

THE INSTITUTE OF PAPER  
CHEMISTRY

Appleton, Wisconsin

Doctor's Dissertation

The Initial Retention of Fibers by Wire Grids

Ronald Estridge

June, 1961

LOAN COPY  
TO BE RETURNED  
EDITION OF 1961

THE INITIAL RETENTION OF FIBERS BY WIRE GRIDS

A thesis submitted by

Ronald Estridge

B.Ch.E. 1956, North Carolina State College  
of Agriculture and Engineering  
M.S. 1958, Lawrence College

0  
in partial fulfillment of the requirements  
of The Institute of Paper Chemistry  
for the degree of Doctor of Philosophy  
from Lawrence College,  
Appleton, Wisconsin

June, 1961

## TABLE OF CONTENTS

	Page
INTRODUCTION	1
ANALYSIS OF THE PROBLEM	8
The Concept of the Retention Probability	8
Evaluation of the Probability Function	14
Application to Initial Retention in Idealized Systems	16
Retention of Fibers by a Grid of Parallel Wires	17
Assuming no Friction Between Wire and Fiber	19
Assuming no Slippage Between Wire and Fiber	23
The Effect of Fiber Orientation	26
Retention of Fibers by a Square-Mesh Grid	28
For $L/b < 1$	29
For $L/b > 2\sqrt{2}$	31
For $L/b = \sqrt{2}$	32
EXPERIMENTAL	36
RESULTS AND DISCUSSION	40
Initial Retention	40
Subsequent Retention	52
Significance of This Work and Suggestions for Future Studies	56
Extension of the Theory	56
Significance to Screening and Classification	60
Significance to Sheet Formation	65
SUMMARY AND CONCLUSIONS	69
NOMENCLATURE	73
LITERATURE CITED	75

	Page
APPENDIX I. DETAILS OF THE CALCULATIONS FOR THE RELATIONSHIPS BETWEEN $\bar{P}_i$ AND $b/L$	76
Method of Obtaining Equation (20)	76
The Relationship Between $\bar{P}_i$ and $L/b$ for Parallel Grid Assuming no Slippage	77
The Relationship Between $\bar{P}_i$ and $L/b$ for Square-Mesh Grid	80
For $L/b < 1$	80
For $L/b > 2\sqrt{2}$	81
For $L/b = \sqrt{2}$	84
Area <u>A</u>	84
Area <u>B</u>	84
Area <u>C</u>	88
Area <u>D</u>	88
Area <u>E</u>	88
Area <u>F</u>	92
Area <u>G</u>	92
APPENDIX II. CALCULATED THEORETICAL POINTS FOR THE CURVES OF FIGURE 9	95
APPENDIX III. EXPERIMENTAL	96
Apparatus	96
Materials	98
Fibers	98
Grids	100
Water	102
Procedure	103
Effects of Operating Variables	105
Flow Rate	105
Wire Diameter	105

	Page
Consistency	107
Permeation Time	107
Distribution of Fiber Orientations	110
APPENDIX IV. EXPERIMENTAL RETENTION DATA	114
APPENDIX V. DETERMINATION OF INITIAL SLOPES	119
APPENDIX VI. PHOTOGRAPHS OF FIBER DEPOSITS	125

## INTRODUCTION

The removal of solid particles from fluid suspensions by direct mechanical interception as in filtration and screening is an important operation in a large number of the chemical process industries. Accordingly, this subject has received a great deal of both theoretical and applied investigation which has greatly increased the understanding of the mechanisms involved.

The production of paper involves such separations at several points in the manufacturing process, e.g., the screening of the pulp to remove oversize and dirt particles and the deposition of fibers on the fourdrinier or cylinder wire to form the sheet. Also, screen classifications are widely used as an index of fiber length and fiber-length distribution. Although these operations are similar in many ways to those used in other industries, the paper industry is faced with a unique problem in that the particles involved have extremely high axis ratios. The dimension along one axis of a papermaking fiber is much greater than those along the two mutually perpendicular axes. Owing to this high axis ratio as compared to granular materials, the determination of whether or not fibrous particles will be retained by the filter medium or screening medium is much less straightforward. For any particles of shape other than spherical, the retention of a particle by an aperture roughly corresponding in size to that of the particle becomes a matter of chance. A particle which in a certain orientation might be retained will not necessarily arrive at the aperture at that orientation. Thus, there is only a certain probability

that the particle will actually be retained. In the case of the screening of granular materials this is often taken into account by the use of empirical shape factors based on the elongation and flakiness of the particles. Granular particles generally have axis ratios of less than five while fibers may be thought of as particles having axis ratios of fifty or more; thus, the element of chance plays a much more important role in the case of fibers. For example, when a screen analysis is performed on a fibrous material, an appreciable amount of long fiber is found in the short fiber fractions and some short fibers in the long fractions; the same test performed on granular materials will give relatively uniform fractions. It is doubtful whether an extension of the empirical concept of shape factors to such extremely different shaped particles as fibers would be justified or of much use in view of the fact that other factors, such as fiber stiffness, also play an important role in fiber retention.

The need for a better understanding of the mechanism of fiber retention has become evident with the rapid growth of the technological understanding of the sheet-forming and drainage processes in the papermaking operation. The advent of high-speed machines and the formation problems that have accompanied them have emphasized the need for increasing our fundamental knowledge of these processes. The formation of paper on a paper machine has been recognized as basically a filtration and thickening process, and much work has been done in recent years in an attempt to apply the established principles of filtration to the sheet-forming operation. Laboratory investigations (1-3) have shown that the filtration laws can be modified to describe the

dewatering of papermaking slurries, but attempts (4, 5) to apply these principles to actual paper machine operation have met with only limited success. One of the complicating factors which arises in studying a paper machine is the loss of a considerable amount of solids through the wire, the quantity passing being greatest as the slurry first contacts the wire and diminishing as a mat of fibers is formed on the wire. This loss is not distributed equally between all particle sizes and species in the slurry, and it has been shown (4) that the change in the loss of fines may account for a threefold increase in the specific filtration resistance between the breast roll and couch roll of a paper machine.

The distributed loss of solids through the wire also profoundly influences the properties of the sheet, causing it to vary in structure and composition through its thickness. This gives rise to a variety of problems ranging from uneven adsorption of additives by the two sides of the sheet to curling due to unequal dimensional stability of the two sides.

The degree of retention of solids in the early stages of formation is controlled by the structure of the wire. The relative importance of the wire will depend on the basis weight of the sheet being formed, being of great importance during the entire formation period of thin sheets such as tissues and decreasing in overall importance as thicker sheets are formed. In the latter case it is the fibers deposited in the early stages that will control retention during the latter stages of the formation period. However, since the wire will,

to a large extent, determine the structure of the first few layers of fibers which will in turn affect the structure of the subsequent layers, the initial retention of fibers by the bare wire must be regarded as an important phase in the formation of any sheet where it is possible for solids to pass through the wire.

It is obvious that by decreasing the size of the openings in the wire, the retention of fibers will be increased. But the resistance to flow will also be increased, making it necessary to compromise between retention and flow resistance in an optimum wire design. The problem of the flow resistance offered by screens and other filter media has been studied by a number of workers (6-8), but studies of the mechanism of fiber retention and the interaction between wire and fibers are almost nonexistent although these might be considered vastly more important problems in the study of sheet formation than the flow resistance of the bare wire. The lack of basic work on the mechanism of fiber retention by the wire is due largely to the fact that studies of sheet formation from a fundamental viewpoint have progressed only in recent years and have for the most part been concerned with formation rate-driving force relationships. In order to apply these relationships to their full advantage in completely describing drainage and sheet formation, it will, however, be necessary to better understand the mechanism of particle retention.

In most other commercial filtration processes, the amount of solids passed through the filter medium is negligible since the filter cake itself acts as the filter medium during all but a short period in

the initial stages of the filtration. The exception to this observation is the area of "filter medium" filtration which includes gas filtration and liquid clarification. The relationship between particle removal from gas streams and the structure of the filter medium has been thoroughly reviewed by Davies (9) and by Chen (10). Liquid clarification has also been studied by several investigators (11-13). Grace (13) has presented a comprehensive review of the earlier work in this field and has attempted to relate the performance of the filter medium to its internal pore structure. These processes differ from the problem of filtration by a monofilament woven material such as wire cloth in that they depend on the depth of the medium for efficient filtration, whereas the wire cloth acts essentially as a two-dimensional medium. However, it would appear that these studies of three-dimensional filter media might be applicable to the problem of retention of the fine particles of a papermaking slurry within the mat of fibers as it is formed.

Due to its regular geometry, the analysis of retention of fibers by wire cloth should lend itself to rigorous treatment much more rapidly than the more or less randomly constructed filter media studied elsewhere. Because of this regular nature of the medium, the problem of fiber retention in the sheet-forming process is closely related to the problem of particle size classification by screening. The relationship between the structure of the screening medium and its particle size retention is the basis of screening operations. The ideal separation of particle sizes by screening is never obtained, and it has been recognized that screening is a statistical process. Steenberg and Kubat (14-16) have presented a statistical analysis of the screening process wherein

they have introduced the concept of a passage probability for a particle through a screen element. Such a concept would appear to be particularly applicable to the screening of fibers where the element of chance plays such an important role. While these authors have not studied the factors which influence the passage probability, they suggest that the most important factors affecting it are the relative geometry and dimensions of the particles and the screen openings, the hydrodynamic field around the openings, and the interactions between particles.

The most obvious factor influencing the passage probability is the relative sizes of the particles and the openings. This has long been used as the basis for fiber-length distribution determinations by screening. The actual relationship between screen number and fiber length retained has not been fully investigated, but other factors such as fiber flexibility and hydrodynamic conditions are known to affect the results. In one investigation of this subject, Andersson and Bartok (17) found a correlation between the fiber length of stiff rayon fibers and their passage probability for 28-mesh screens in a modified Bauer-McNett classifier. For pulp fibers a correlation was also established between the weights of fractions collected and the average fiber length with the standard deviation as a parameter. No general conclusions can be drawn from their correlations, however, owing to the rather restricted set of conditions used.

A detailed theoretical analysis of the general problem of retention of fibers by wire grids would be extremely involved and would require a much more thorough understanding of the hydrodynamics and flocculation of fiber suspensions than is presently available. This

shortcoming in our present knowledge precludes a vigorous fundamental attack on the problem from a quantitative standpoint. However, it would appear very worthwhile to begin developing a fundamental analysis of the mechanism involved in the retention of fibers on grids with the objective of expanding it to the more general case as our knowledge in these related areas increases. When initially attacking a problem of great complexity it is often worthwhile to try to resolve the problem into simpler components and to study the most important factors under ideal conditions isolated from as many of the complicating interactions as possible. Even though the results of such studies are seldom of immediate value in a practical sense, this procedure enables one to obtain a clearer view of the fundamental phenomena involved, and as the complex process is reconstructed by combining these basic components one obtains a better understanding of the interactions involved.

The objective of the work reported here was to carry out the first stage of such an attack on the problem of the retention of fibers by wire grids. The approach used in this study was to develop very generalized expressions describing fiber retention in terms of a probability function which is dependent on the properties of the fibers and the grid, the hydrodynamic field, and the interactions between fibers. The probability function was then investigated for the case of the initial retention of fibers by the bare grid under a restricted set of conditions in order to illustrate this approach to the problem and to test its validity. Since the relative geometry and dimensions of the fibers and the openings in the grid are probably two of the most important factors which affect retention, these were the variables chosen for investigation in this study.

ANALYSIS OF THE PROBLEM

THE CONCEPT OF THE RETENTION PROBABILITY

Consider a suspension of fibers approaching some type of grid which will intercept some of the particles from the suspension and will allow others to pass through. The grid is in the  $x$ - $y$  plane and the suspension is approaching from the  $z$  direction with no lateral components of velocity. If the average point concentration expressed as the number of fiber centers per unit volume of suspension is  $\underline{n}$ , the probability of finding a fiber center in an infinitesimal volume  $\underline{dx dy dz}$  at a point  $(\underline{x}, \underline{y})$  in a plane parallel to and at a short distance  $\underline{z}$  ahead of the grid is  $\underline{n dx dy dz}$ . If the probability that a fiber will be in a position to be retained by the grid is  $\underline{P}$ , then the number of fibers  $\underline{dN}$  removed from a volume  $\underline{dV}$  of suspension which reaches the plane of the grid in time  $\underline{dt}$  can be expressed as

$$\underline{dN} = \underline{dt} \iint \underline{nPu} \, \underline{dx} \, \underline{dy} = (\underline{dV}/\underline{A}\bar{u}) \iint \underline{nPu} \, \underline{dx} \, \underline{dy} \quad (1)$$

where  $\underline{u}$  is the velocity perpendicular to the grid at the point  $(\underline{x}, \underline{y})$  and  $\bar{u}$  is the average value of  $\underline{u}$  over the area  $\underline{A}$  which is the area in the  $x$ - $y$  plane under consideration and over which the indicated integration is performed. In the most general case,  $\underline{n}$ ,  $\underline{P}$ , and  $\underline{u}$  will be functions of  $\underline{x}$  and  $\underline{y}$ , and the grid may be either of regular geometry such as a wire cloth or irregular such as a deposit of fibers retained from the suspension that has previously passed the grid. The probability function  $\underline{P}$  will also be dependent on the structure and properties of both the grid and the fibers as well as the nature of the hydrodynamic

field in the vicinity of the grid and fiber interactions such as flocculation.

If all the particles in the suspension are identical, Equation (1) can be rewritten in terms of the mass of fibers  $\frac{dW}{dr}$  retained on the grid:

$$\frac{dW}{dr} = (\lambda \frac{dV}{A\bar{u}}) \iint nPu \, dx \, dy \quad (2)$$

where  $\lambda$  is the mass per fiber. In general, there will be, however, more than one type of particle present, and it becomes necessary to write Equation (2) as the summation over all these types of particles:

$$\frac{dW}{dr} = (\frac{dV}{A\bar{u}}) \sum_{i=1}^j \lambda_i \iint \frac{n_i P_i u}{\bar{u}} \, dx \, dy \quad (3)$$

where there are  $j$  types of particles present.

For convenience, average values of  $\frac{n_i}{\bar{u}}$  and  $\frac{P_i}{\bar{u}}$  over the area  $A$  may be defined as

$$\frac{\overline{n_i P_i}}{\bar{u}} = \frac{\iint \frac{n_i P_i u}{\bar{u}} \, dx \, dy}{\iint u \, dx \, dy} = \frac{\iint \frac{n_i P_i u}{\bar{u}} \, dx \, dy}{\bar{u} A} \quad (4)$$

so that

$$\frac{dW}{dr} = \frac{dV}{A} \sum \lambda \frac{\overline{n_i P_i}}{\bar{u}} \quad (5)$$

When the average point concentration  $\underline{n}_i$  is not a function of  $\underline{x}$  and  $\underline{y}$ , the mean product  $\overline{\underline{n}_i \underline{P}_i}$  can be replaced by  $\overline{\underline{n}_i} \overline{\underline{P}_i}$ . The quantity  $\lambda_i \overline{\underline{n}_i}$  is equivalent to  $\overline{\rho} \overline{\underline{s}_i}$  where  $\overline{\rho}$  is the mean density of the suspension over  $\underline{A}$  and  $\overline{\underline{s}_i}$  is the mean concentration expressed as the mass of fibers of type  $\underline{i}$  per unit mass of suspension. Hence, Equation (5) can be written as

$$\underline{dW}_r = \overline{\rho} \underline{dV} \sum_i \overline{\underline{s}_i \underline{P}_i} \quad (6)$$

It is often more convenient to express the weight of material retained by the grid in terms of the volume of filtrate  $\underline{V}_f$  rather than in terms of the volume of suspension approaching the grid. The two volumes are related by the total material balance.

$$\overline{\rho} \underline{dV} = \underline{m} \underline{dW}_r + \overline{\rho}_f \underline{dV}_f \quad (7)$$

where  $\underline{m}$  is a measure of the moisture content of the deposit expressed as the mass ratio of the wet deposit to dry deposit, and  $\overline{\rho}_f$  is the density of the filtrate. Combining Equations (6) and (7) gives

$$\underline{dW}_r / \underline{dV}_f = (\overline{\rho}_f \sum_i \overline{\underline{s}_i \underline{P}_i}) / (1 - \underline{m} \sum_i \overline{\underline{s}_i \underline{P}_i}). \quad (8)$$

The concentration of particles in the filtrate  $\overline{\underline{s}_f}$  can be determined by a fiber balance:

$$\underline{dW}_r / \underline{dV}_f = \overline{\rho}_f (\overline{\underline{s}} - \overline{\underline{s}_f}) / (1 - \underline{m} \overline{\underline{s}}) \quad (9)$$

which when combined with Equation (8) yields

$$\overline{\underline{s}_f} = (\overline{\underline{s}} - \sum_i \overline{\underline{s}_i \underline{P}_i}) / (1 - \underline{m} \sum_i \overline{\underline{s}_i \underline{P}_i}). \quad (10)$$

Another useful way of expressing the removal of particles from the suspension is as the weight fraction  $\alpha$  of particles removed from an element of slurry.

$$\alpha = \frac{dW_r / \bar{s} \bar{\rho} dV}{(1/\bar{s}) \sum \frac{\bar{s}_i \bar{P}_i}{\bar{s}_i \bar{P}_i}} \quad (11)$$

When the mass of material deposited on the grid  $\underline{W}_r$  is plotted as a function of the total mass of material that has reached the grid  $\underline{W}_t$  (i.e., the mass of the deposit plus the mass of solids that has passed the grid) as in Fig. 1, the slope at any point is  $\alpha$ . Such a curve will have a finite initial slope  $\alpha_0$  which can be interpreted as the fraction of fibers retained by the bare grid from the first element of suspension passing through it. This initial slope, which will hereafter be referred to as the initial rate of retention, or simply as the "initial retention," will be a direct function of the relative geometry and dimensions of the grid and fibers, while the slope at any other point will depend on the size and shape of the interfiber spaces in the bed of fibers already deposited. As the fiber deposit grows, the slope will increase eventually approaching a value of unity when the openings in the grid are effectively closed and no more particles can pass through. If the portion of the curve having unit slope is extended to  $\underline{W}_r = 0$ , it intercepts the  $\underline{W}_t$  axis at a value  $\underline{W}_T$  which is equal to the total amount of solids passed by the grid. Thus, for a perfect sieve the curve would be a straight line of unit slope passing through the origin. The point at which the relationship becomes linear is important in describing the structure of the deposit if more than one fiber type is present. Until this point is reached the composition of each layer deposited will

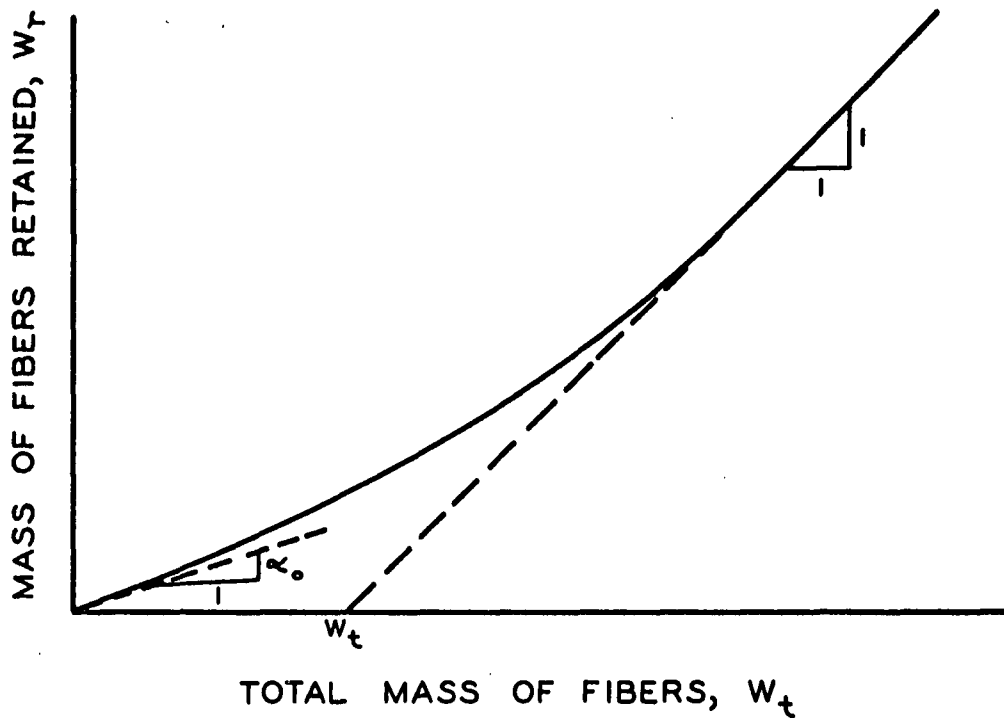


Figure 1. Retention Curve

vary in composition; after this point the composition of each layer will be the same unless there is some redistribution of components within the bed.

The equations developed in the preceding pages should describe the build-up of a fiber deposit on a grid. Integrated forms of Equations (3), (5), (6), (8), or (11) could be used in combination with a knowledge of the flow schedule to predict the weight of the deposit at any time. Integration of these equations, however, require that  $\bar{P}_{i1}$  be known as a function of  $\underline{W}_r$ . It is probably not feasible to determine this relationship analytically since it would require a complete description of the geometry of the system formed by the deposit of fibers on the grid at any time and a knowledge of how  $\underline{P}_{i1}$  is

affected by this geometry. In fact, the determination of  $\underline{P}_{-i}$  becomes too involved to be of use at the present time except for the simplest grid geometries and fiber systems. In very simple systems it is possible to evaluate  $\underline{P}_{-i}$  for the first fibers that approach the bare grid, and therefore to predict the initial retention. Since the initial retention will determine to some extent how the succeeding elements of the deposit are formed, this would be useful in an initial study of factors which affect fiber retention by grids.

In many cases assumptions can be made which greatly simplify the relationships presented thus far. For instance, if the suspensions are dilute,  $\underline{V} = \underline{V}_f$ ,  $\bar{\rho} = \bar{\rho}_f$ , and  $\underline{m}\bar{s} \ll 1$ . In this case, Equation (8) becomes

$$\underline{dW}/\underline{dV}_f = \bar{\rho}_f \sum \bar{s}_{-i} \bar{P}_{-i} \quad (12)$$

and Equation (10) becomes

$$\bar{s}_{-f} = \bar{s} - \sum \bar{s}_{-i} \bar{P}_{-i}. \quad (13)$$

Where it can be assumed that the values of  $\underline{n}$  and  $\underline{u}$  are not functions of  $\underline{x}$  and  $\underline{y}$ , then  $\underline{n}_{-i} = \bar{n}_{-i}$  and  $\underline{u} = \bar{u}$ . In this case  $\bar{P}_{-i}$  can be defined without the use of these quantities simply as

$$\bar{P}_{-i} = \frac{\iint \underline{P}_{-i} \underline{dx} \underline{dy}}{\underline{A}} \quad (14)$$

rather than by Equation (4). Equation (11) can then be written as

$$\alpha = (1/\bar{s}) \sum \bar{s}_{-i} \bar{P}_{-i} = \sum \underline{w}_{-i} \bar{P}_{-i} \quad (15)$$

where  $w_i$  is the weight fraction of the  $i$ th type of fiber in the suspension.

### EVALUATION OF THE PROBABILITY FUNCTION

In order to evaluate the probability function  $P$  at any point  $(x,y)$ , it is necessary to know the distribution of angular orientations of fibers passing this point and to know at which angles a fiber will be in position to be retained.

A fiber's orientation may be specified by two angles  $\theta$  and  $\phi$ . The distribution of orientations can be represented by a distribution function  $n_{\theta,\phi}$  such that the probability is  $n_{\theta,\phi} d\omega$  that a fiber at  $(x,y)$  lies within a differential solid angle  $d\omega$  with the angular orientation given by  $\theta$  and  $\phi$ . A fiber at this point will be in position to be retained if it lies within a certain solid angle defined by a functional relationship between  $\theta$  and  $\phi$ . Thus, the probability function can be reduced to

$$P = \iint n_{\theta,\phi} d\omega \quad (16)$$

and the problem is now to determine the relationship which specifies the limits on the integral.

This relationship which defines the conditions for retention of a fiber is dependent upon the fiber's position with respect to the members of the grid and a number of other important variables. These may be categorized as follows:

- (1) structure of the grid,
- (2) properties of the fibers,
- (3) hydrodynamic conditions,
- (4) fiber interactions.

Obviously, the geometry and dimensions of the grid are very important in establishing the conditions for retention. Also, the surface condition of the grid is important since this will determine the frictional forces between the fiber and grid. Properties of the fiber that would be expected to be important are its length, stiffness, and surface condition. The importance of the length in relation to the size of the openings in the grid is obvious, and the surface condition is again important in determining the frictional forces which might play a part in holding the fibers on the grid. The fiber's stiffness controls how much the fiber will deform, and thus determines whether a fiber can be retained by bridging between two adjacent members of the grid or by stapling over a single member. If a fiber bridges initially, it still may deform enough under the fluid drag to be carried on through the grid. The hydrodynamic field is important as it affects the drag on deposited fibers and as it affects the motions of the approaching fibers. Fiber interactions such as flocculation will cause the fibers to assume collective properties which become important. The individual fiber properties will become less important as the degree of interaction increases and factors such as the size and strength of flocs become the variables which control retention. Needless to say, most of these variables are not unrelated.

In order to mathematically describe the conditions which determine if a fiber will be retained, it would be necessary to be able to quantitatively describe all of these variables and the interrelationships between them. This, of course, is not possible at this time.

APPLICATION TO INITIAL RETENTION IN IDEALIZED SYSTEMS

The foregoing considerations can now be applied to the analysis of the initial retention of fibers by grids. Since the objective of this work was to study the effects of fiber length and grid geometry and because many of the other variables cannot be satisfactorily described, the following analysis will be limited to a rather idealized system. Two simple grid geometries have been chosen for study, infinite parallel mesh and square mesh. It should be recognized that these are the two limiting cases of the general rectangular geometry. The analysis will also be restricted as follows:

- (1) only rigid fibers are considered,
- (2) the fiber suspensions are dilute enough that each fiber acts independently,
- (3) all flow is perpendicular to the grid and is not affected by the grid,
- (4) the fibers are uniformly dispersed in the fluid,
- (5) the rotational motion of the fibers is small compared to the translational velocity,
- (6) the diameter of the wires forming the grid is small in comparison to the size of the openings.

Under these conditions Equations (14) and (15) can be used to predict the initial rate of retention.

Since the grids to be studied are composed of simple repeating units and conditions are assumed to be identical over all of these units, it is possible to carry out the analysis over only one of them.

RETENTION OF FIBERS BY A GRID OF PARALLEL WIRES

Consider a uniformly dispersed suspension of rigid fibers differing only in length approaching a grid composed of infinite parallel wires with a uniform spacing  $\underline{b}$  between axes. Considering half the distance between two adjacent wires as a repeating unit, Equation (14) can be applied to give

$$\underline{\bar{P}}_i = (2/\underline{b}) \int_0^{\underline{b}/2} \underline{P} \underline{dx} \quad (17)$$

If the conditions for retention can be established,  $\underline{P}$  can be evaluated by Equation (16) and values of  $\underline{\bar{P}}_i$  and  $\alpha_o$  can be obtained.

In order to establish the conditions necessary for a fiber to bridge between two wires, consider a fiber of length  $\underline{L}$  whose center is approaching the grid at a distance  $\underline{x} < \underline{b}/2$  from one of the wires as in Fig. 2. This fiber is oriented at an angle  $\phi$  with the plane of the grid and its projection makes an angle  $\theta$  with the  $\underline{x}$ -axis which is perpendicular to the axes of the wires composing the grid. Since both ends of the fiber are identical, the position of the fiber can be described by values of  $\theta$  and  $\phi$  lying between  $\pi/2$  and  $-\pi/2$ . If  $\phi$  is between 0 and  $\pi/2$ , the fiber must strike the nearest wire(I) before it strikes the adjacent wire(II) if it is to bridge across them and be retained by the grid. Likewise, if  $\phi$  is between 0 and  $-\pi/2$ , it must strike the adjacent wire(II) first if bridging is to occur.

When the fiber strikes the grid, some slippage may take place depending on the frictional forces between the fiber and the grid. The two extreme cases of slippage will be considered; no friction between fiber and wire, and enough friction such that no slippage takes place.

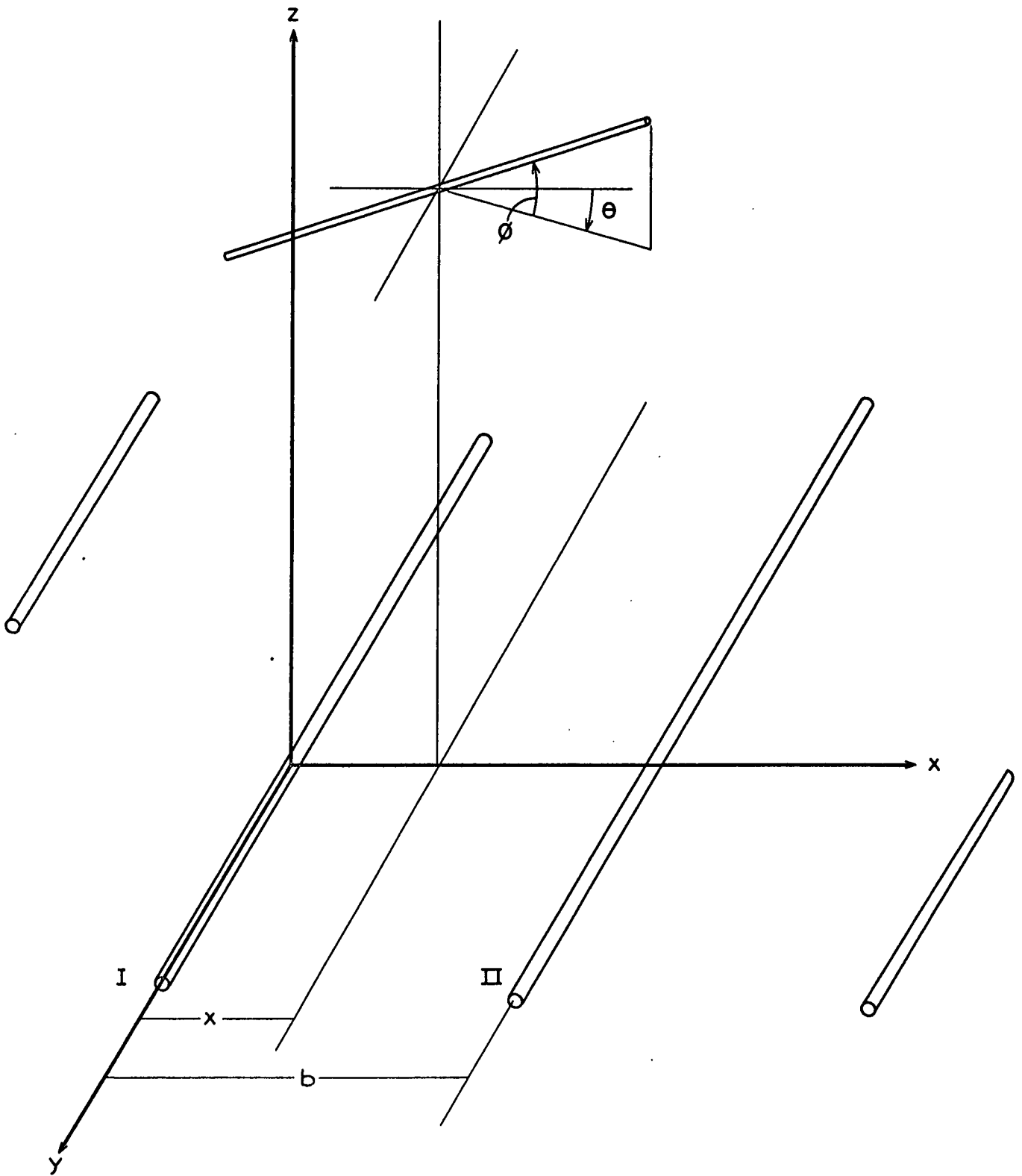


Figure 2. Fiber Approaching Grid of Parallel Wires

Assuming no Friction Between Wire and Fiber

First assume that when the fiber strikes one of the wires, it rotates with the angle  $\theta$  remaining constant and that slippage occurs such that the  $\underline{x}$ - $\underline{y}$  co-ordinates of the fiber midpoint remain unchanged. From Fig. 3 it is evident that if  $\phi$  is negative, the necessary and sufficient condition for bridging to occur is that the fiber be in position to strike wire(II), i.e.,  $(\underline{L}/2) \cos\theta \cos\phi > (\underline{b} - \underline{x})$ . If the fiber approaches with  $\phi$  positive, the conditions for bridging to occur are that the fiber be in position to strike wire (I), i.e.,  $(\underline{L}/2) \cos\theta \cos\phi > \underline{x}$ , and that upon rotation to  $\phi = 0$ , it be in position to also strike wire(II), i.e.,  $(\underline{L}/2)\cos\theta > (\underline{b} - \underline{x})$ . These conditions are met if the fiber lies in the solid angle formed by the center of a sphere of diameter  $\underline{L}$  and the area on the surface of the sphere defined by:

$$\cos\theta \geq 2(\underline{b} - \underline{x})/\underline{L} \cos\phi \quad \text{for } 0 > \phi > -\pi/2 \quad (18a)$$

and

$$\begin{aligned} \cos\theta &\geq 2(\underline{b} - \underline{x})/\underline{L} \\ \cos\theta &\geq 2\underline{x}/\underline{L} \cos\phi \quad \text{for } 0 < \phi < \pi/2. \quad (18b) \end{aligned}$$

The area defined by (18a) is simply half the area of a spherical segment of diameter  $\underline{L}$  and height  $(1/2\underline{L} - \underline{b} + \underline{x})$ , while that defined by (18b) is formed by the intersection of a spherical segment of height  $(1/2\underline{L} - \underline{x})$  and a great circle of the sphere as illustrated in Fig. 4(only half of the area is shown in the figure). Applying these conditions as the limits for integration, Equation (16) becomes for this case:

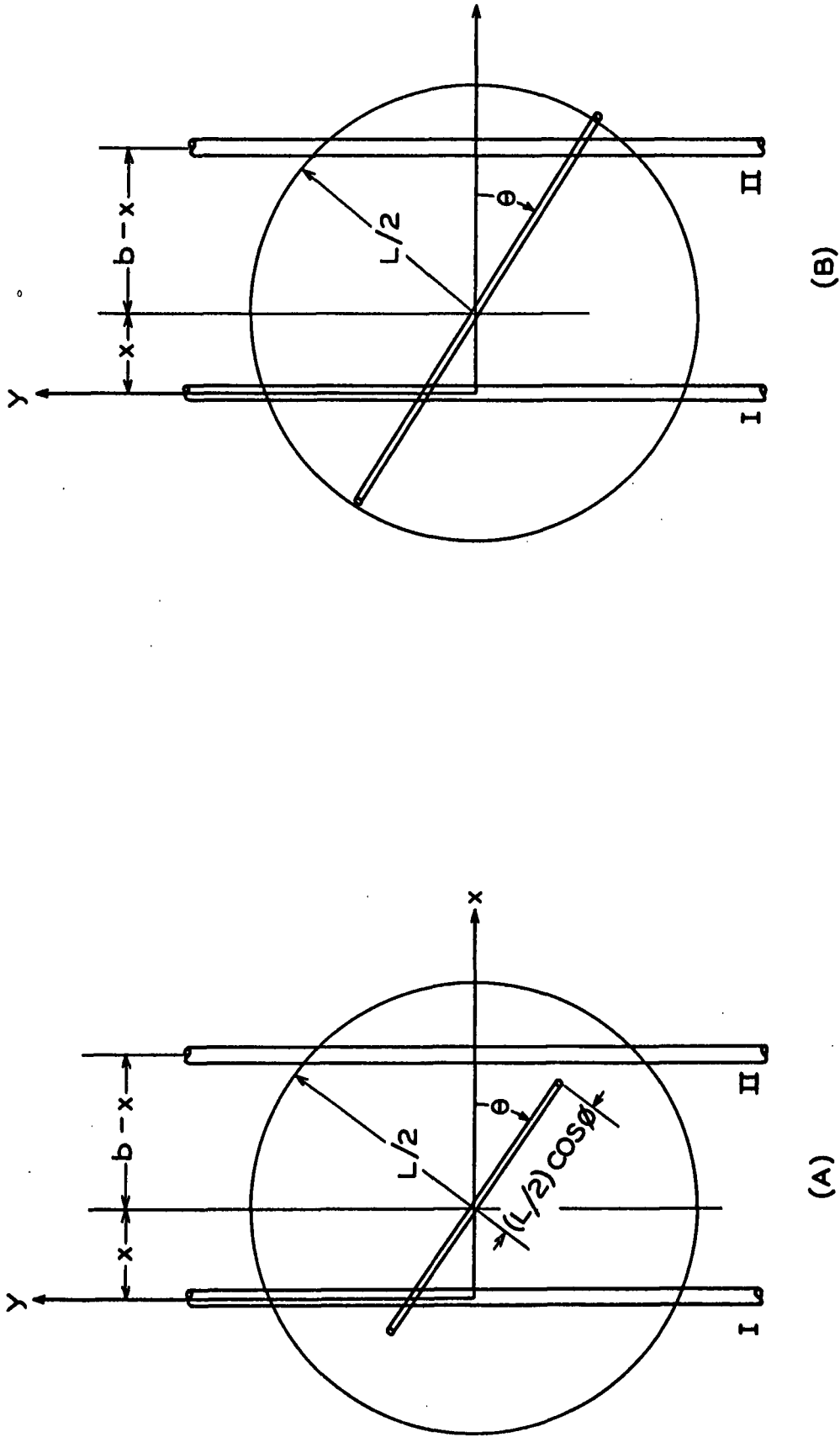


Figure 3. Projection of Fiber on Parallel Grid  
(A) Before Striking Grid  
(B) After Striking Grid and Rotating to  $\phi = 0$

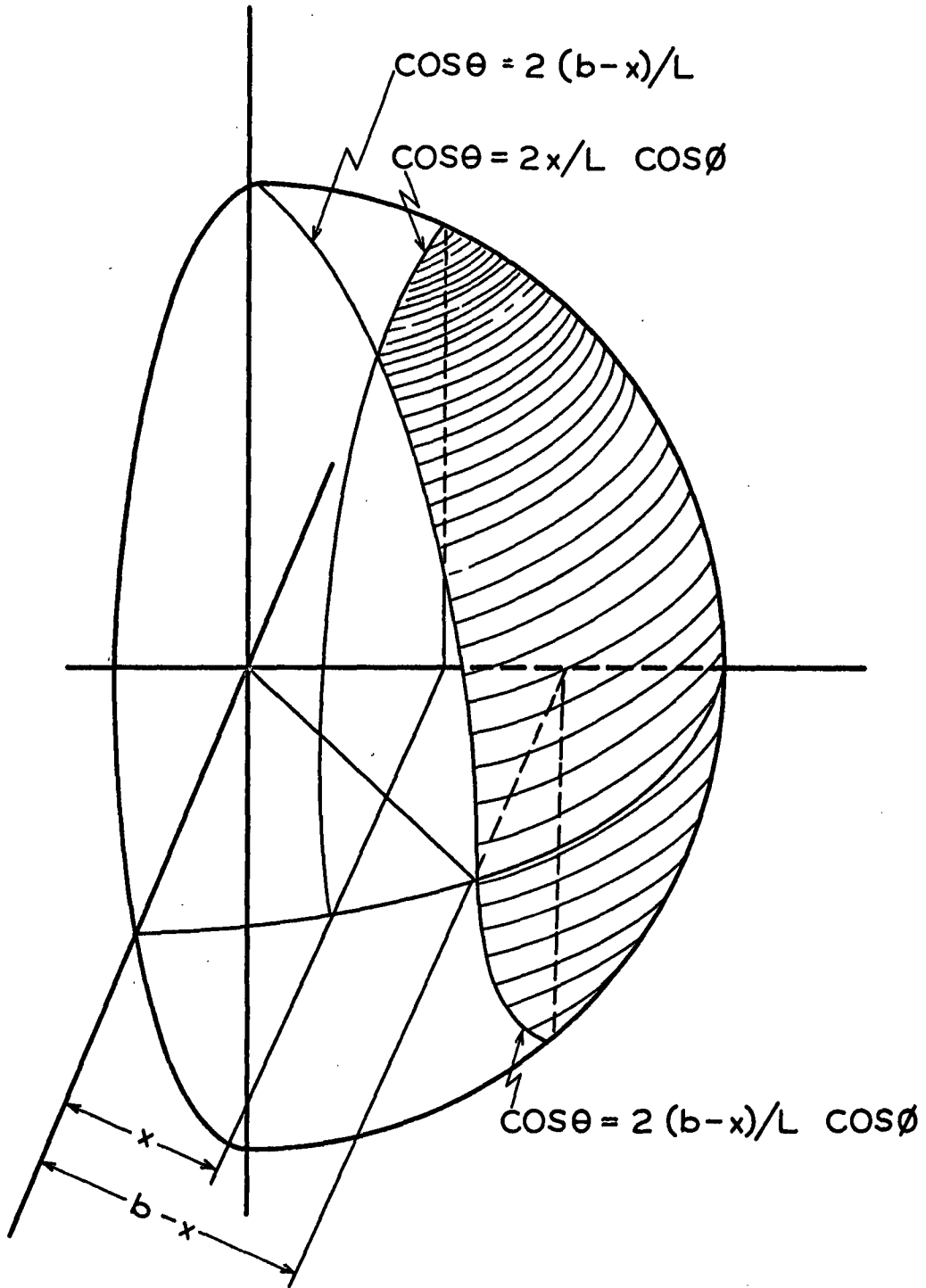


Figure 4. Representation of the Area Described by Equation (18)

$$\underline{P} = \int_{-\cos^{-1}2(\underline{b}-\underline{x})/\underline{L}}^{\cos^{-1}2(\underline{b}-\underline{x})/\underline{L}} \left( \begin{array}{l} \cos^{-1}2\underline{x}/\underline{L} \cos\theta \\ \underline{n}_{\theta,\phi} \cos\phi \frac{d\theta}{d\phi} \\ -\cos^{-1}2(\underline{b}-\underline{x})/\underline{L} \cos\theta \end{array} \right) \quad (19)$$

If it is assumed that the fibers are randomly oriented, then  $\underline{n}_{\theta,\phi} = 1/2\pi$ , and, upon integration, Equation (19) yields\*

$$\underline{P} = 1/2 - \underline{b}/\underline{L} + \underline{x}/\underline{L} + (1/\pi)[\tan^{-1}\underline{v} - (2\underline{x}/\underline{L})\tan^{-1}2\underline{x}\underline{v}/\underline{L}] \quad (20)$$

where  $\underline{v} = [L^2/4 - (\underline{b}-\underline{x})^2]^{1/2}/[(\underline{b}-\underline{x})^2 - \underline{x}^2]^{1/2}$

which is just the ratio of twice the area shown in Fig. 4 to the area of the hemisphere. This result can now be substituted in Equation (17) to obtain an expression for  $\underline{\bar{P}}_1$  as a function of the relative fiber length. When this is done, the integration indicated in Equation (17) must be carried out from 0 to  $\underline{b}/2$  for fibers longer than  $2\underline{b}$  and from  $\underline{b} - \underline{L}/2$  to  $\underline{b}/2$  for fibers shorter than  $2\underline{b}$  but longer than  $\underline{b}$ . This results in the expression:

$$\underline{\bar{P}}_1 = 1/2 - 3\underline{b}/4\underline{L} + (2/\pi\underline{b}) \int_0^{\underline{b}/2} [\tan^{-1}\underline{v} - (2\underline{x}/\underline{L})\tan^{-1}2\underline{x}\underline{v}/\underline{L}] d\underline{x}$$

for  $\underline{L}/\underline{b} > 2$ , and (21)

$$\underline{\bar{P}}_1 = \underline{b}/4\underline{L} + \underline{L}/4\underline{b} - 1/2 + (2/\pi\underline{b}) \int_{\underline{b}-\underline{L}/2}^{\underline{b}/2} [\tan^{-1}\underline{v} - (2\underline{x}/\underline{L})\tan^{-1}2\underline{x}\underline{v}/\underline{L}] d\underline{x}$$

for  $1 < \underline{L}/\underline{b} < 2$ .

Knowing the distribution of fiber lengths in the suspension one can now determine the initial slope  $\alpha_0$ . If all of the fibers are of the same length  $\alpha_0$  is just equal to  $\underline{\bar{P}}_1$ .

\*See Appendix I, Page 76.

Assuming no Slippage Between Wire and Fiber

If the frictional forces between the fiber and wire are large enough so that no slippage occurs, the fiber will rotate about the point of initial contact with the grid with the angle  $\theta$  remaining essentially constant. During this rotation, the x-y co-ordinates of the midpoint will change, and the chances of the fiber bridging will be greater than in the case discussed previously. Looking at Fig. 5, it is evident that if  $\phi$  is negative, the necessary and sufficient condition for bridging to occur is again that the fiber strike wire(II), i.e.,  $(L/2) \cos\theta \cos\phi > (b - x)$ . And, if  $\phi$  is positive, it can be deduced that the conditions for bridging are that the fiber strike wire(I), i.e.,  $(L/2) \cos\theta \cos\phi > x$ , and that upon rotating to  $\phi = 0$ , it be in position to also strike wire(II). This last condition is now represented by the statement:

$$(L/2) + x/\cos\theta \cos\phi > b/\cos\theta.$$

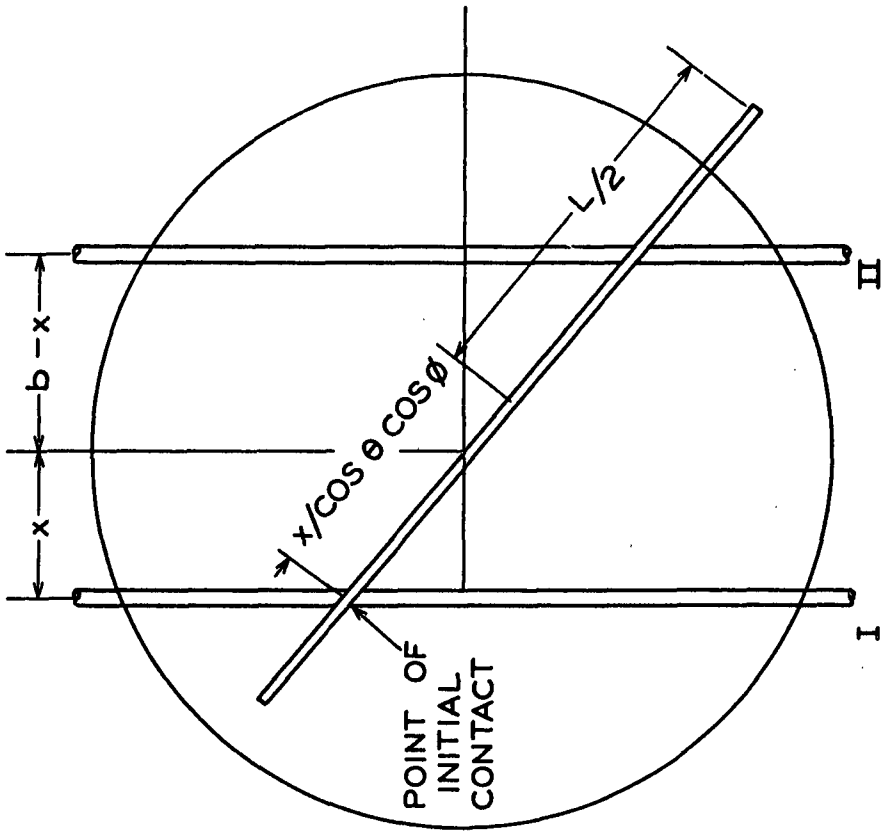
These conditions are met if the fiber lies in the solid angle formed by the center of a sphere of diameter L and the area on the surface of the sphere defined by

$$\cos\theta \geq 2(b - x)/L \cos\phi \quad \text{for } 0 > \phi > -\pi/2 \quad (22a)$$

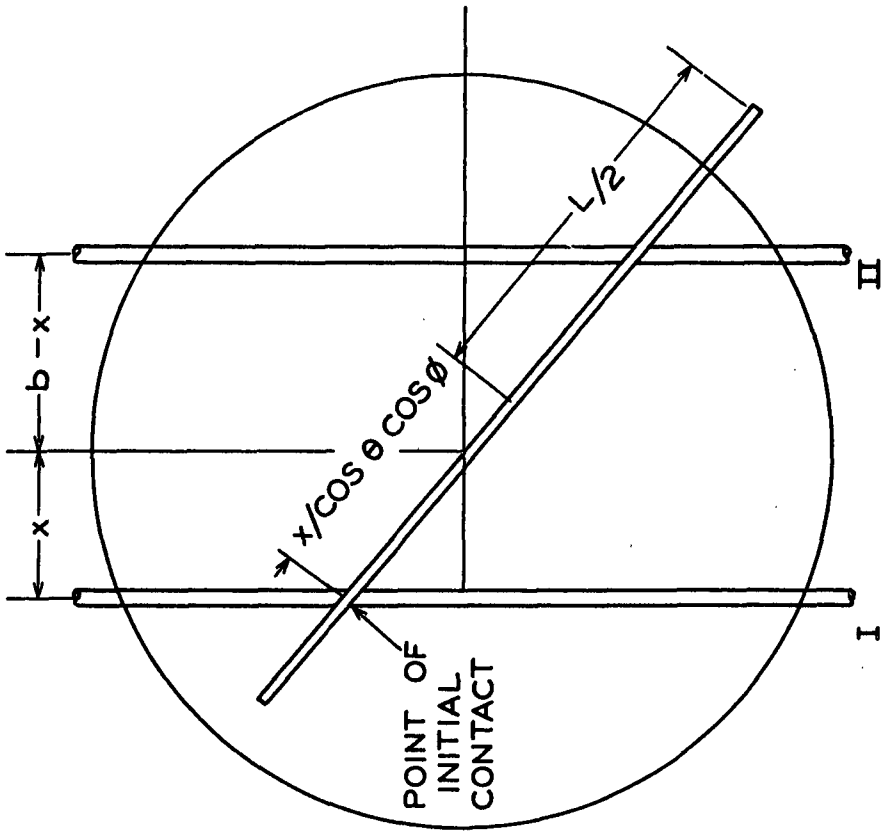
and

$$\begin{aligned} \cos\theta &\geq 2x/L \cos\phi \\ \cos\theta &\geq 2b/L - 2x/L \cos\phi \quad \text{for } 0 < \phi < \pi/2 \quad (22b) \end{aligned}$$

This area is illustrated in Fig. 6 for L > 2b and for b < L < 2b when x is between b - L/2 and b/2. For the case where b < L < 2b when x is between 0 and b - L/2, the area defined by (22a) vanishes and that defined



(A)



(B)

Figure 5. Projection of Fiber on Parallel Grid  
(A) Before Striking Grid  
(B) After Striking Wire(I) and Rotation to  $\phi = 0$   
Assuming no Slippage

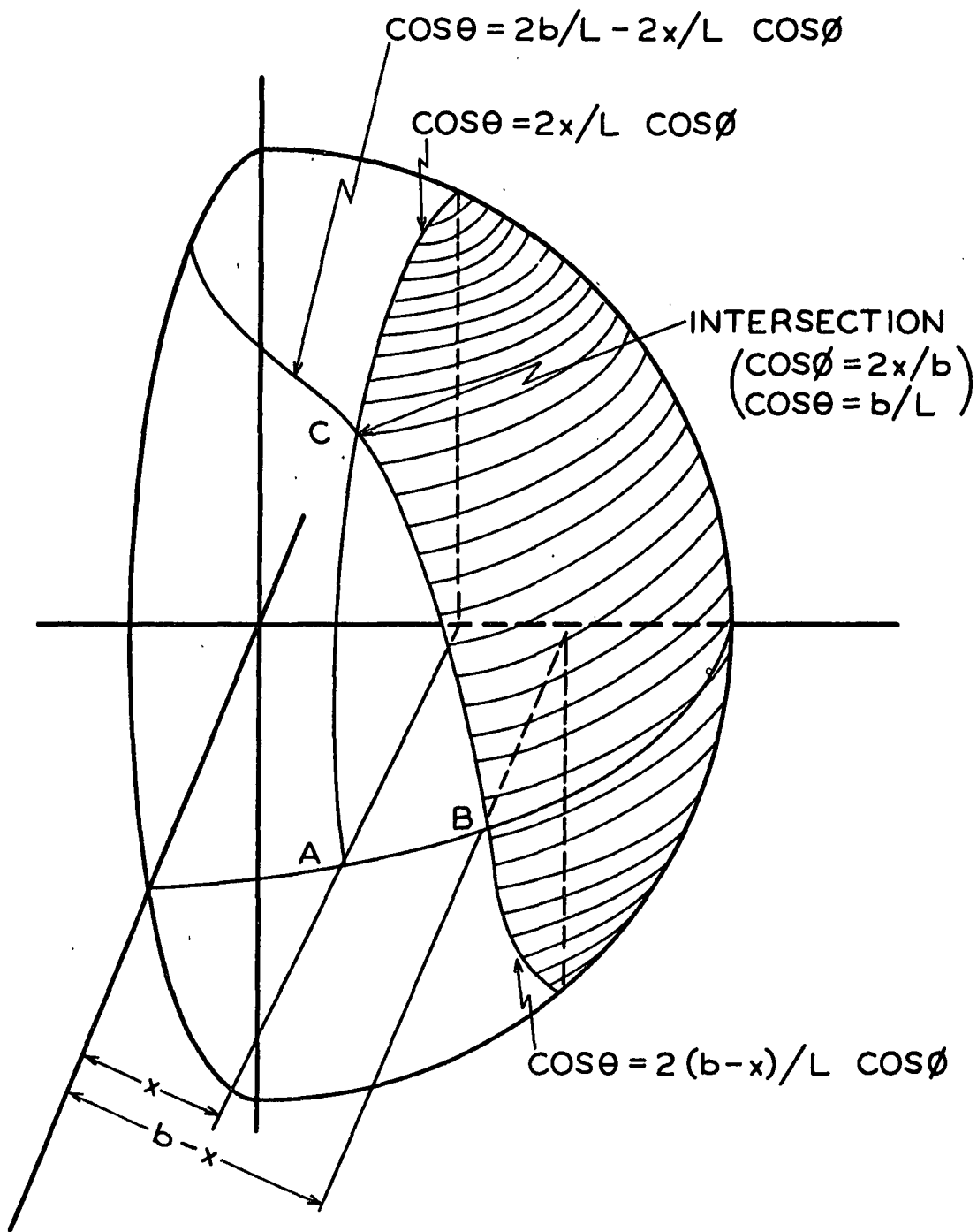


Figure 6. Representation of the Area Described by Equation (22)

by (22b) is as illustrated in Fig. 7. The occurrence of two cases leads to a probability function composed of two parts when these conditions are used to find the limits of integration in the application of Equation (16) to this case:

$$\begin{aligned} \underline{P} = & \int_{-\cos^{-1}2(\underline{b}-\underline{x})/\underline{L}}^{\cos^{-1}2(\underline{b}-\underline{x})/\underline{L}} \int_{-\cos^{-1}2\underline{x}/\underline{L} \cos\theta}^{\cos^{-1}2\underline{x}/\underline{L} \cos\theta} \underline{n}_{\theta,\phi} \cos\phi \, d\phi \, d\theta + \\ & 2 \int_{\cos^{-1}2(\underline{b}-\underline{x})/\underline{L}}^{\cos^{-1}\underline{b}/\underline{L}} \int_{-\cos^{-1}2\underline{x}/(2\underline{b} - \underline{L} \cos\theta)}^{\cos^{-1}2\underline{x}/\underline{L} \cos\theta} \underline{n}_{\theta,\phi} \cos\phi \, d\phi \, d\theta \end{aligned} \quad (23a)$$

for  $\underline{L} > 2\underline{b}$  and for  $\underline{b} < \underline{L} < 2\underline{b}$  when  $\underline{x}$  is between  $\underline{b} - \underline{L}/2$  and  $\underline{b}/2$ , and

$$\underline{P} = \int_{-\cos^{-1}\underline{b}/\underline{L}}^{\cos^{-1}\underline{b}/\underline{L}} \int_{\cos^{-1}2\underline{x}/(2\underline{b} - \underline{L} \cos\theta)}^{\cos^{-1}2\underline{x}/\underline{L} \cos\theta} \underline{n}_{\theta,\phi} \cos\phi \, d\phi \, d\theta \quad (23b)$$

for  $\underline{b} < \underline{L} < 2\underline{b}$  when  $\underline{x}$  is between 0 and  $\underline{b} - \underline{L}/2$ .

If the fibers are randomly oriented as they approach the grid, this again reduces to just the ratio of the area on the spherical surface defined by Equation (22) to the area of the hemisphere. When this is substituted in Equation (17) and the integration is performed, the desired expression for  $\underline{P}_{-1}$  is obtained\*.

### The Effect of Fiber Orientation

In the previous analysis, random orientation of the fibers approaching the grid was assumed. This places a severe limitation on

\*See Appendix I, Page 78.

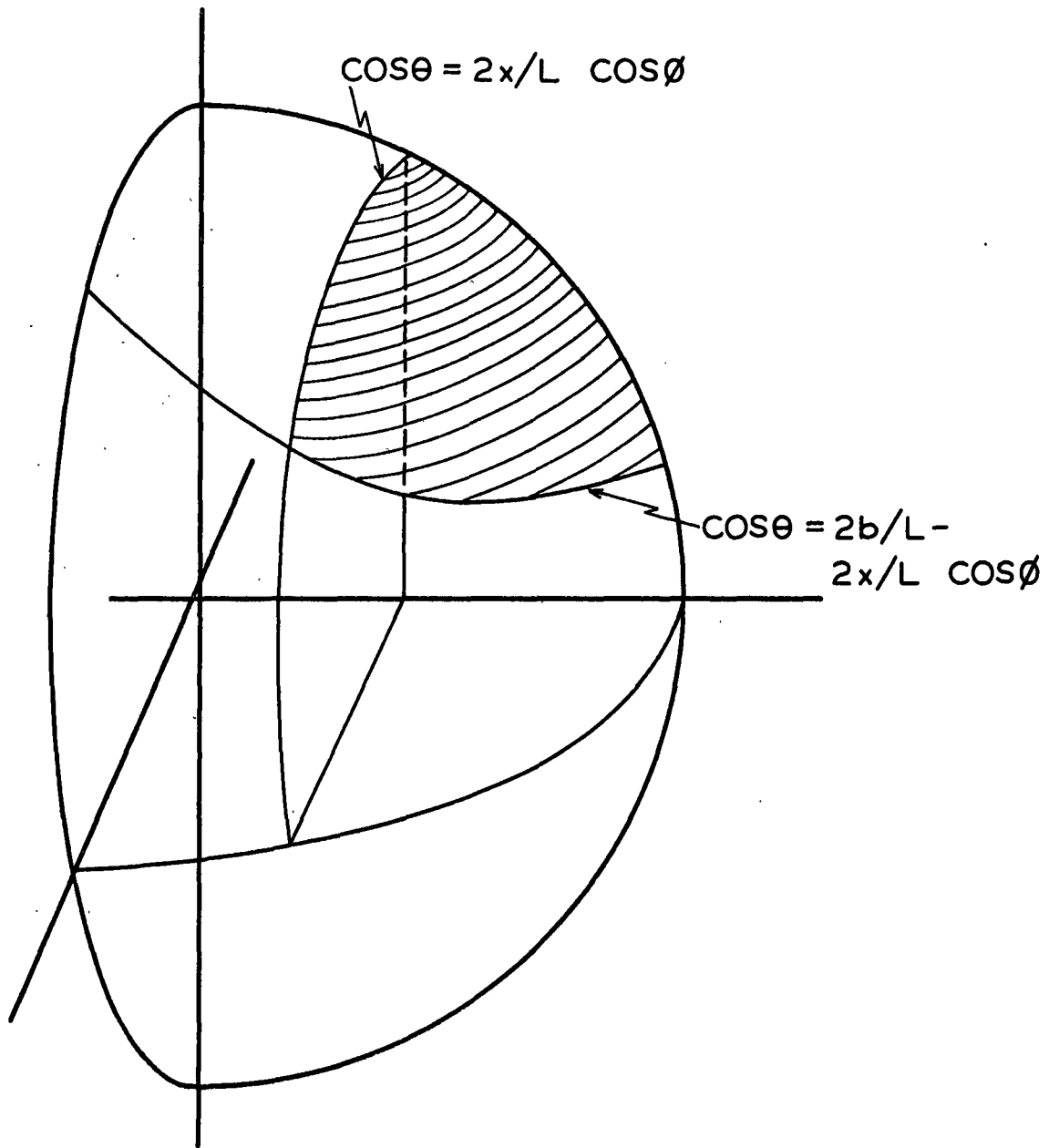


Figure 7. Representation of the Area Described by Equation (22) when  $\underline{b} < \underline{L} < 2\underline{b}$  and  $\underline{x}$  is Between 0 and  $\underline{b} - \underline{L}/2$

the relationships presented in the previous sections. The orientation function  $n_{\theta, \phi}$  will obviously be a major factor in determining the initial retention, and will be governed largely by the hydrodynamic field. In a turbulent field the assumption of random orientation is probably valid, but in a laminar shear field this would be a poor approximation for the fibers tend to show definite preferential orientations as has been shown by Mason (19).

Another distribution of orientations which is of interest is where all fibers approach the grid with  $\phi = 0$ , and are randomly oriented in the  $x$ - $y$  plane. The probability function reduces to:

$$\underline{P} = \int_{-\cos^{-1}2(\underline{b}-\underline{x})/\underline{L}}^{\cos^{-1}2(\underline{b}-\underline{x})/\underline{L}} (1/\pi) \underline{d}\theta \quad (24)$$

which when integrated and combined with Equation (17) yields:

$$\bar{P}_{\underline{i}} = (2/\pi) [\cos^{-1}(\underline{b}/\underline{L}) - 2\cos^{-1}(2\underline{b}/\underline{L}) - \sqrt{(\underline{b}/\underline{L})^2 - 1} + \sqrt{(\underline{b}/\underline{L})^2 - 4}] \quad (25a)$$

for  $\underline{L}/\underline{b} > 2$ , and

$$\bar{P}_{\underline{i}} = (2/\pi) \left[ \sqrt{(\underline{b}/\underline{L})^2 - 1} - \cos^{-1}(\underline{b}/\underline{L}) \right] \quad (25b)$$

for  $1 < \underline{L}/\underline{b} < 2$ . This relationship is also shown in Fig. 9.

#### RETENTION OF FIBERS BY A SQUARE-MESH GRID

The preceding sections have illustrated the procedure for predicting the initial rate of fiber retention by a simple parallel grid.

The same procedure can be applied to a square-mesh geometry, but the analysis is much more complicated due to the possibility of the fiber bridging across several combinations of the sides of the square. The analysis must be subdivided into a number of cases depending upon the value of  $\underline{L}/\underline{b}$ . Only the two limiting cases of  $\underline{L}/\underline{b} < 1$  and  $\underline{L}/\underline{b} > 2\sqrt{2}$  and one intermediate case will be considered here. Also, only the case of no friction between the fiber and grid will be considered. In this case the  $\underline{x}$ - $\underline{y}$  position of the fiber midpoint does not change as the fiber rotates after striking the grid.

For the square-mesh geometry, an octant\* of the square can be taken as the repeating unit for purposes of the analysis, and Equation (14) can be written as

$$\bar{P}_1 = (8/\underline{b}^2) \int_0^{\underline{b}/2} \int_0^{\underline{x}} \underline{P} \underline{dx} \underline{dy} \quad (26)$$

When the conditions necessary for retention are established,  $\underline{P}$  can again be evaluated by Equation (16) and values of  $\bar{P}_1$  and  $\alpha_0$  can be calculated.

For  $\underline{L}/\underline{b} < 1$

The only way a fiber whose length is less than  $\underline{b}$  can be retained is by bridging across the corner of the opening as in Fig. 8. If  $\phi$  is negative, the fiber must strike the wire along the  $\underline{x}$ -axis first, i.e.,  $(\underline{L}/2) \sin\theta \cos\phi > \underline{y}$ , and upon rotating to  $\phi = 0$  it must strike the

\* An octant of the square is defined here as one of the eight equal right isosceles triangles formed by the diagonal of the square and the perpendicular bisectors of the four sides.



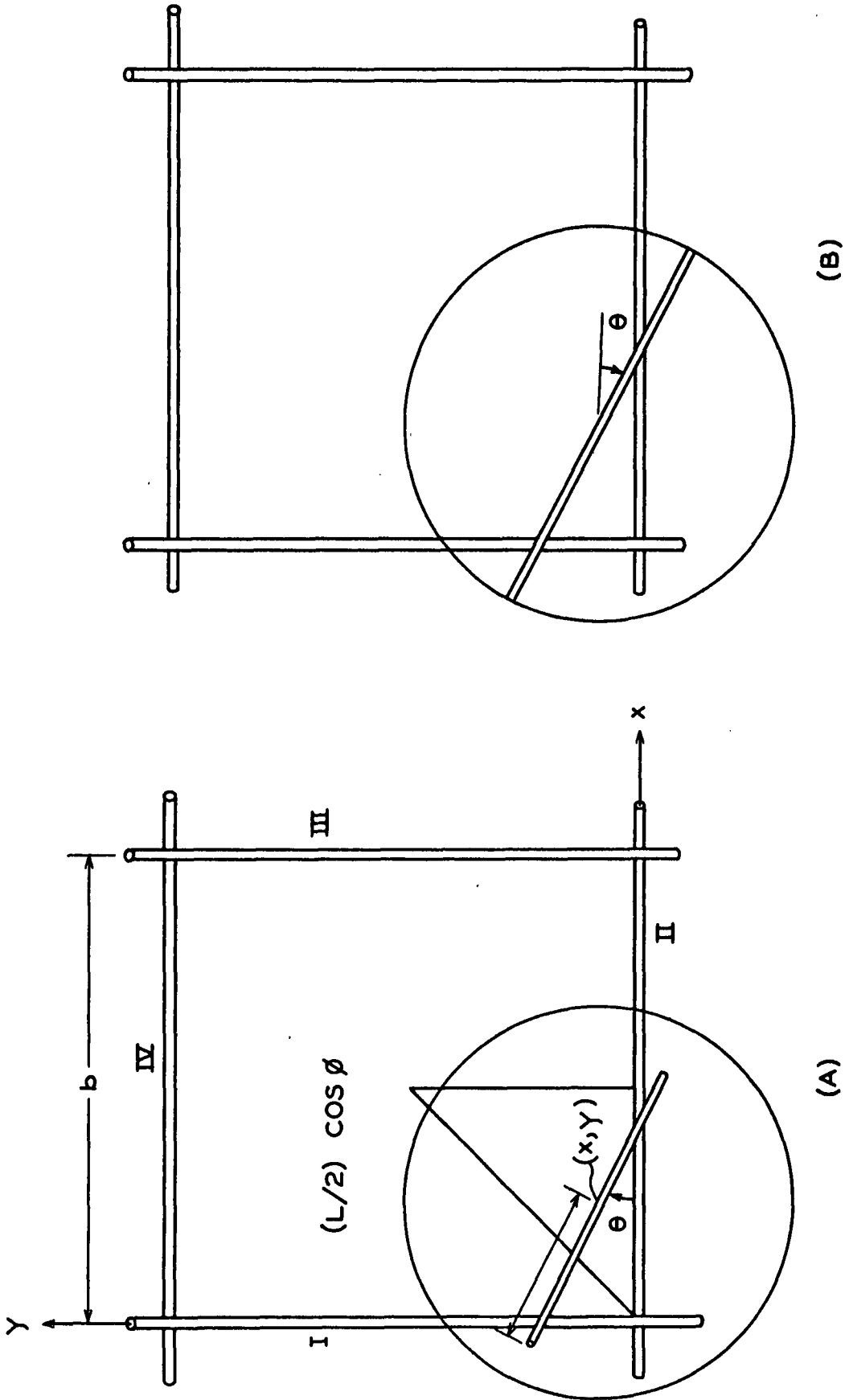


Figure 8. Projection of Fiber on Square-Mesh Grid for  $L/b < 1$   
(A) Before Striking the Grid  
(B) After Striking the Grid and Rotation to  $\phi = 0$

y-axis, i.e.,  $(L/2) > x/\cos\theta$ . If  $\phi$  is positive, it must first strike the y-axis,  $(L/2) \cos\theta \cos\phi > x$ , and upon rotation also strike the x-axis,  $(L/2) > y/\sin\theta$ . These conditions describe the solid angle in which the fiber must lie if it is to bridge across the corner of the opening and can be used to find the limits of integration when applying Equation (16) to evaluate the probability function. In this instance

$$\begin{aligned} \underline{P} = & \int_0^{\cos^{-1} 2x/(L^2 - 4y^2)^{1/2}} \int_{\sin^{-1} 2y/L}^{\cos^{-1} 2x/L \cos\phi} \underline{n}_{\theta, \phi} \cos\phi \, d\phi \, d\theta + \\ & \int_0^{\cos^{-1} 2y/(L^2 - 4x^2)^{1/2}} \int_{\sin^{-1} 2x/L}^{\cos^{-1} 2y/L \cos\phi} \underline{n}_{\theta, \phi} \cos\phi \, d\phi \, d\theta \end{aligned} \quad (27)$$

Of course this only applies to the region where the fiber is near enough to the corner to strike the sides of the square. This region is defined by  $x^2 + y^2 \leq L^2/4$ ; outside this region  $\underline{P}$  is equal to zero. Taking this into account, and using Equation (26), the desired relationship for randomly oriented fibers is found to be simply\*

$$\underline{\bar{P}}_1 = (1/8)(L/b)^2 \quad (28)$$

for  $L/b < 1$ .

For  $L/b > 2\sqrt{2}$

When the length of the fiber is greater than twice the length of the diagonal of the square opening, it is obvious that if it is in a

\*See Appendix I, Page 80.

position such that the lower half of the fiber will hit any side of the opening, its rotation will carry it into position to be retained. To simplify the determination of the probability function, a fiber approaching the point  $(\underline{x}, \underline{y})$  may be thought of as having its midpoint at the center of a sphere of diameter  $\underline{L}$ . The lower end of the fiber will occupy a point on the surface of the lower half of the sphere. If the projection of this point on the plane of the grid falls outside the square opening under consideration the fiber is in position to strike one of the sides and will be retained. If the projection falls inside the square, it is not in position to be intercepted. If the fibers approaching the grid are randomly oriented, the lower end of the fiber can occupy any point on the hemisphere with equal probability. The probability that the fiber will be retained is then the ratio of the surface of the portion of the hemisphere which projects outside the square opening to the total area of the hemisphere. When this is evaluated and used in conjunction with Equation (26), the relationship\* shown in Fig. 9 as the portion of Curve IV for  $\underline{L}/\underline{b} > 2\sqrt{2}$  is obtained.

For  $\underline{L}/\underline{b} = \sqrt{2}$

The two limiting portions of the relationship for the square-mesh geometry fairly well establish the nature of the relationship. However, one intermediate point will be calculated to better establish the relationship and to illustrate the method used. To establish the conditions necessary for bridging to take place, the octant of the square under consideration is broken down into seven parts as shown in

\* See Appendix I, Page 81.

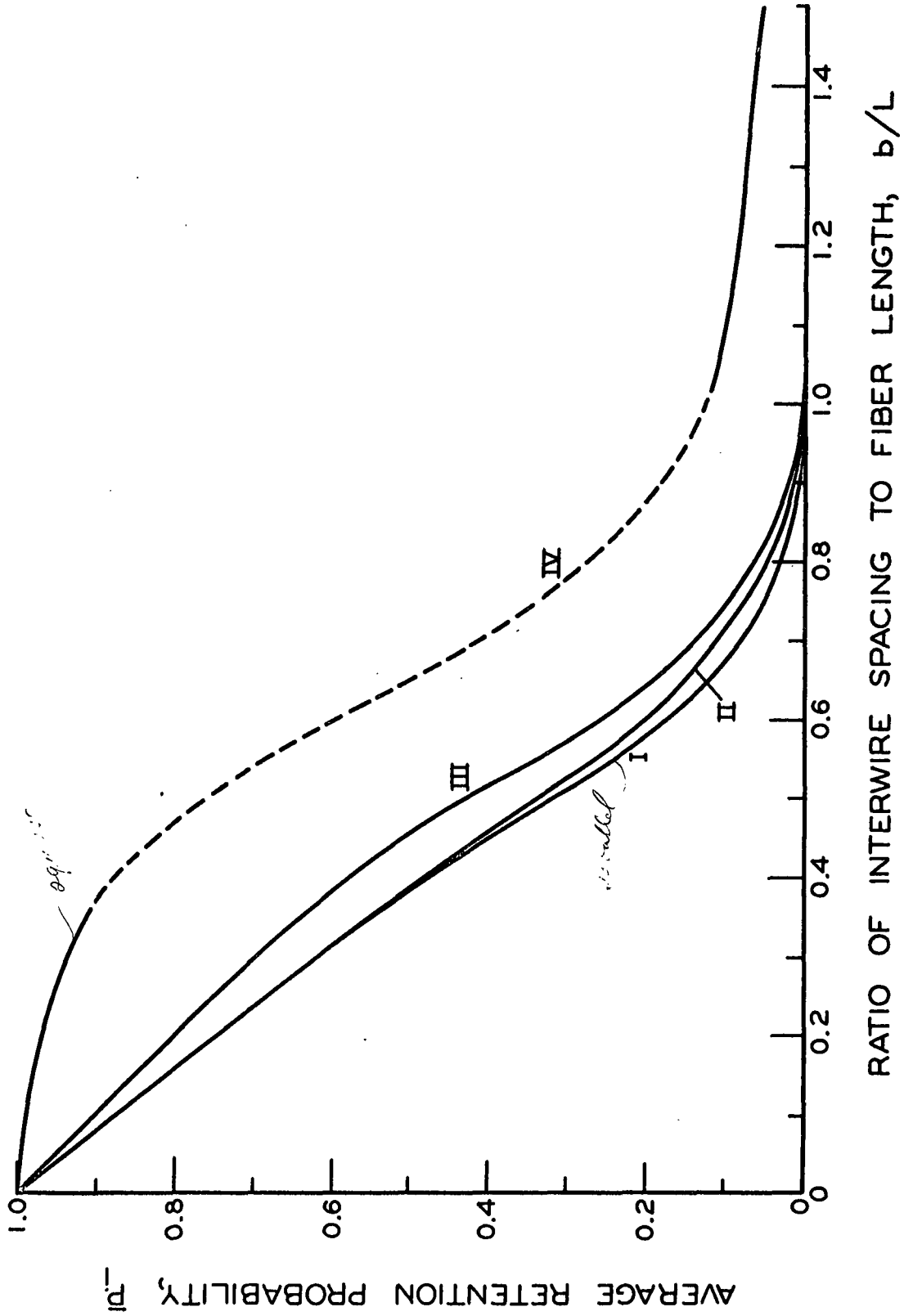


Figure 9. The Theoretical Relationships Between the Average Retention Probability and the Ratio of Interwire Spacing to Fiber Length

Fig. 21 (Appendix I). This is necessary since if a fiber approaches with its midpoint in area A, the only possible way of bridging is across sides I and II, while if it is in area B, it can bridge across sides I and II or I and III, and if it is in area C, it can bridge across I and II, I and III, or II and IV, and so forth for the other areas. Thus,  $\underline{P}$  is represented by a different function for each of these areas, and the integration indicated in Equation (26) must be carried out over these areas individually. The procedure is the same as before, but the details will be confined to the Appendix\*.

The relationships between  $\underline{\bar{P}}_i$  and  $\underline{b/L}$  for simple parallel and square-mesh grids as derived in the preceding sections are shown in Fig. 9. Evaluation of these relationships required numerical integrations which were performed using an IBM 610 computer. The curves shown in Fig. 9 represent the following conditions:

- Curve I. Parallel-mesh grid and randomly oriented fibers assuming no friction between the fibers and the wires composing the grid.
- Curve II. Parallel-mesh grid and randomly oriented fibers assuming no slippage between the fibers and the wires composing the grid.
- Curve III. Parallel-mesh grid and all approaching fibers oriented with their long axes parallel to the plane of the grid.
- Curve IV. Square-mesh grid and randomly oriented fibers assuming no friction between grid and fibers.

The solid portions of Curve IV represent the two limiting cases of  $\underline{L/b}$  which were analyzed, and the intermediate portion shown as the dashed line represents an interpolation guided by the intermediate calculated point for  $\underline{L/b} = \sqrt{2}$ .

\* See Appendix I, Page 84.

Within the limitations set forth, these curves should now predict the initial rate of retention of rigid fibers by such grids.

## EXPERIMENTAL

If the relationships derived in the previous section are proved valid within the limitations imposed, then it can be assumed that the method used is basically sound and can be used to predict the initial retention in more complex systems if the additional variables are properly taken into account in the derivation. The experimental portion of this work was designed for the purpose of establishing the validity of the derived relationships. This program consisted of developing a method of obtaining retention curves such as that illustrated in Fig. 1 under conditions ~~as~~ nearly the same as those imposed on the derived relationships, and using this method to obtain curves for different fiber length-grid combinations from which the initial slopes could be determined for comparison with the predicted values.

There are two possible methods for determining the desired retention curves. The first is by passing a fiber suspension through the grid and following continuously the buildup of a fiber deposit by recording the weight of fibers on the grid as a function of the total amount of fibers which have reached the grid. A possible method of doing this would be by continuously monitoring the fiber concentration both directly above and below the grid by some technique such as light scattering or a tracer method. The second alternative is to pass varying amounts of fibers onto the grid and each time collect and measure separately the amount of fibers collected and passed by the grid. In this manner the retention curve could be constructed by a number of

points each obtained from a separate run. The latter method was chosen for this study because it appeared to be more straightforward and to offer fewer experimental problems.

The experimental apparatus that was developed for this purpose is shown schematically in Fig. 10 and is described in detail in Appendix III. Briefly, it consisted of a flow tube C into which a grid could be inserted, a means for collecting separately the fibers retained by and passed by the grid, two tanks, a pump, and auxiliary piping, meters, etc. The over-all length of the flow tube was approximately seven feet. The tube and the grids were eight inches in diameter. A large diameter was chosen to reduce wall effects, to obtain a high Reynolds number at low linear flow velocities, and to increase the accuracy in weighing the fibers retained and passed by the grid. This last reason was very important since deposits of very small mass per unit area were of particular interest in this study.

To simulate as nearly as possible the conditions imposed upon the derived relationships, grids made of very small diameter wire and essentially rigid 15-denier nylon fibers were used. The fibers were cut to relatively narrow length ranges, and samples with average lengths of 1.8, 2.1, 2.6, 3.4, and 4.9 mm. were used. Parallel-mesh grids with interwire spacings of 0.05 and 0.07 inch and square-mesh grids with spacings of 0.07 and 0.10 inch were used. The fiber suspensions were of such low concentrations that each fiber acted essentially independently. The flow rate in the flow tube (2.2 cm./sec. average linear velocity) was sufficiently high to insure turbulent flow which would tend to keep the

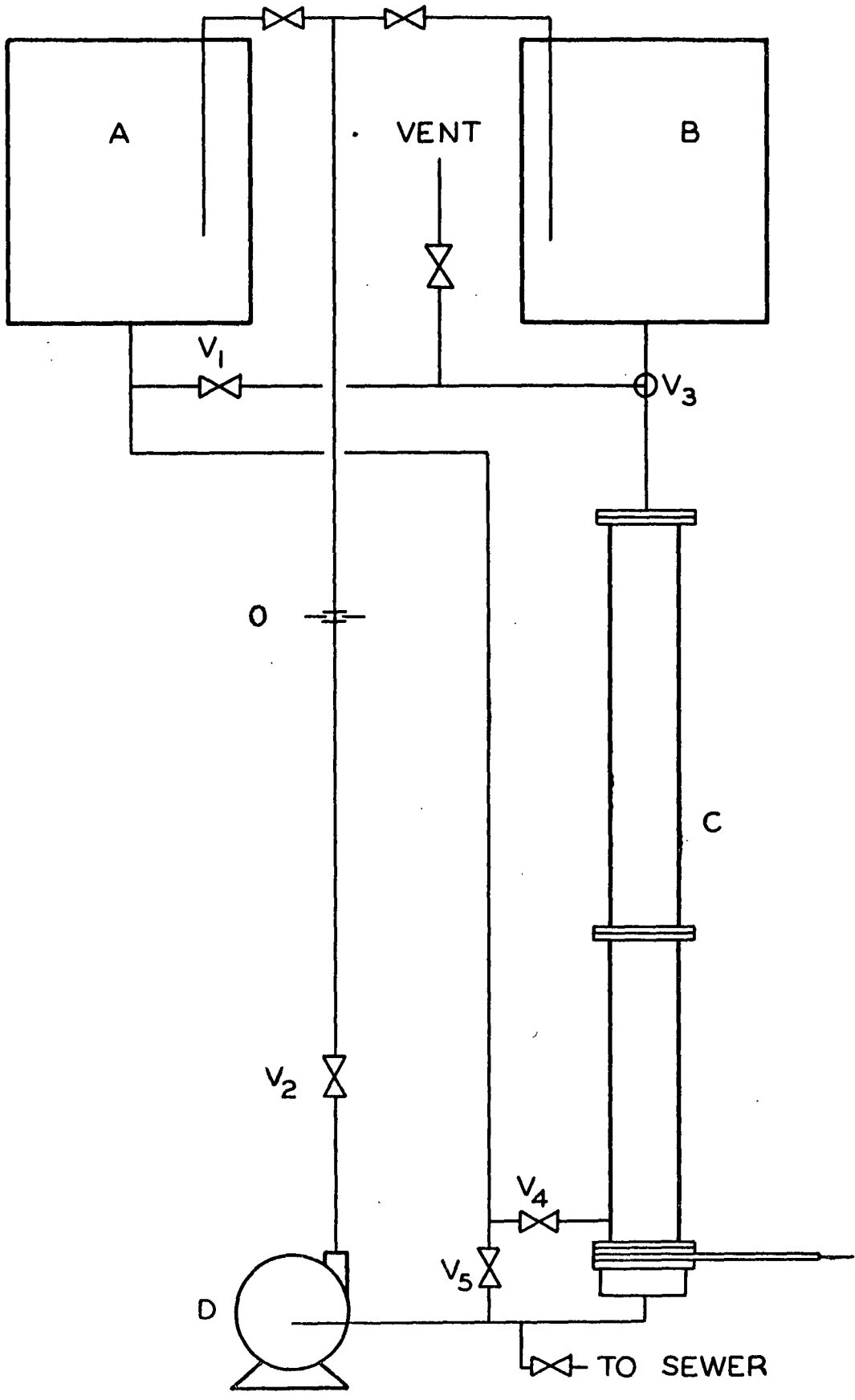


Figure 10. Schematic Diagram of Apparatus

fibers randomly oriented as they approached the grid but low enough so that the fluid drag forces would not appreciably deform the grid or the deposited fibers.

The procedure for making runs is also described in detail in Appendix III. Briefly, the procedure consisted of establishing the desired flow rate in the flow tube with clear water, introducing the desired amount of fiber suspension into the top of the tube, and then shifting back to clear water to maintain a constant flow rate until all the fibers had reached the grid. The tube was then drained, and the fibers intercepted by the grid were collected, dried, and weighed. Those passing through the grid were collected on a tared nylon filter cloth below the grid and also dried and weighed.

It was felt that certain of the operating variables which were not taken into account by the derived relationships might affect the experimentally determined retention curves. Special series of runs were made to determine the effects of flow rate, fiber concentration, time of permeation of the fiber deposit by water after it was formed, and the diameter of the wire used in constructing the grids. As is shown in Appendix III, none of these were found to have an appreciable effect on the retention curves within the ranges of the variables that were studied.

## RESULTS AND DISCUSSION

### INITIAL RETENTION

The experimental retention data are presented in the form of retention curves in Fig. 11-14 and in tabular form in Appendix IV. The curves are of the expected shape, the slope having a finite initial value and increasing to a value of unity as the deposit is formed.

For this study, the primary interest in the data is centered about the initial slopes of the retention curves. It can be shown that the initial slope is equal to the limiting value of the ratio  $\frac{W_r}{W_t}$  as  $W_r$  approaches zero. If the retention data are plotted as  $\frac{W_r}{W_t}$  versus  $W_r$ , then the value of  $\frac{W_r}{W_t}$  extrapolated to  $W_r = 0$  is the initial slope of the curve. This was the method used for determining the initial slopes of all the retention curves. The plots used for this purpose are shown in Appendix V.

The initial retention values obtained by this technique are shown as functions of  $b/L$  in Fig. 15 for both parallel- and square-mesh data. Since the samples of fibers used had narrow fiber-length distributions, the initial slopes of the experimental retention curves can be compared directly with the theoretical values of  $\bar{P}_1$  presented in Fig. 9. Thus, the theoretical curves of Fig. 9 are also shown in Fig. 15 for comparison with the experimental results.

Within the limits of experimental error, the predicted curves fit the data very well. Due to inaccuracies in the extrapolation technique, the precision of the data is not good enough to determine which

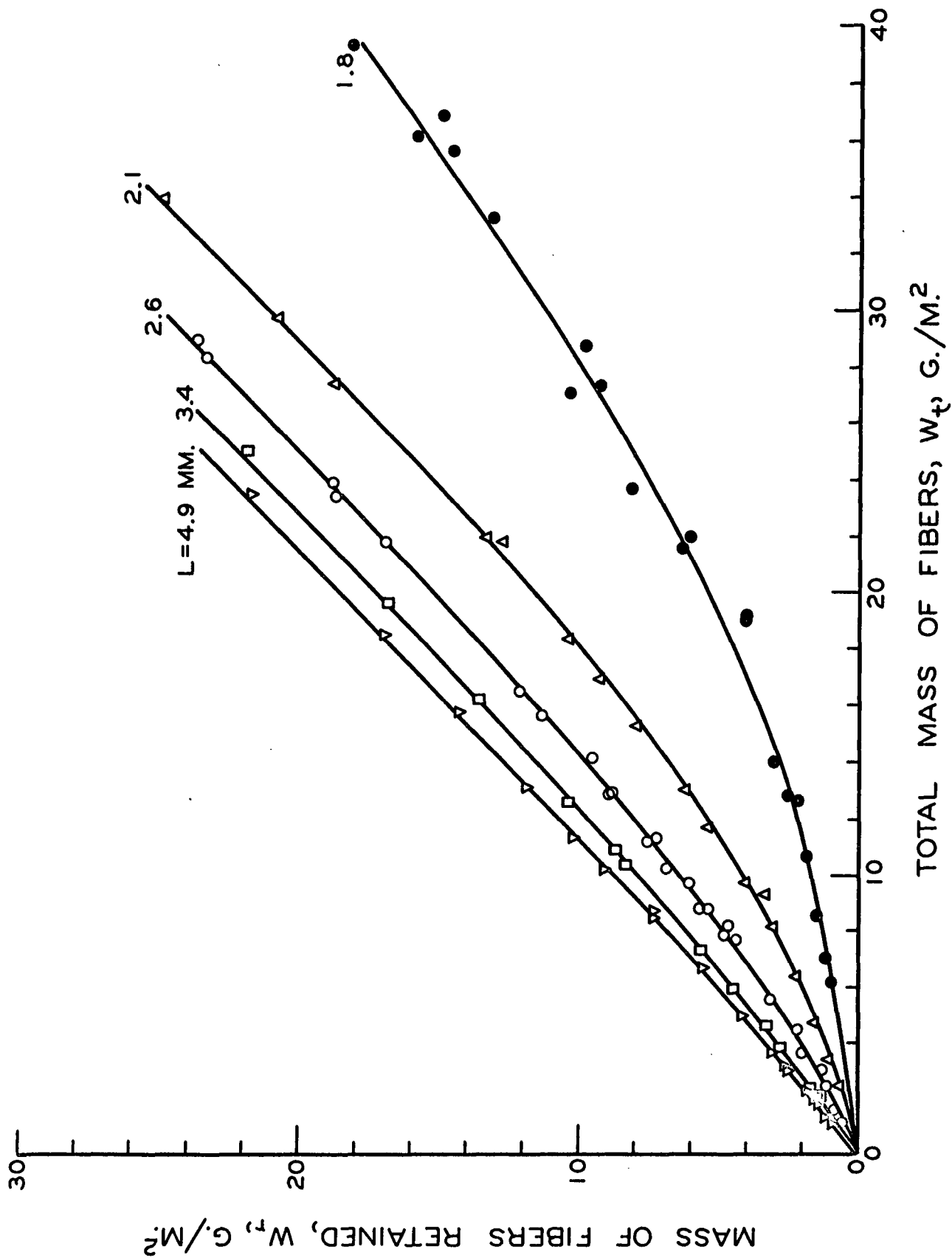


Figure 11. Retention Curves for Parallel-Mesh Grid,  $b = 0.05$  in.  $\approx 1.3$  mm

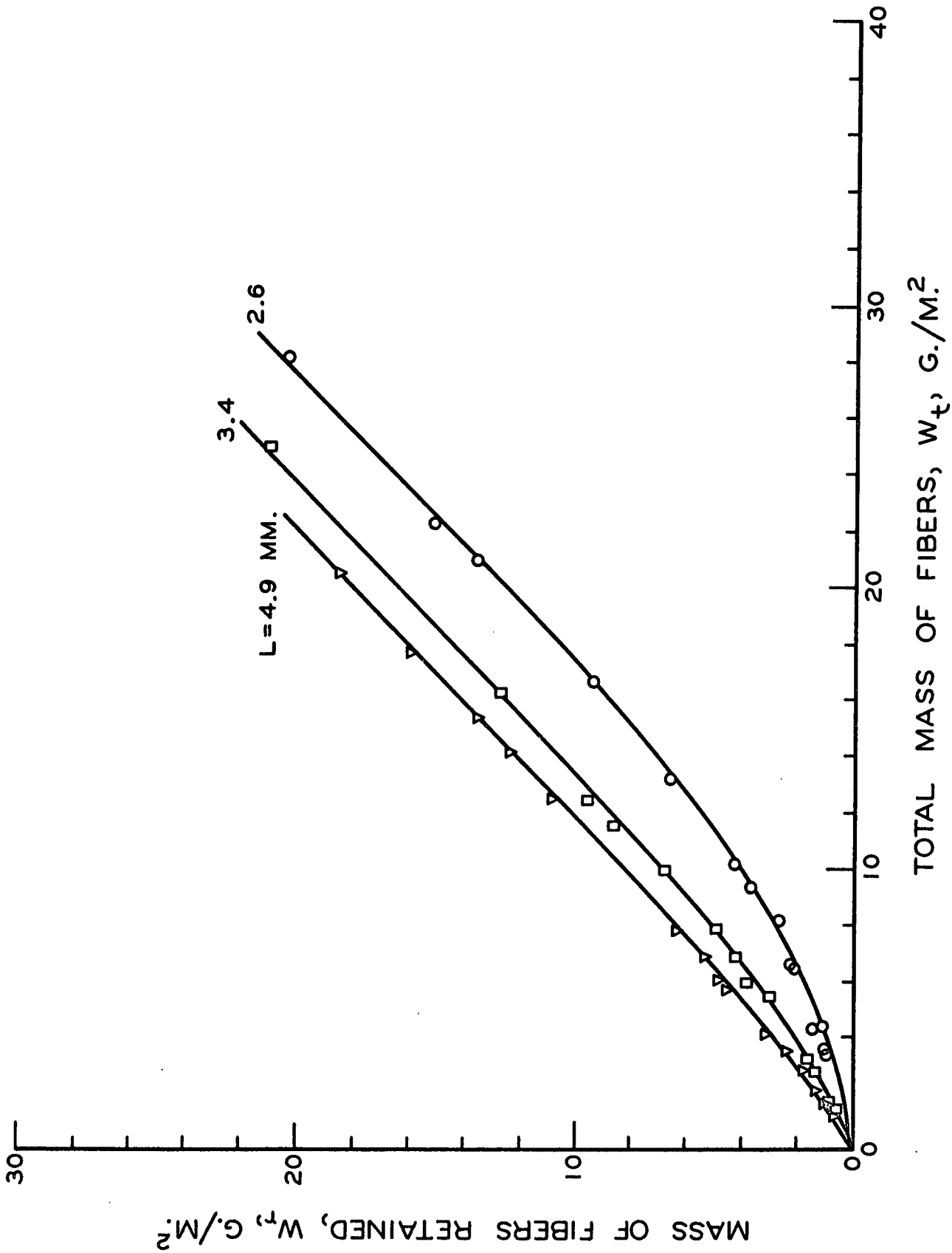
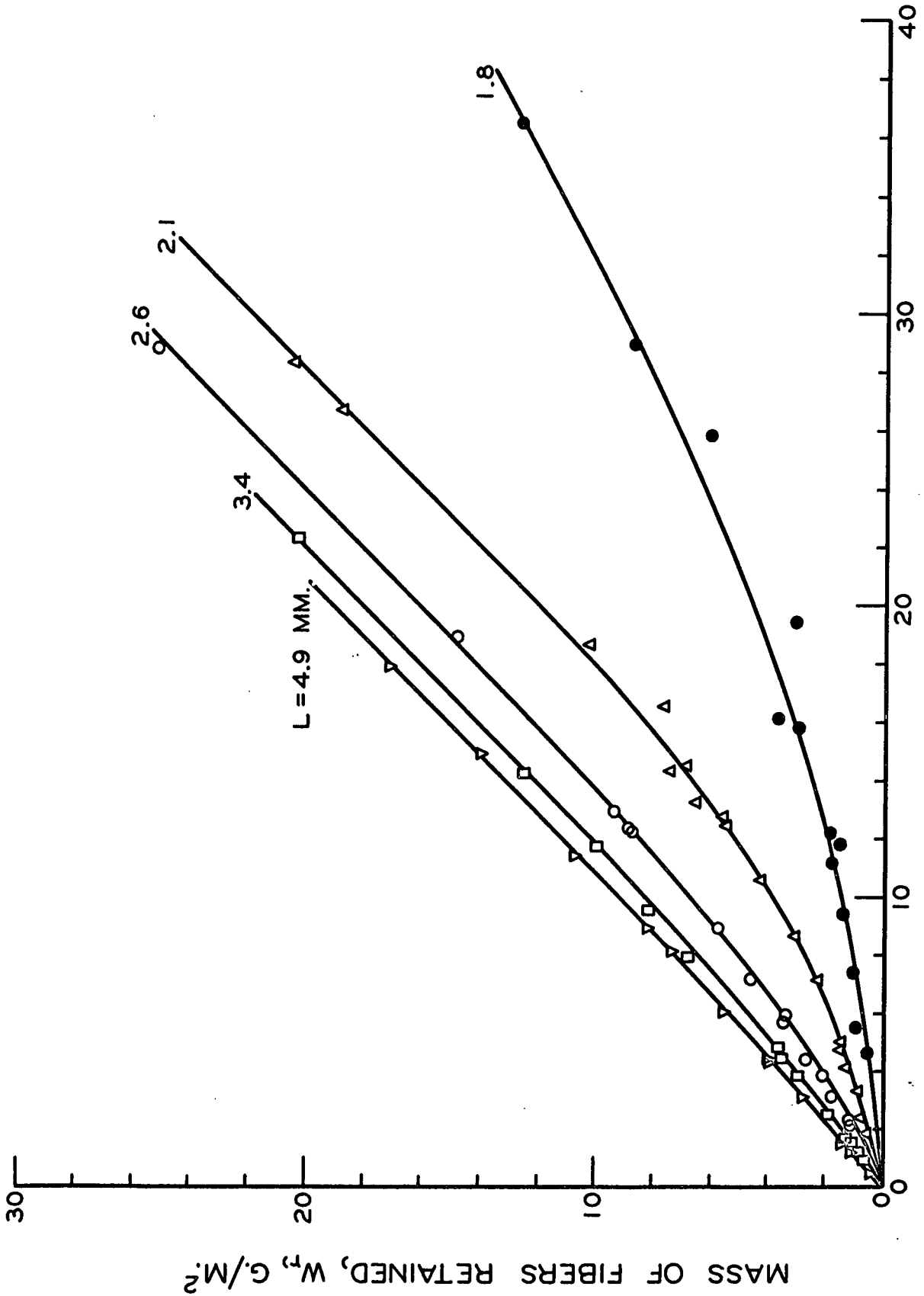
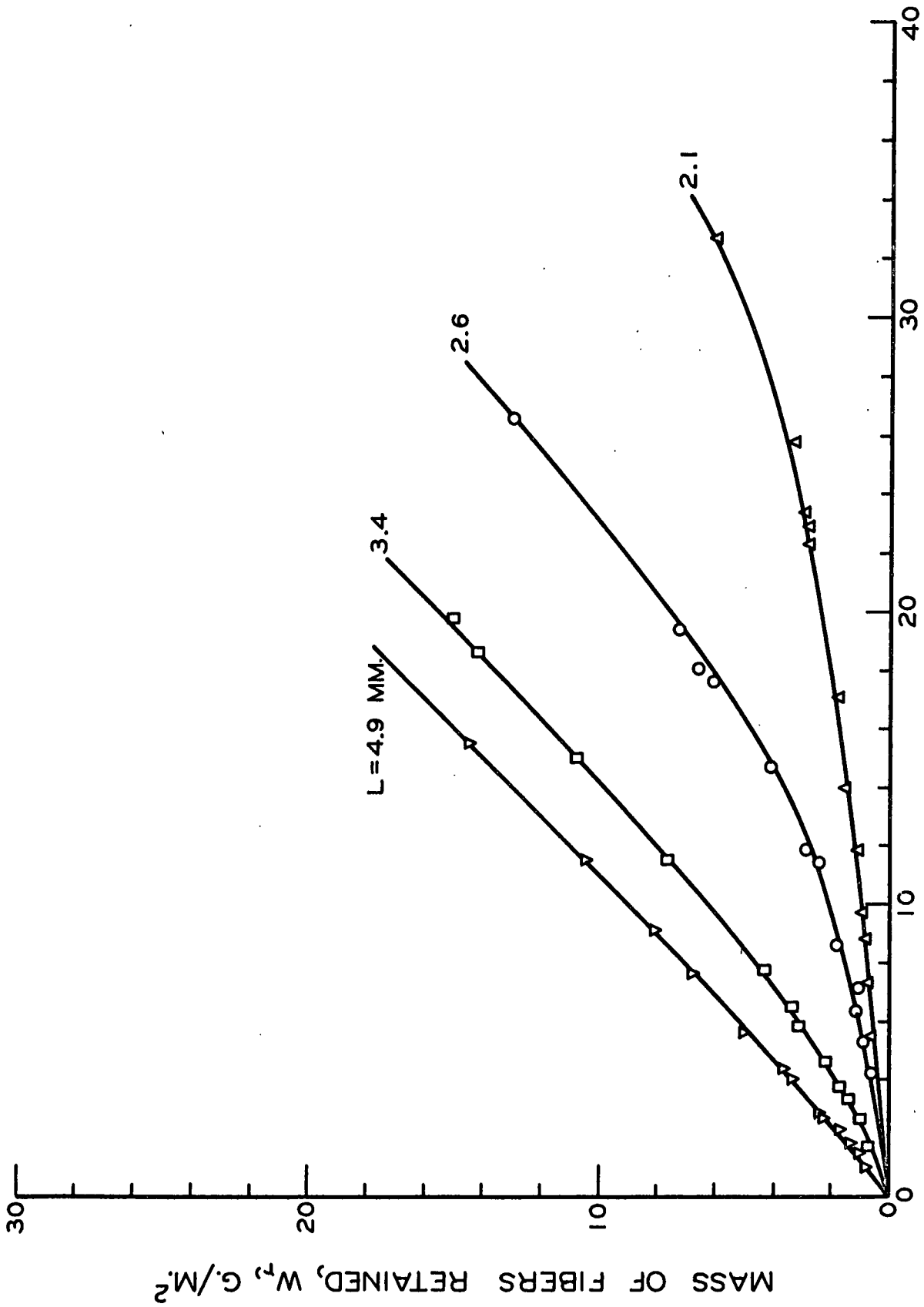


Figure 12. Retention Curves for Parallel-Mesh Grid,  $b = 0.07$  in.



TOTAL MASS OF FIBERS,  $w_t$ , G./M.<sup>2</sup>

Figure 13. Retention Curves for Square-Mesh Grid,  $\beta = 0.07$  in.



TOTAL MASS OF FIBERS,  $W_t$ , G./M.<sup>2</sup>

Figure 14. Retention Curves for Square-Mesh Grid,  $b = 0.10$  in.

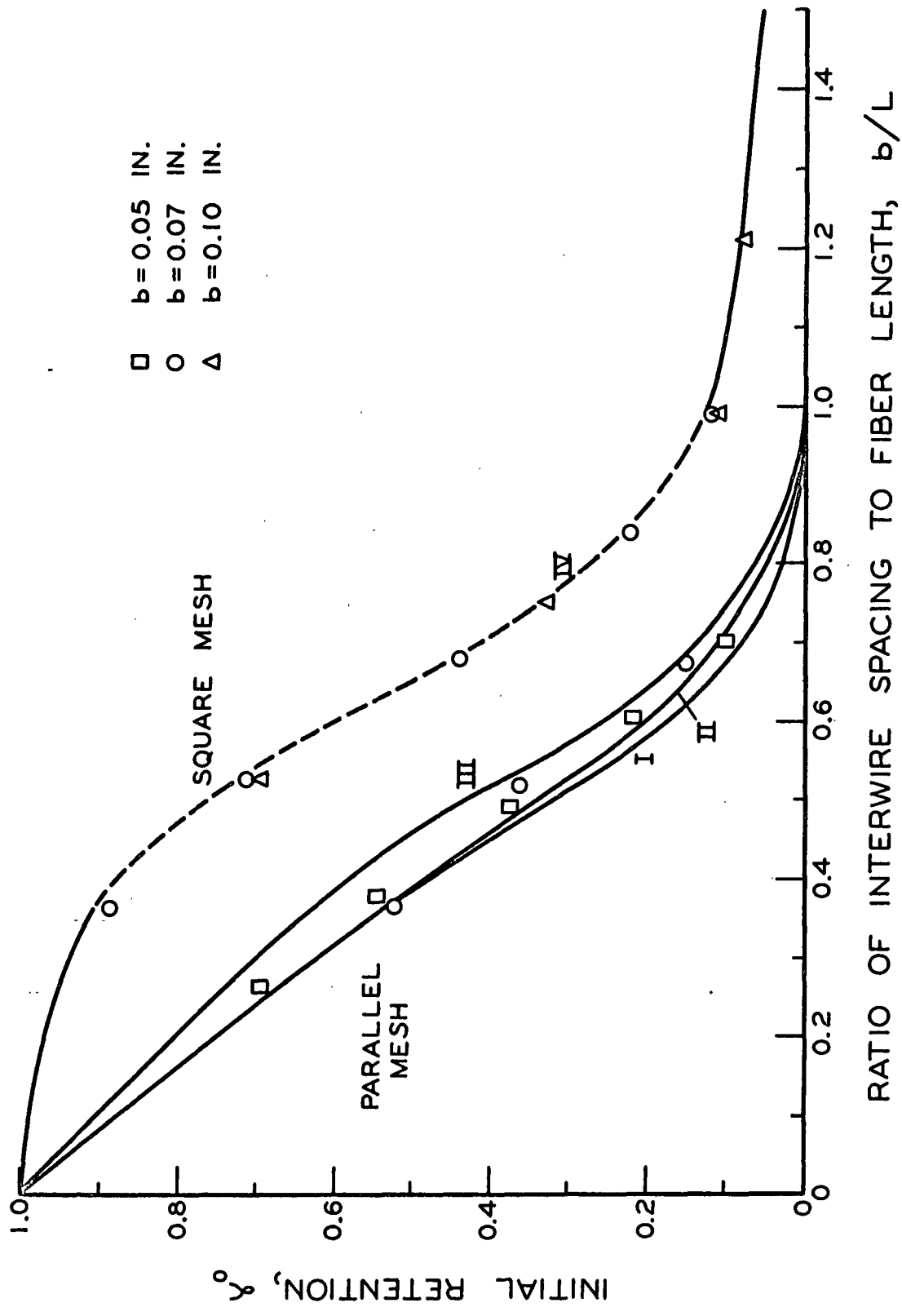


Figure 15. Comparison of Experimental Results with the Predicted Relationships

of the curves for parallel grids would better fit the data. Curve III, derived assuming the extreme case of  $\phi = 0$  fiber orientation, represents an upper limit of the values which would be expected for the experimental system used in this work. All of the points for parallel grids fall well below this curve as would be expected in view of the results of the direct measurements of angular orientations (Appendix III). The indications are that Curve II might give the best agreement at the higher values of  $\underline{b}/\underline{L}$  where Curves I and II deviate most, but this must be considered a mere speculation in view of the precision of the experimental results.

For the square-mesh grids, the extrapolation procedure for determining the initial slope is subject to less error than for the parallel grids as will be discussed later. The experimental values of the initial slopes are in good agreement with the predicted relationship for square-mesh grids, and fill in nicely the interpolated portion of the curve. Therefore, it can be concluded that the predicted relationships do represent the effect of relative fiber length on the initial retention of rigid individual fibers by simple parallel and square-mesh grids. More important, however, is the fact that the method used for predicting this effect has been substantiated as a valid approach to the general problem of fiber retention by grids.

It should be recognized that the parallel- and square-mesh geometries are the two extreme cases of the general rectangular geometry. Thus, if  $\underline{b}$  is the short dimension and  $\underline{a}$  the long dimension of the rectangle, the relationship between initial retention and  $\underline{b}/\underline{L}$  for any

rectangular mesh grid should lie between those for parallel- and square-mesh grids with a as the parameter.

The initial retention relationships are important both to the process of retention of fibers during the formation of a deposit during filtration and to the process of screening of fibers. The importance to filtration of fiber slurries has been discussed in an earlier section. It was pointed out that the initial rate of retention was very important in describing the formation of a fiber deposit, but much more would have to be known to completely describe the process. In the classification of fibers by screening, no deposit is allowed to form, and the initial retention relationship would be expected to apply during the entire process.

Some interesting observations can be made from the curves of Fig. 15 concerning the efficiency of the grid in either idealized filtration or screening operations. For instance, one might ask whether a parallel or elongated rectangular geometry would be more efficient than a square-mesh geometry for initially retaining fibers of a given length. If the length of wire per unit area of grid surface is used as a basis for comparison, then the initial retention of a square-mesh grid at  $\underline{b}/\underline{L} = 0.4$  must be compared with that of a parallel grid at  $\underline{b}/\underline{L} = 0.2$ , and a square grid at  $\underline{b}/\underline{L} = 0.8$  would be compared with a parallel grid at  $\underline{b}/\underline{L} = 0.4$ , etc. Such a comparison also may be considered as being on the basis of equal hydraulic radii for the simple grids where the diameter of the wire is small. For the two numerical examples mentioned, Fig. 15 shows that the square-mesh grid has a higher rate of initial retention in the first case, while in the latter the parallel grid is more efficient.

Analyzing the relationships over the entire range of  $b/L$  values shows that the square grid is a much more efficient screening or classifying medium, retaining a larger proportion of longer fibers and passing a greater portion of short ones than the parallel grid. This is more readily evident if, for the comparison, the initial retention is shown as a function of  $L/b'$  where  $b'$  is an equivalent dimension of the openings in the grid defined by

$$b' = \frac{ab}{(a + b)}$$

This is similar to the hydraulic radius concept often used in fluid mechanics. This method of comparison is shown in Fig. 16; now each point on the abscissa represents the same fiber length for both geometries. Obviously, the most efficient classifying medium is the one which gives the sharpest rate of change of initial slope with changes in fiber length. Thus, it can be concluded that a square mesh is theoretically the most efficient form of a rectangular-mesh grid for classifying fibers according to length.

The area where the most immediate use of the average retention probability or initial retention relationships might be expected to be made is in the field of screening and fiber classification. The present work illustrates the procedure for calculating the theoretical probability relationships required by the theories of Steenberg and Kubat (14-16) and Andersson and Bartok (17). The "permeabilities" experimentally determined by Andersson and Bartok offer the only data that have been found in the literature which can be compared with the present work. Their data, which were obtained using stiff rayon fibers and a 28-mesh screen in a modified

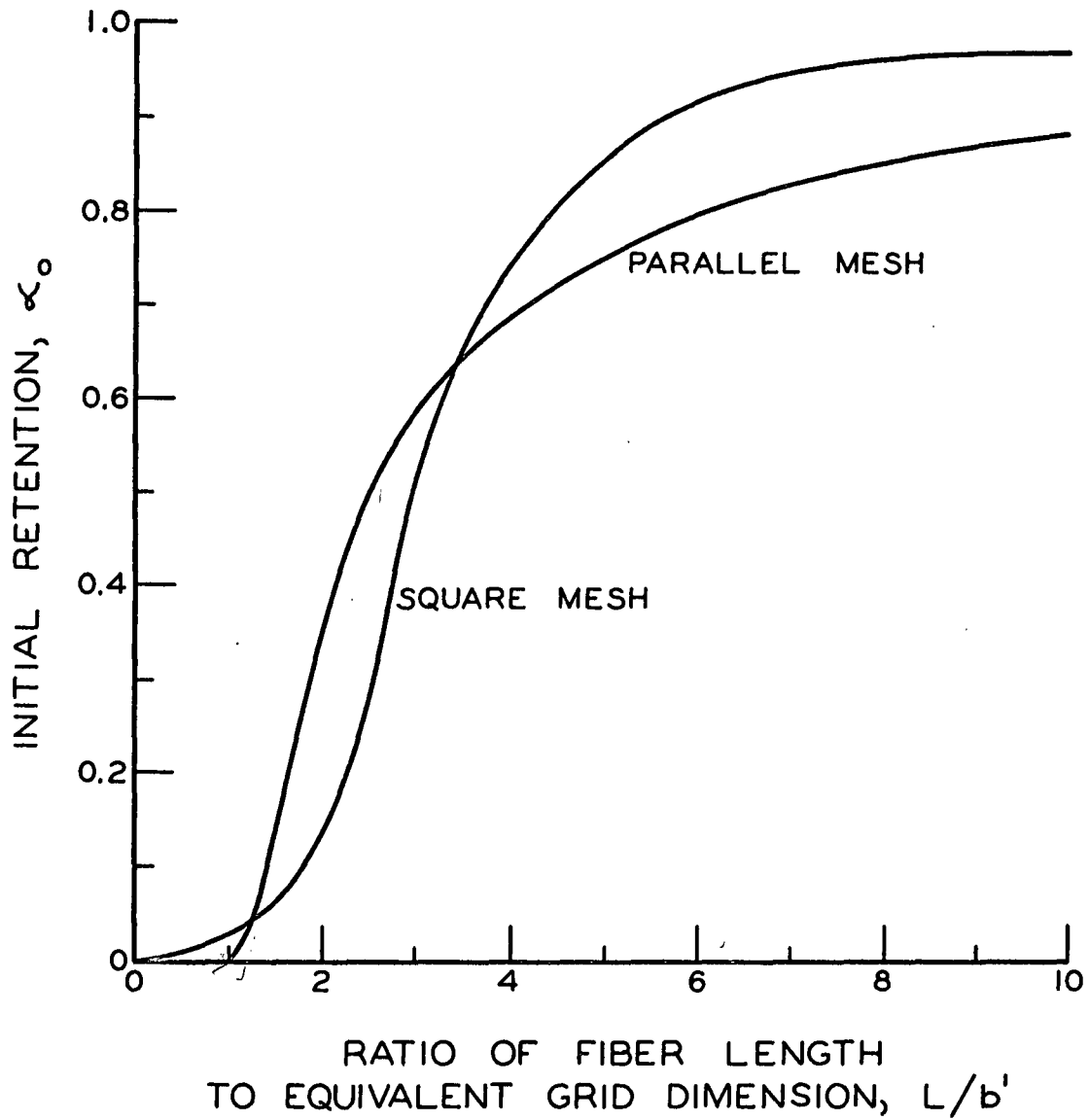


Figure 16. Comparison of Initial Retention of Parallel and Square-Mesh Grids Using the Equivalent Dimension  $b'$

Bauer-McNett classifier, is shown in Fig. 17. The diameter of the wires in a standard 28-mesh screen is certainly not negligible in comparison to the interwire spacing as was assumed in the theoretical development of this study. Therefore, their data has been plotted assuming  $\underline{b} = 0.0232$  inch, the dimension of the opening in a standard 28-mesh screen, rather than the actual distance between individual wire centers which is 0.0357 inch. Considering that Andersson and Bartok used an entirely different method of obtaining their results and that their conditions were far from ideal, their results are in remarkable agreement with the theoretical relationship and the experimental results of this study. This agreement suggests that the effect of wire diameter on initial retention can be taken into account by a rather simple means.

The compartments of a Bauer-McNett classifier were designed to present the fibers at the screen openings with their long axes parallel to the plane of the screen. If this is achieved by the design, then the distribution of fiber orientations might be expected to approach that assumed in deriving Equation (25) for parallel grids. An analogous relation can be derived for square-mesh grids. It is obvious that if all the fibers approach the grid with  $\phi = 0$ ,  $\bar{P}_i$  must be unity for  $\underline{b}/\underline{L} < 1/2\sqrt{2}$ , and it can be shown easily that for  $\underline{b}/\underline{L} > 1$ ,  $\bar{P}_i = 1/4(\underline{L}/\underline{b})^2$ . This relationship is shown in Fig. 17 as the dashed line, the locus of the intermediate portion of the curve only being estimated. This curve would be expected to represent an upper limit for the retention relationship for individual rigid fibers in a Bauer-McNett classifier. Owing to the large amount of turbulence in a Bauer-McNett compartment, it is highly unlikely that the  $\phi = 0$  orientation is achieved, and it is felt that the

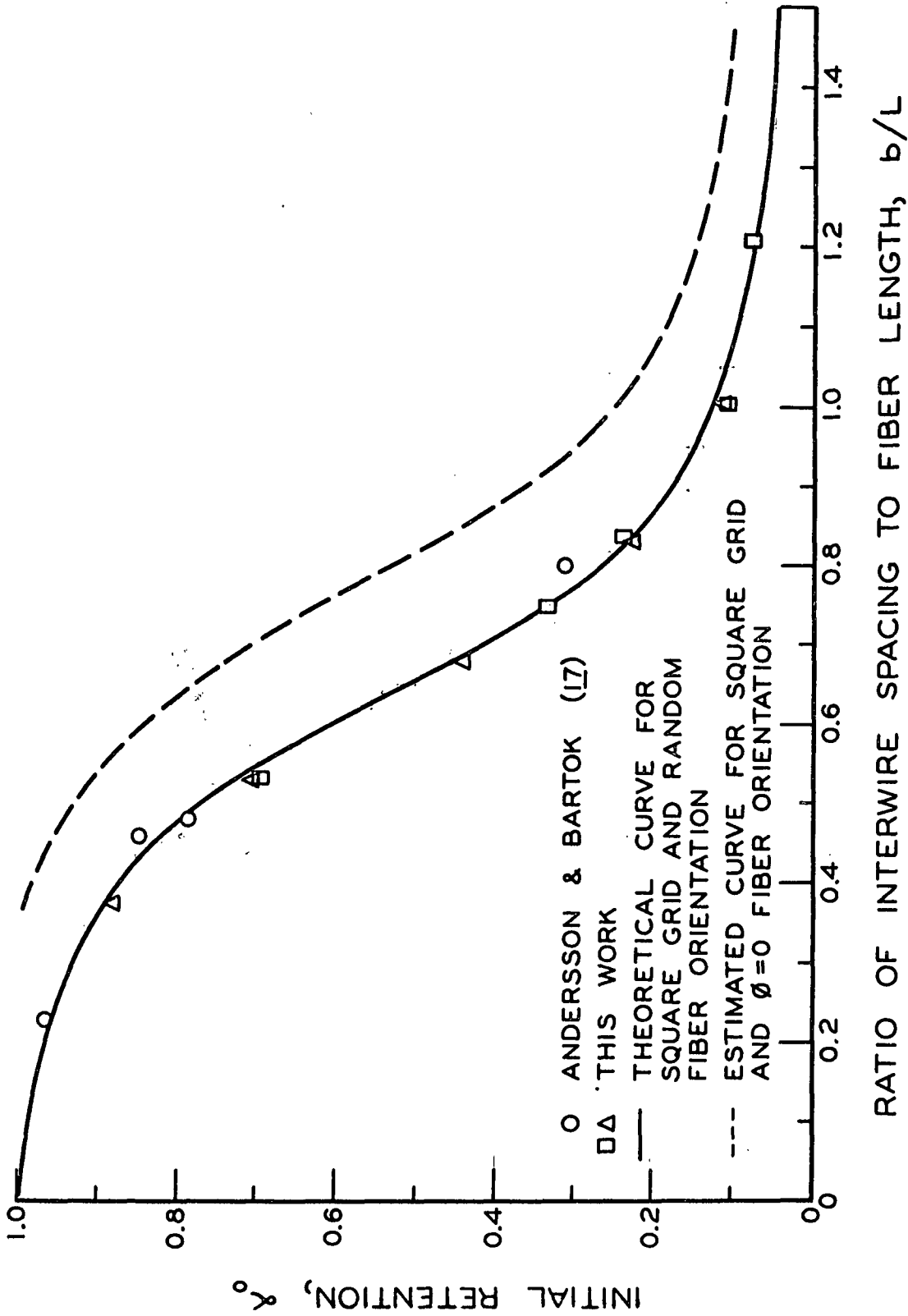


Figure 17. Comparison of the Results of Andersson and Bartok with the Present Work

random orientation would be a better approximation to the real situation. This belief is strongly supported by the data of Andersson and Bartok. Although the agreement of this Bauer-McNett data with the theoretical relationship could be only coincidental, it is felt that this is highly unlikely. The excellent agreement over a rather wide range of fiber lengths suggests very strongly that the theoretical relationship derived here can be applied directly to the screen analysis of rigid individual fibers in the Bauer-McNett and other classifiers.

#### SUBSEQUENT RETENTION

In the process of obtaining the initial retention data by the extrapolation technique, a considerable portion of the retention curve was experimentally defined for each fiber length-grid combination. While it was not an objective of this work to study the entire retention curve, several worthwhile observations can be made concerning the subsequent buildup of a fiber deposit after the first fibers strike the grid.

The ultimate goal in the study of fiber retention would be to obtain a theoretical expression which would completely describe the retention curve for any fiber-grid system. Even for an ideal system such as the ones considered in this work, the expression would be very complex. As was suggested in a previous section, this would require a knowledge of how the geometry of the openings changes with the deposition of fibers and how this affects the retention probability. The description of the changing geometry will be very difficult because the fiber deposit is not formed uniformly over the entire area of the grid. Where several fibers are initially deposited close together, the probability

that succeeding fibers will be retained in that area is much greater than for the areas of the grid where there are still no fibers. This results in a spotty formation with definite open areas in the deposit as can be seen in the photographs in Appendix VI. The degree of this nonuniformity is a function of the relative fiber length, the deposit being extremely nonuniform for relatively short fibers. One of the effects of this situation is immediately obvious in the retention curves. If the deposit was formed uniformly over the grid area, it would be expected that the point where the slope of the retention curve becomes unity would occur at about the same value of  $\frac{W}{r}$  for all the curves obtained with any one grid. As can be seen in Fig. 11-14, this is not the case, and the deviation is greatest at short fiber lengths. Any expression describing the entire retention curve must take this into account.

An important quantity that can be measured from the retention curve is  $\underline{W}_T$ , the total amount of fibers passed by the grid before the openings are effectively closed. As has been pointed out, this is equivalent to the intercept of the straight-line portion of the curve if it is extended to  $\underline{W}_r = 0$ . In filtration operations, this is a better criterion of grid efficiency than is initial retention. The efficiency of the two grid geometries studied can be compared with respect to the total amount of fibers passed in a manner similar to that used earlier for comparing initial-retention rates. If the same basis of comparison is used as before, i.e., equal length of wire per unit area of grid surface, the parallel grid with  $\underline{b} = 0.05$  in. can be directly compared with the square grid having  $\underline{b} = 0.10$  in. Comparing the values of  $\underline{W}_T$  at a

given fiberlength shows that the square grid passes much more material than does the parallel grid up to a value of  $L/b'$  equal to about 3.5. This is illustrated graphically in Fig. 18. The relationship here parallels very closely the comparison of initial retentions of Fig. 16 and indicates that initial retention is a valid measurement of the efficiency of a grid with respect to retaining fibers in a separation by filtration. From the comparisons of Fig. 16 and 18 it can be concluded that in constructing a grid for removal of fibers in filtration-type operations, the most efficient use of the wire is made when the openings have a parallel or elongated rectangular shape if the fibers are not longer than 3.5 times the equivalent dimension  $b'$ . Since very few fibers longer than this are passed by either grid geometry the parallel geometry might be thought to be the most efficient, but the final decision will depend on the fiber-length distribution of the suspension being filtered. It should be noted that the two curves in Fig. 18 must intersect at some point in the low fiber-length range. The parallel grid can retain no fibers for  $L/b' < 1$  and so the curve must approach this value asymptotically. The ideal square-mesh grid is not so limited because very short fibers can bridge across the corners of the openings. This is also the reason for the lower intersection of the curves in Fig. 16. For woven screens this bridging across corners would not be expected to be of great importance, and these intersections of the curves would not occur, or at least would be of little significance.

For each of the two grid geometries studied, two interwire spacings were used. The different values of  $b$  were shown to have no

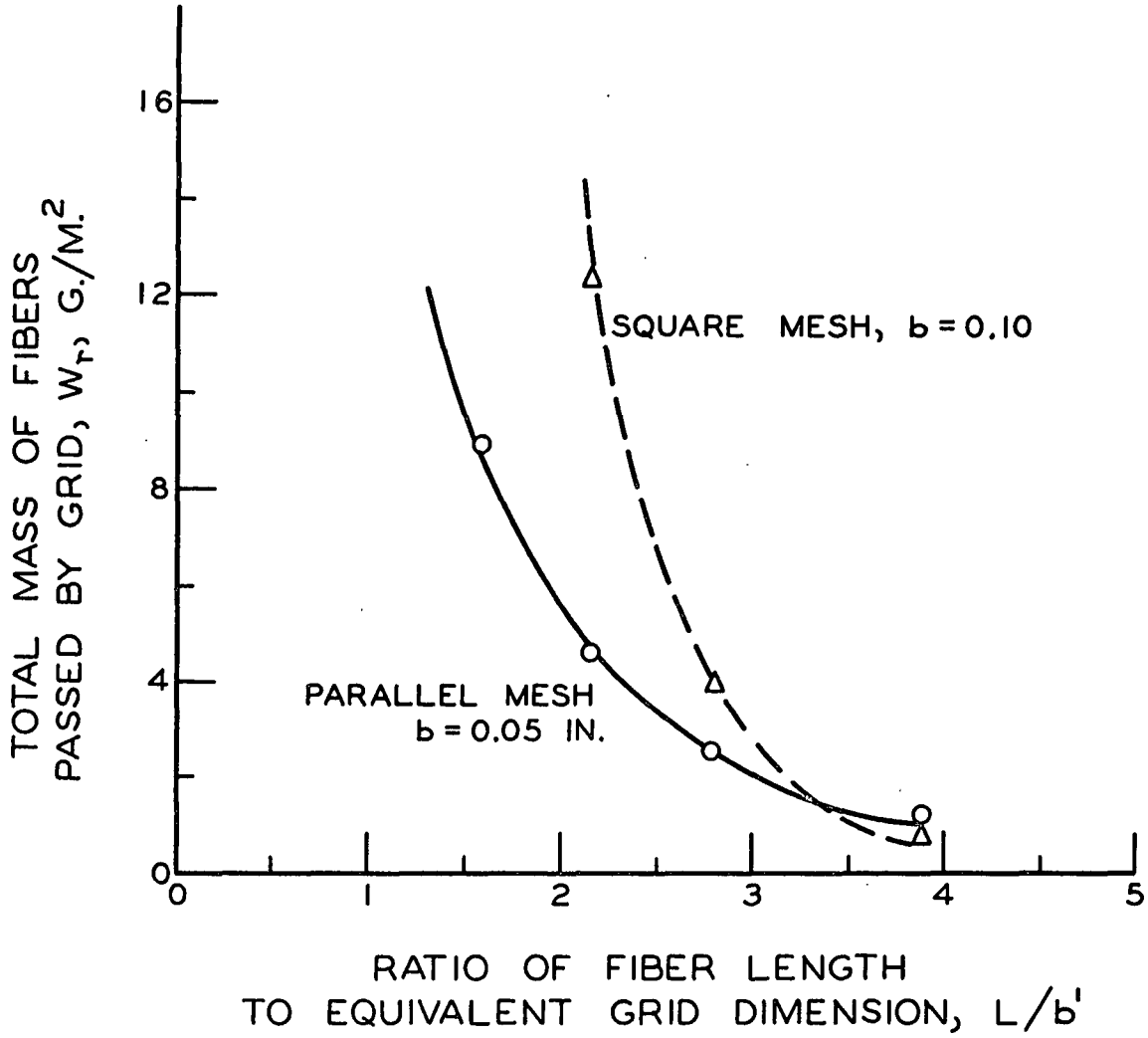


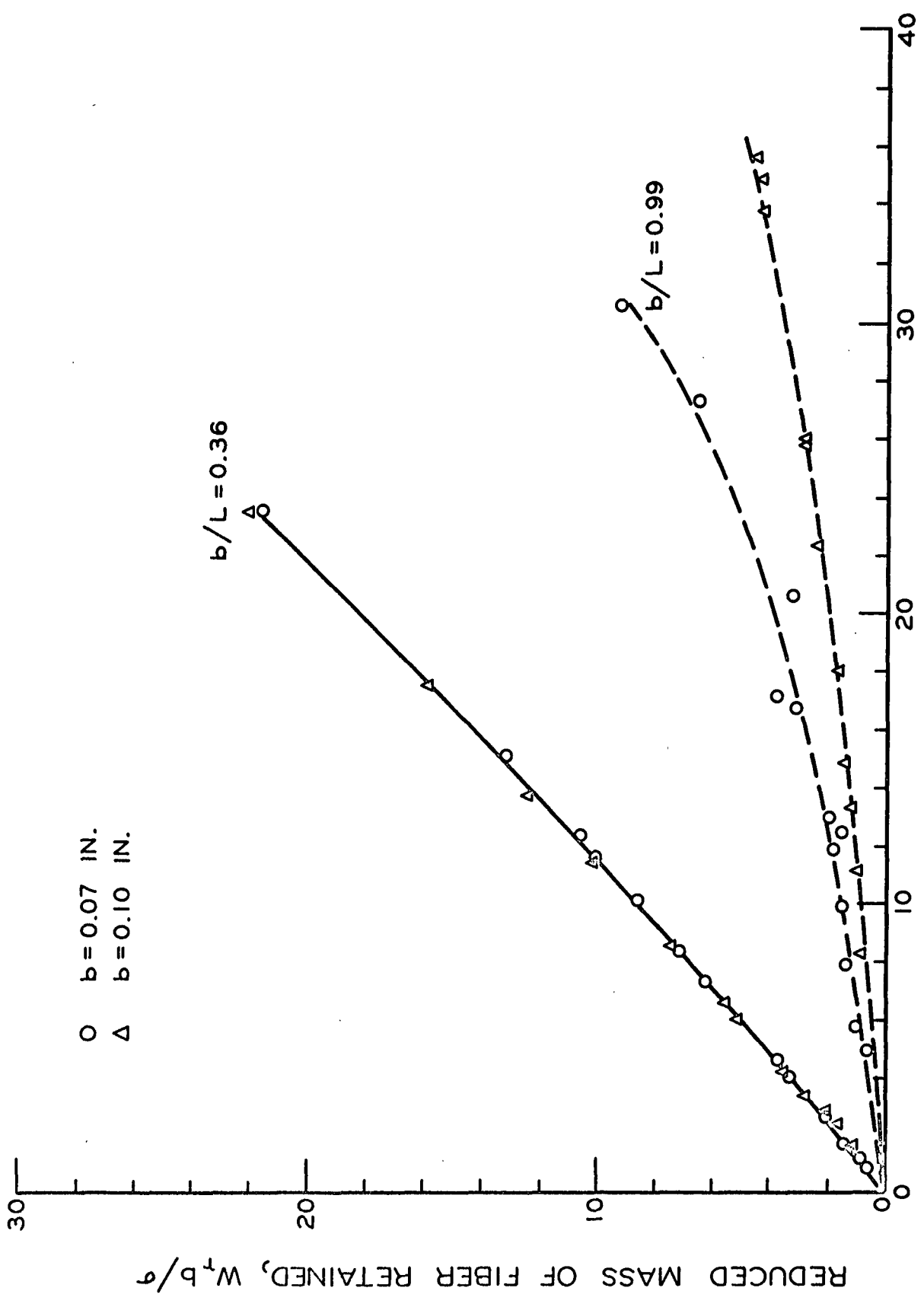
Figure 18. Comparison of Parallel and Square-Mesh Grid with Respect to Total Amount of Fibers Passed

effect on the initial retention as long as the ratio  $\underline{b}/\underline{L}$  was kept constant. However, for the same  $\underline{b}/\underline{L}$  value, the retention curves for the two values of  $\underline{b}$  do not coincide. For example, the square-mesh curves for  $\underline{b} = 0.07$ ,  $\underline{L} = 3.4$  mm. and for  $\underline{b} = 0.10$  in.,  $\underline{L} = 4.9$  mm. have identical values of  $\underline{b}/\underline{L}$  but differ considerably; the same is true for the square-mesh curves  $\underline{b} = 0.07$  in.,  $\underline{L} = 1.8$  mm. and  $\underline{b} = 0.10$  in.,  $\underline{L} = 2.6$  mm. Since the geometries are identical, the differences are only a matter of scale, and if the proper scale factor is used when plotting, the curves should be made to coincide. To place the curves for the two interwire spacings on the same scale, it should readily be observed that the co-ordinates to be plotted are the dimensionless quantities  $\underline{W}_r \underline{b}^2 / \underline{L} \sigma$  vs.  $\underline{W}_t \underline{b}^2 / \underline{L} \sigma$ . These dimensionless numbers represent the number of fibers per grid opening at any time. Of course the same reduction can be obtained by plotting  $\underline{W}_r \underline{b} / \sigma$  vs.  $\underline{W}_t \underline{b} / \sigma$ . This is done in Fig. 19 for the examples mentioned. For the longer fibers, the curves are brought together nicely, but for the shorter ones, an inconsistency in the data is indicated. This can be attributed to the rather large difference in the relative fiber-length distributions of the two fiber samples. Because of this difference, the geometries of the two systems are significantly different even though the average values of  $\underline{b}/\underline{L}$  are identical.

#### SIGNIFICANCE OF THIS WORK AND SUGGESTIONS FOR FUTURE STUDIES

##### EXTENSION OF THE THEORY

In this study a theory of retention has been presented and illustrated with experimental verification for an idealized system.



REDUCED TOTAL MASS OF FIBERS,  $w_t b / \sigma$

Figure 19. Retention Curves for Square-Mesh Grid Plotted on Reduced Coordinates

With appropriate extension and modification the theory should also be applicable to more complex systems. To be of greatest practical value the analysis should be extended to account for flexible fibers, more complex grid geometries, hydrodynamic effects, and fiber interactions. Fiber flexibility and more complex grid geometries would be the logical variables to consider next. The effects of hydrodynamic conditions and fiber interactions would be somewhat more difficult to analyze due to the lack of basic understanding of the phenomena, and any studies of these effects would probably of necessity be largely empirical. The inclusion of only the effect of fiber flexibility in the analysis would make it immediately applicable to the screen classification of pulp fibers. To apply the analysis to flexible fibers it would be necessary to define the conditions necessary for retention of a fiber in such a manner that the limits on the integral of Equation (16) would be known. This would undoubtedly require experimental work with individual fibers to define the conditions, and it would require a method of measuring flexibility. When this is accomplished the remainder of the analysis would be the same as presented in the illustration given by this work.

For flexible fibers to be retained by bridging across an opening, it would be necessary for the fibers to overhang the wires to a certain degree depending upon the degree of flexibility. The effect of flexibility will then be to cause the fiber to appear to be shorter than it actually is, and the relationships presented in the present study might then apply if the true fiber length is replaced by an apparent length. This apparent length could be determined by considering the change in shape of a fiber supported at two points and uniformly

loaded by the fluid drag and its own weight. Such an analogy would only be useful for fibers which are not flexible enough to be retained by stapling themselves over individual wires in the grid. As the flexibility increases the apparent length and the retention of fibers of a given length would decrease until the flexibility becomes great enough for the stapling mechanism of retention to become important. Because of this stapling effect, further increases in flexibility could conceivably increase the amount of retention. A further complicating effect that must be accounted for when dealing with flexible fibers is the curved and coiled positions that the fibers can assume when approaching the grid. If this effect is great enough they may no longer act like fibers approaching the grid but more like spherical particles. A method of describing the apparent fiber length in such cases will be necessary.

Extension of the analysis to more complex grid geometries will likely be laborious but should be rather straightforward as long as two dimensional grids are considered. For three dimensional grids such as woven screens of low pitch-to-diameter ratios, the analysis could be quite difficult since the wires forming the sides of the openings make considerable angles with the plane of the grid. In studies of retention by such grids, it would probably be useful to describe them in terms of equivalent two-dimensional grids. Once the equivalent dimensions are established experimentally, the relationships for this equivalent grid could be used.

In order to apply the theory during the formation of a fiber deposit by filtration it will be necessary to deal with a changing grid

geometry. This changing geometry can be described mathematically for a simple system like the one used in this work, but even for this system the description promises to become unmanageable. For more immediate results, a semiempirical approach to the problem might prove of more value. Description of the geometry in terms of an average property similar to the hydraulic radius or mean pore size concepts might be useful. For instance, one might assume that the size and geometry of the openings in the grid-fiber deposit combination could be characterized by some dimension  $\bar{b}$  and that the relative change in  $\bar{b}$  is proportional to the amount of fibers deposited, i.e.,  $\frac{d\bar{b}}{\bar{b}} = -k \frac{dW_r}{W_r}$ . If it is further assumed that  $\alpha$ , the slope of the retention curve, is a linear function of  $\bar{b}$ , i.e.,  $\frac{dW_r}{dW_t} = 1 - a\bar{b}$ , then one can arrive at the form,

$$\frac{W_r}{W_t} + (1/k) \log \frac{1 - ce^{-kW_r}}{1 - c} = \frac{W_t}{W_t}$$

where  $k$  and  $c$  are constants, for the equation of the retention curves. In fact, this simple equation fits several of the experimental curves very well. Obviously, the assumptions made in deriving this equation are gross oversimplifications, but this serves to illustrate the type of approach that might be used.

#### SIGNIFICANCE TO SCREENING AND CLASSIFICATION

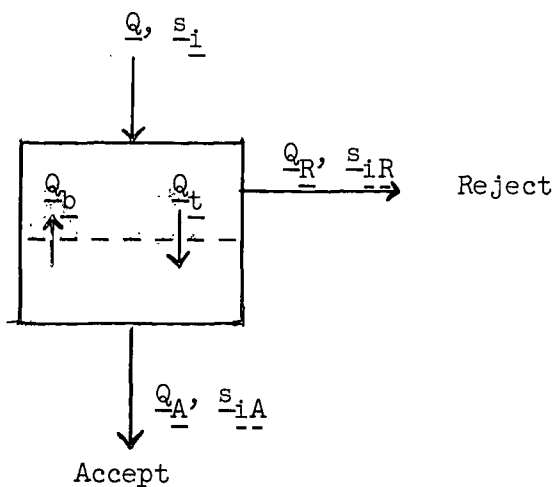
Some of the results of the analysis of initial retention presented in this work should be of immediate value to the theory of screening and size classification of particles having high axis ratios. In systems where the major assumptions of this analysis (rigid, individual,

approximately randomly oriented fibers and grids of high pitch-to-diameter ratio) are reasonably valid, the predicted relationships between initial retention and relative fiber length can be used to guide the selection of screens for particular uses. It has been pointed out that the square-mesh grid geometry is the most efficient for classifying fibers according to length. Similar use can be made of the relationships to pick the best geometries for other uses. For example, if one wishes to remove spherical particles from a fiber suspension by retaining them on the screen and allowing the fibers to pass through, the comparison shows that the parallel geometry would be best. This fact has been recognized in screening practice and utilized in the design of slotted screen plates for removing oversize and dirt particles in the screening of pulp. When the theory is extended to account for flexible fibers, other facts that have been recognized in practice may receive theoretical explanations. Poor performance of screen plates with certain drill patterns has been attributed at times to the blinding of the screen by fibers stapling over the members separating adjacent holes. This should be readily substantiated or refuted by the application of the theory.

A greater value of the theory presented here and any extensions or modifications that may be made will be its use in theoretically describing the processes of screening and fiber-length classification. There are no basic differences between commercial screening operations and laboratory fiber-length classifications that depend upon screen separations. Any system of screens can be used in conjunction with material balances and the initial retention relationships to determine fiber-length distributions. In practice, screening operations are usually

operated continuously while particle-size classifications are done batch-wise. All fiber-length classifiers in present use depend upon the different rates of passage of fibers of different lengths through the same screen element rather than upon some equilibrium condition. With the infinite number of possibilities for arranging and operating sets of screens, it is surprising that all of these instruments are so similar and operate on nearly identical principles. The ability to analyze screening systems from a theoretical standpoint may lead to better classifier operating principles and designs as well as eliminating the empirical methods of interpreting results.

For the purpose of illustrating the application of the initial retention relationship to screening and classification operations, a screen element operating at steady state in a continuous system will be analyzed. A stream of fibers is flowing into the screen compartment at a mass flow rate  $\underline{Q}$  and has a concentration of fibers  $\underline{s}_i$  of a particular length.



The screen splits the incoming stream into an accepted fraction and a rejected fraction as shown in the diagram. If the screen vibrates to

keep the openings clear, then there will be a back flow  $\underline{Q}_b$  through the screen and a forward flow  $\underline{Q}_t = \underline{Q}_A + \underline{Q}_b$ . If mixing is complete in both sides of the compartment a material balance shows that

$$\underline{Q}_A \underline{s}_{iA} = (1 - \bar{P}_i)(\underline{Q}_t \underline{s}_{iR} - \underline{Q}_b \underline{s}_{iA}) \quad (29)$$

which leads to

$$\underline{s}_{iR}/\underline{s}_{iA} = 1 + (\underline{Q}_A/\underline{Q}_t)[\bar{P}_i/(1-\bar{P}_i)] = \underline{K}_i \quad (30)$$

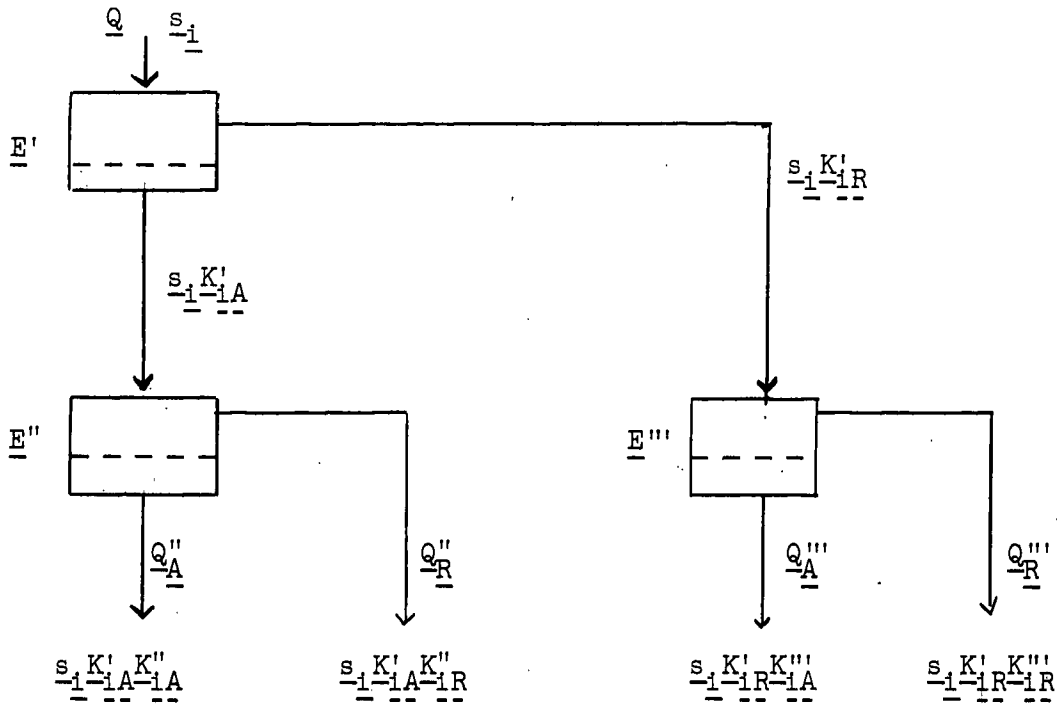
$$\underline{s}_{iA}/\underline{s}_i = \left\{ \underline{K}_i - (\underline{Q}_A/\underline{Q}_t)(\underline{Q}_A/\underline{Q})[\bar{P}_i/(1-\bar{P}_i)] \right\}^{-1} = \underline{K}_{iA} \quad (31)$$

$$\underline{s}_{iR}/\underline{s}_i = \underline{K}_i \underline{K}_{iA} = \underline{K}_{iR} \quad (32)$$

These relationships show that fibers with high values of  $\bar{P}_i$  can be almost completely removed from the accepted stream, but short fibers with low values of  $\bar{P}_i$  are distributed between both outflowing streams. They also show that the concentrations in the outflowing streams can be adjusted to some extent by adjusting the various flow rates.

Any number of screen elements such as this can be operated with different overflows and backflows in an endless number of arrangements to produce desired separations. It is not possible to discuss the merits and drawbacks of various methods of operation. However, a simple arrangement will be described for illustrative purposes which might be used for continuously monitoring the fiber-length distribution of a flowing suspension of fibers such as the discharge from a refiner. The stream would be continuously sampled and the sample diluted to meet the conditions of negligible fiber interactions. This sample is fed into

a screen element  $E'$  and the overflow and reject are fed into two other screens  $E''$  and  $E'''$  as shown in the diagram below. The concentrations of fiber type  $\underline{i}$  in each of the streams will be as shown when the steady state is reached. If there are four different fiber lengths in the



sample (or four length ranges for which average values of  $\bar{P}_{\underline{i}}$  can be determined), the amounts of each can be determined by measuring the total concentration of each of the four exit streams, and solving the system of equations shown in Equation (33). The quantities  $\underline{s}''_{\underline{A}}$ ,  $\underline{s}''_{\underline{R}}$ ,  $\underline{s}'''_{\underline{A}}$ , and  $\underline{s}'''_{\underline{R}}$  are the measured concentrations of the exit streams and the values of  $\underline{K}$  can be calculated from the initial retention relationships, the flow rates, and a knowledge of the screen structures. By continuously monitoring the concentrations, a continuous record of fiber-length distribution would be obtained. This has been only one example of the use of the theory. Examples of the use of the probability concept in

unsteady-state operations have been given by Kubat (16) and by Andersson and Bartok (17). This analysis of screening is similar to that presented by these workers, but the significance of the present work lies in the theoretical prediction of the retention probability, a quantity which was only assumed to exist in their analyses.

$$\begin{aligned}
 \sum_{i=1}^4 \frac{s_{-i} K'_{-iA} K''_{-iA}}{s_{-i} K'_{-iA} K''_{-iA}} &= \underline{s''_A} \\
 \sum_{i=1}^4 \frac{s_{-i} K'_{-iA} K''_{-iR}}{s_{-i} K'_{-iA} K''_{-iR}} &= \underline{s''_R} \\
 \sum_{i=1}^4 \frac{s_{-i} K'_{-iR} K'''_{-iA}}{s_{-i} K'_{-iR} K'''_{-iA}} &= \underline{s'''_A} \\
 \sum_{i=1}^4 \frac{s_{-i} K'_{-iR} K'''_{-iR}}{s_{-i} K'_{-iR} K'''_{-iR}} &= \underline{s'''_R} \\
 \underline{Q} \sum_{i=1}^4 s_{-i} &= \underline{Q''_A} \underline{s''_A} + \underline{Q''_R} \underline{s''_R} + \underline{Q'''_A} \underline{s'''_A} + \underline{Q'''_R} \underline{s'''_R}
 \end{aligned}
 \tag{33}$$

SIGNIFICANCE TO SHEET FORMATION

The other area in which initial retention is of significance to the paper industry is that of sheet formation. This has been discussed briefly in earlier sections, and it was pointed out that initial retention and retention in general were of importance from the aspects of drainage phenomena on the paper machine and the structure of the finished sheet. The initial retention represents only a small but a

quite significant part of the sheet-forming process. The structure of the first few layers of fibers not only controls the deposition and structure of succeeding layers of the sheet but must also have a considerable effect on the flow resistance of the wire. It is suspected that the resistance of the bare wire is somewhat less than the apparent wire resistance during a filtration. This is likely due to fibers in the first layers of the deposit being forced into the wire openings and causing it to appear to have a much finer mesh than it actually does and thus a higher resistance than the bare wire with a layer of fibers above it. If this is the case, the properties and arrangement of the fibers composing these first layers along with the compressive forces driving them into the wire openings would be the factors which control the apparent increase in wire resistance. Thus, a knowledge of how these fibers are deposited would be necessary in a study of the effects of wire-fiber interactions on flow resistance, a subject of great interest to sheet formation and drainage.

The results of this work show that even for very open grids the deposits of fibers closed up the openings rather rapidly, and the total amounts of fibers passing were relatively small except for very short fibers. The high losses through the wire on a paper machine must then be attributed to small fibers and fines or unfavorable hydrodynamic conditions. It has been observed that the losses on a paper machine are much greater than for laboratory filtrations of the same pulp slurry using identical wires. This leads one to compare the conditions on a paper machine with the simple flow conditions used for forming the fiber deposits in this and other laboratory studies. As the papermaking slurry

first contacts the machine wire the formation process begins and probably proceeds similar to a laboratory filtration but with greater drag on the fibers and more fiber interaction. The concepts of retention presented earlier in this thesis would then apply. But as the wire passes over a table roll some water is driven back through the wire disrupting the deposit, and as suction is applied on leaving the table roll the fibers in the first layers of the deposit have another opportunity to pass through the wire. The probability analysis could be applied again to the loss of fibers during this period and could be repeated for each succeeding table roll. During this period the fiber interactions would have a major effect upon the retention, and as the deposit grows and is compacted more as it passes over each table roll, the degree of interaction will increase. Also, as the sheet is compacted the tendency for the deposit to be disrupted would become less, and the losses due to this effect would decrease.

Only fibers have been considered in the present study while in an actual papermaking slurry there are nonfibrous particles such as fillers and fiber fragments as well as a wide range of sizes of particles which can be classified as fibers. With regard to initial retention, however, it is probably safe to assume that all the fine particles except those attached to the larger fibers by surface forces will pass through the wire. The deposition of the first elements of the sheet composed mostly of long fibers will be followed by the deposition of layers with increasing amounts of short fibers until a fine pore structure is developed. As this fine structure begins developing the removal and deposition within the mat of fine particles suspended alone in the water can begin to take place. The

retention of these fine particles can be described in a manner analogous to that for fiber retention for their retention is also a matter of probability. In this case, however, the probability function must account for retention by surface adsorption as well as by direct mechanical interception. It must also provide for the three-dimensional nature of the medium whereas for fibers it was possible to treat the medium as two dimensional.

Thus, each elementary layer of the sheet would be expected to have a different composition and structure and therefore a different resistance to drainage during the sheet-forming process. As has been pointed out previously, the initial rate of retention and the structure of the first layer of fibers retained will have a major role in determining the degree of this nonuniformity.

The theoretical description of the entire formation process would be very difficult for it is obviously a highly complex process. But through increased efforts towards theoretical analysis and more thorough experimental studies our knowledge can be greatly improved, and eventually it should be possible to predict or measure quantities which will serve to characterize the sheet-forming process.

## SUMMARY AND CONCLUSIONS

The mechanism of retention of fibers by screens and wire cloth is of particular importance to the understanding of screening and sheet-forming operations in the paper industry. A better understanding of this mechanism is necessary if a theoretical approach is to be taken in the study of these and related operations. The study reported here was undertaken with the objective of increasing our fundamental knowledge of the retention process. Since the formation of a deposit of fibers on the grid during the filtration of a fiber suspension is a complex process, this study was limited to the period of initial retention of fibers by the bare grid. Specifically, the effects of fiber length and grid geometry on the initial rate of retention were to be studied.

It was recognized that the retention of fibers by a grid is a statistical process. There is only a certain probability that a particle which in a certain orientation might be retained by the grid will actually arrive at that orientation. On this basis a general expression describing the retention process was derived. This expression involves a probability function which is dependent upon the properties of the fibers, and grid, the hydrodynamic field in the vicinity of the grid, and the interactions between fibers. This general expression was then applied to the specific case of the initial retention of rigid individual fibers by simple parallel and square-mesh grids. This resulted in relationships between the initial retention and the relative fiber length for each of the grid geometries.

An apparatus was then designed and constructed for the purpose of conducting experiments to verify the predicted relationships. Stiff

nylon fibers cut to narrow fiber-length ranges and grids constructed of small diameter wire were used to simulate the conditions of the mathematical model. The apparatus was designed so that differing amounts of fibers could be passed onto a grid and the amounts retained and passed by the grid could be collected and measured. In this manner the data for the different fiber length-grid combinations could be used to construct retention curves, plots of the amount of material retained as a function of the total amount passed onto the grid. From the retention curves the initial rate of fiber retention was measured. This initial rate is defined as the initial slope of the retention curve and is equivalent to the fraction of fibers retained from the first increment of the fiber suspension that reaches the bare grid.

The initial retention rates measured in this manner agreed very well with the predicted values. This agreement is taken as very strong evidence in favor of the validity of not only the method of predicting initial retention but also the general approach to the problem of fiber retention used in this study. It is suggested that the analysis can now be modified to account for more variables and will be of use in predicting initial retention in more complex systems.

The parallel and square-mesh geometries studied in this work are the limiting cases of the general rectangular mesh geometry. By comparing results for these two cases, some general conclusions can be made concerning the most efficient use of wire in constructing rectangular-mesh grids for the screening and filtration of fiber suspensions. For classifying mixtures of fibers of different lengths, this

comparison has shown that the square-mesh geometry gives the sharpest separation according to length. For obtaining the greatest initial retention of fibers during filtration of a fiber suspension, the efficiency depends upon the relative fiber length. The parallel mesh is more efficient than the square mesh if the length of the fibers is between about 1.3 and 3.5 times the spacing between the parallel wires; otherwise the square mesh is more efficient. This fiber-length dependence means that for designing the best grid for retaining fibers in a given system, it would be necessary to know the fiber-length distribution of the suspension. A comparison of the experimental results on the basis of total retention revealed an identical dependence of efficiency upon relative fiber length. This suggests that initial retention is a direct indication of total retention during the formation of a deposit by filtration of a fiber suspension. This is of great importance since initial retention can be predicted much more easily than total retention, and it will therefore be possible to compare the efficiencies of different grid structures on this basis. These conclusions apply strictly only to the ideal systems studied here, but it is reasonable to assume that they would be valid qualitatively for less ideal systems as well.

The area in which the analysis of initial retention will probably be of most immediate value is that of screening and classification of fiber suspensions. In these operations no deposit is allowed to form on the screen and the initial retention relationships would apply at all times. Results of a limited amount of experimental work reported in the literature indicate that the relationships derived in this work for idealized systems might apply directly to the classification of stiff fibers

in the Bauer-McNett classifier. If this is true it should be possible to use the relationship to calculate average fiber lengths and fiber-length distributions from screen classification data. Also, it will provide a means for choosing screens for separating fiber-length mixtures into the desired length fractions. The relationships will be of great value to the theories of screening and classification in a very practical sense if they are modified to account for fiber flexibility and more complex grid geometries.

The significance of this work will depend to a large degree upon the ability of future studies to apply the analysis to more complex systems of initial retention and the subsequent formation of a fiber deposit on the grid. Through these future studies it is hoped that the present work will serve to increase the understanding of the screening and sheet-forming operations in the paper industry.

NOMENCLATURE

- $\underline{A}$  = Area in the plane of the grid.
- $\underline{a}$  = Long dimension of opening in rectangular-mesh grid.
- $\underline{b}$  = Spacing between parallel wires in a square- or parallel-mesh grid. Short dimension of opening in rectangular-mesh grid.
- $\underline{L}$  = Fiber length.
- $\underline{L}_r$  = Reduced fiber length, equal to  $\underline{L}/\underline{b}$ .
- $\underline{n}$  = Average point concentration expressed as the number of fiber centers per unit volume.
- $\underline{n}_{\phi, \theta}$  = Distribution function for orientations of fibers approaching the grid.
- $\underline{N}$  = Number of fibers intercepted by the grid.
- $\underline{m}$  = Moisture content of deposited fibers expressed as the mass ratio of wet deposit to dry deposit.
- $\underline{P}$  = Probability a particular fiber will be retained.
- $\underline{P}_i$  = Probability a fiber of type  $\underline{i}$  will be retained.
- $\overline{\underline{P}_i}$  = Average of  $\underline{P}_i$  over the area  $\underline{A}$ .
- $\underline{Q}$  = Mass flow rate of fiber suspension.
- $\underline{s}_i$  = Point concentration of fibers of type  $\underline{i}$  expressed as mass of fibers per unit mass of suspension.
- $\overline{\underline{s}_i}$  = Average of  $\underline{s}_i$  over the area  $\underline{A}$ .
- $\underline{s}$  = Point concentration of all types of fibers, equal to  $\sum \underline{s}_i$ .
- $\overline{\underline{s}}$  = Average of  $\underline{s}$  over the area  $\underline{A}$ .
- $\underline{u}$  = Point velocity of suspension perpendicular to grid.
- $\overline{\underline{u}}$  = Average of  $\underline{u}$  over the area  $\underline{A}$ .
- $\underline{V}$  = Volume of suspension that has reached the plane of the grid at any time.
- $\underline{V}_f$  = Volume of filtrate at any time.
- $\underline{W}_r$  = Mass of fiber deposited on the grid.

$\underline{W}_t$  = Total mass of fibers that have reached the plane of the grid at any time.

$\underline{W}_T$  = Total mass of fibers that will be passed by the grid before the openings are effectively closed.

GREEK LETTERS

$\alpha$  =  $\frac{d\underline{W}_r}{d\underline{W}_t}$

$\alpha_0$  =  $\frac{d\underline{W}_r}{d\underline{W}_t}$  at  $\underline{W}_r = 0$ .

$\rho$  = Point density of the suspension approaching the grid.

$\bar{\rho}$  = Average value of  $\rho$  over the area  $\underline{A}$ .

$\bar{\rho}_f$  = Average density of the filtrate over  $\underline{A}$ .

$\sigma$  = Weight per unit length of fiber.

$\phi$  = The angle between the long axis of the approaching fiber and the plane of the grid.

$\theta$  = The angle between the projection of the fiber on the grid and the  $\underline{x}$  axis.

SUBSCRIPTS

$\underline{i}$  = Refers to  $\underline{i}$ th type of fiber.

$\underline{f}$  = Refers to filtrate.

$\underline{o}$  = Refers to  $\underline{W}_r = 0$ .

$\underline{r}$  = Refers to weight of fibers retained on grid. Also to a reduced value.

$\underline{t}$  = Refers to total amount of fibers.

$\underline{R}$  = Refers to rejected fraction.

$\underline{A}$  = Refers to accepted fraction.

LITERATURE CITED

1. Ingmanson, W. L., Tappi 35, no. 10:439 (1952).
2. Ingmanson, W. L., and Whitney, R. P., Tappi 37, no. 11:523 (1954).
3. Whitney, R. P., Ingmanson, W. L., and Han, S. T., Tappi 38, no. 3:157 (1955).
4. Ingmanson, W. L., Tappi 40, no. 12:936 (1957).
5. Ingmanson, W. L., Tappi 42, no. 6:449 (1959).
6. Halladay, J. F., Paper Trade J. 118, no. 6:32 (1944).
7. Bergstrom, J., and Knell, H., Svensk Papperstidn. 57, no. 1:1 (1954).
8. Brecht, W., and Rosenlew, N., Das Papier 7:381 (1953).
9. Davies, C. N., Proc. Inst. Mech. Engrs. (London) 1B:185 (1952).
10. Chen, C. Y., Chem. Rev. 55, no. 3:595 (1955).
11. Hermans and Bredee, Rec. trav. chim. 54:680 (1935).
12. Heertjes, P. M., and Hass, H., Rec. trav. chim. 68:361 (1949).
13. Grace, H. P., A.I.Ch.E. Journal 2, no. 3:307 (1956).
14. Steenberg, B., and Kubat, J., Svensk Papperstidn. 58, no. 9:319 (1955).
15. Kubat, J., Svensk Papperstidn. 59, no. 5:175 (1956).
16. Kubat, J., Svensk Papperstidn. 59, no. 7:251 (1956).
17. Andersson, O., and Bartok, W., Svensk Papperstidn. 58, no. 10:367 (1955).
18. Mason, S. G., Tappi 37, no. 11:494 (1954).
19. Mason, S. G., Svensk Papperstidn. 61, no. 3:61 (1958).

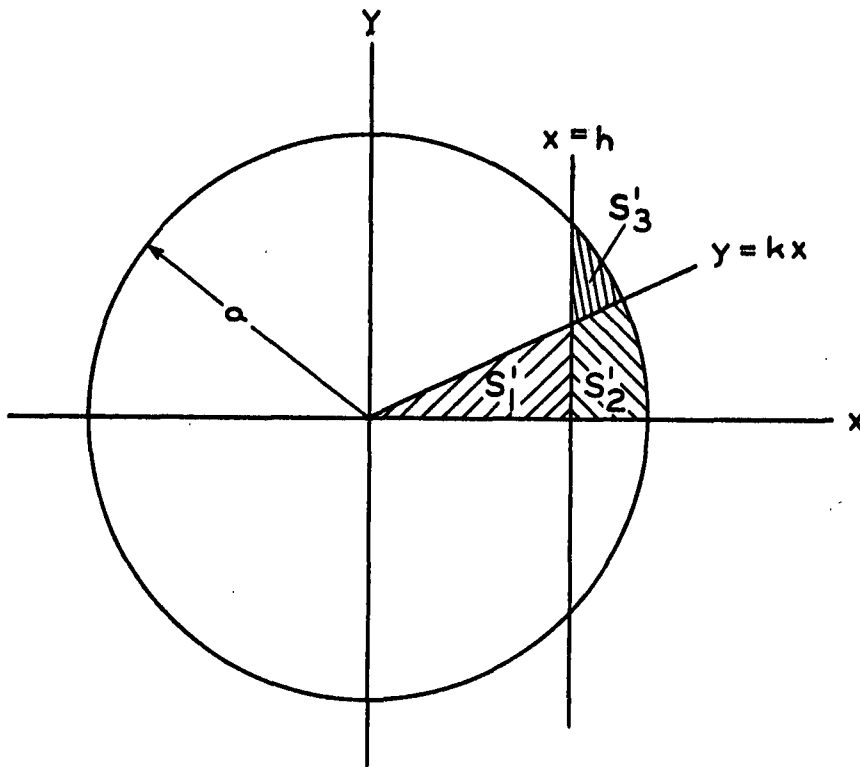
APPENDIX I

DETAILS OF THE CALCULATIONS FOR THE RELATIONSHIPS  
BETWEEN  $\bar{P}_1$  AND  $b/L$

METHOD OF OBTAINING EQUATION (20)

As stated in the text, Equation (20) represents the ratio of twice the area shown in Fig. 4 to the area of the hemisphere. The portion of the area defined by Equation (18a) is half the area of a spherical segment of diameter  $L$  and height  $(1/2L - b + x)$ , or  $(\pi L/2)(1/2L - b + x)$ . The area defined by (18b) can be determined as follows.

Consider a sphere,  $x^2 + y^2 + z^2 = a^2$ , which is intersected by the planes,  $x = h$  and  $y = kx$ . The projection of the sphere and planes on the  $x$ - $y$  plane is shown in the following diagram:



An element of area on the surface of a sphere can be represented by

$$dS = \underline{a}(\underline{a}^2 - \underline{x}^2 - \underline{y}^2)^{-1/2} \underline{dy} \underline{dx} \quad (34)$$

The area  $S_1$  on the upper portion of the spherical surface which projects as the shaded area  $S'_1$  in the diagram can then be represented as

$$S_1(\underline{a}, \underline{h}, \underline{k}) = \int_0^{\underline{h}} \int_0^{\underline{kx}} \underline{a} (\underline{a}^2 - \underline{x}^2 - \underline{y}^2)^{-1/2} \underline{dy} \underline{dx} \quad (35)$$

or upon integration

$$S_1(\underline{a}, \underline{h}, \underline{k}) = \underline{ah} \tan^{-1} \underline{h}/\underline{v}' + \underline{a}^2 \tan^{-1} \underline{v}'/\underline{a} - \underline{a}^2 \tan^{-1}(1/\underline{k}) \quad (36)$$

where  $\underline{v}' = (1/\underline{k}) [\underline{a}^2 - \underline{h}^2(1+\underline{k}^2)]^{1/2}$

The area  $S_2$  which projects as  $S'_2$  is given by

$$S_2(\underline{a}, \underline{h}, \underline{k}) = \underline{a}^2 \tan^{-1} \underline{k} - S_1(\underline{a}, \underline{h}, \underline{k})$$

or

$$S_2(\underline{a}, \underline{h}, \underline{k}) = \underline{a}^2 \tan^{-1} \underline{a}/\underline{v}' - \underline{ah} \tan^{-1} \underline{h}/\underline{v}' \quad (37)$$

The area defined by Equation (18b) is equivalent to twice  $S_2(L/2, \underline{x}, \sqrt{L^2/4(\underline{b}-\underline{x})^2 - 1})$ . (This notation is used to indicate the same relationship as  $S_2(\underline{a}, \underline{h}, \underline{k})$  except that  $\underline{a}$  is replaced by  $L/2$ ,  $\underline{h}$  by  $\underline{x}$ , and  $\underline{k}$  by  $\sqrt{L^2/4(\underline{b}-\underline{x})^2 - 1}$ ). Taking the ratio of the area defined by Equation (18) to the area of the hemisphere results in Equation (20).

THE RELATIONSHIP BETWEEN  $\bar{P}_1$  AND  $L/b$  FOR  
PARALLEL GRID ASSUMING NO SLIPPAGE

Assuming randomly oriented fibers, Equation (23a) represents the ratio of twice the area illustrated in Fig. 6 to the area of the

hemisphere. The lower portion of the area, that defined by Equation (22a), is the area of half a spherical segment of diameter  $\underline{L}$  and height  $(1/2\underline{L} - \underline{b} + \underline{x})$ , or  $(\pi\underline{L}/2)(1/2\underline{L} - \underline{b} + \underline{x})$ . The upper portion, defined by (22b), is half the area of a spherical segment of diameter  $\underline{L}$  and height  $(1/2\underline{L} - \underline{x})$  less twice the area  $\underline{ABC}$ , or

$$(\pi\underline{L}/2)(1/2\underline{L} - \underline{x}) - 2\underline{ABC} \quad (38)$$

The area  $\underline{ABC}$  can be represented by

$$\underline{ABC} = (\underline{L}/2) \int_0^{\cos^{-1}2\underline{x}/\underline{b}} \underline{F}_1(\underline{x}, \phi) \cos\phi \, d\phi \quad (39)$$

where  $\underline{F}_1(\underline{x}, \phi) = \cos^{-1}2\underline{x}/\underline{L} \cos\phi - \cos^{-1}(2\underline{b}/\underline{L} - 2\underline{x}/\underline{L} \cos\phi)$

Utilizing these observations, Equation (23a) becomes

$$\underline{P} = 1 - \underline{b}/\underline{L} - (1/\pi) \int_0^{\cos^{-1}2\underline{x}/\underline{b}} \underline{F}_1(\underline{x}, \phi) \cos\phi \, d\phi \quad (40)$$

Combining this with Equation (17) yields for the case of  $\underline{L} > 2\underline{b}$

$$\bar{\underline{P}}_1 = 1 - \underline{b}/\underline{L} - (2/\pi\underline{b}) \int_0^{\underline{b}/2} \int_0^{\cos^{-1}2\underline{x}/\underline{b}} \underline{F}_1(\underline{x}, \phi) \cos\phi \, d\phi \, d\underline{x} \quad (41)$$

which can be further reduced by changing the order of integration to

$$\bar{\underline{P}}_1 = 1 - 1/\underline{L}_r - 1/4\underline{L}_r - 1/2 [\cos^{-1}(1/\underline{L}_r) - \cos^{-1}(2/\underline{L}_r) + (\underline{L}_r^2/4 - 1)^{1/2} - (\underline{L}_r^2 - 1)^{1/2}] \quad (42)$$

where  $\underline{L}_r = \underline{L}/\underline{b}$ .

For the case where  $\underline{b} < \underline{L} < 2\underline{b}$ , the portion of the probability function given by Equation (23b) must also be taken into account. Equation (23b) can be reduced to

$$\underline{P} = (1/\pi) \int_0^{\cos^{-1} \underline{b}/\underline{L}} \underline{F}_2(\underline{x}, \theta) \underline{d}\theta \quad (43)$$

$$\text{where } \underline{F}_2(\underline{x}, \theta) = \sqrt{1 - 4\underline{x}^2/\underline{L}^2 \cos^2 \theta} - \sqrt{1 - 4\underline{x}^2/(2\underline{b} - \underline{L} \cos \theta)^2}$$

When the integration indicated by Equation (17) is carried out, the limits must be from  $\underline{b} - \underline{L}/2$  to  $\underline{b}/2$  for the portion of the probability function given by Equation (23a) and from 0 to  $\underline{b} - \underline{L}/2$  for the portion given by (23b). This results in

$$\begin{aligned} \bar{\underline{P}}_1 = & (1 - \underline{b}/\underline{L})(\underline{L}/\underline{b} - 1) - (2/\pi \underline{b}) \int_{\underline{b}-\underline{L}/2}^{\underline{b}/2} \int_0^{\cos^{-1} 2\underline{x}/\underline{b}} \underline{F}_1(\underline{x}, \phi) \cos \phi \underline{d}\phi \underline{d}\underline{x} + \\ & (2/\pi \underline{b}) \int_0^{\underline{b}-\underline{L}/2} \int_0^{\cos^{-1} \underline{b}/\underline{L}} \underline{F}_2(\underline{x}, \theta) \underline{d}\theta \end{aligned} \quad (44)$$

By again changing the order of integration, this can be reduced to

$$\begin{aligned} \bar{\underline{P}}_1 = & (1 - 1/\underline{L}_r)(\underline{L}_r - 1) - \\ & (1/\pi) [\cos^{-1}(1/\underline{L}_r) - \sqrt{\underline{L}_r^2 - 1}] [\cos^{-1}(2-\underline{L}_r) - (2-\underline{L}_r) \sqrt{1-(2-\underline{L}_r)^2}] \\ & + (\underline{L}_r/\pi) \int_0^{\cos^{-1}(2-\underline{L}_r)} [\underline{t} \cos^{-1} \underline{t} + \underline{s} \cos^{-1} \underline{s} - \sqrt{1-\underline{t}^2} - \sqrt{1-\underline{s}^2}] \cos^2 \phi \underline{d}\phi \\ & + (2/\pi) \int_0^{\cos^{-1} 1/\underline{L}_r} \left\{ (1-\underline{L}_r/2) (\sqrt{1-\underline{p}^2} - \sqrt{1-\underline{q}^2}) + (\underline{L}_r/2) \cos \theta \sin^{-1} \underline{p} - \right. \\ & \left. [1 - (\underline{L}_r/2)] \cos \theta \sin^{-1} \underline{q} \right\} \underline{d}\theta \end{aligned} \quad (45)$$

$$\begin{aligned} \text{where } \underline{s} &= (2/\underline{L}_r - 1)/\cos\phi \\ \underline{t} &= 2/\underline{L}_r - \underline{s} \\ \underline{p} &= (2/\underline{L}_r - 1)/\cos\theta \\ \underline{q} &= (2/\underline{L}_r - 1)/(2/\underline{L}_r - \cos\theta) \end{aligned}$$

The integrals in this relationship were evaluated numerically, and the results are presented as Curve II in Fig. 9.

THE RELATIONSHIP BETWEEN  $\bar{P}_i$  AND  $L/b$  FOR SQUARE-MESH GRID

FOR  $L/b < 1$

Referring to the diagram on page 76, the area on the spherical surface  $S_3$  which projects as  $S'_3$  is represented by

$$S_3(\underline{a}, \underline{h}, \underline{k}) = 1/2\pi\underline{a}(\underline{a} - \underline{c}) - S_2(\underline{a}, \underline{h}, \underline{k})$$

or

$$S_3(\underline{a}, \underline{h}, \underline{k}) = \underline{a}^2 \tan^{-1} \underline{v}'/\underline{a} - \underline{a}\underline{h} \tan^{-1} \underline{v}'/\underline{h} \quad (46)$$

where  $\underline{v}'$  is as defined previously on page 77.

The first term of Equation (27) is the ratio of

$S_3(L/2, \underline{x}, \underline{y}/\sqrt{L^2/4 - \underline{y}^2})$  to the area of the hemisphere of diameter  $L$ .

Likewise, the second term is the ratio of  $S_3(L/2, \underline{y}, \underline{x}/\sqrt{L^2/4 - \underline{x}^2})$  to the area of the hemisphere. Thus,

$$\underline{P} = (2/\pi L^2)[S_3(L/2, \underline{x}, \underline{y}/\sqrt{L^2/4 - \underline{y}^2}) + S_3(L/2, \underline{y}, \underline{x}/\sqrt{L^2/4 - \underline{x}^2})] \quad (47)$$

Combining this with Equation (26) and remembering that it is valid only for  $\underline{x}^2 + \underline{y}^2 \leq (L/2)^2$  gives

$$\bar{P}_1 = (16/b^2 L^2) \int_0^{L/2\sqrt{2}} \int_x^{\sqrt{L^2/4 - y^2}} [S_3(L/2, x, y/\sqrt{L^2/4 - y^2}) + S_3(L/2, y, x/\sqrt{L^2/4 - x^2})] dx dy \quad (48)$$

This can be shown to be equivalent to

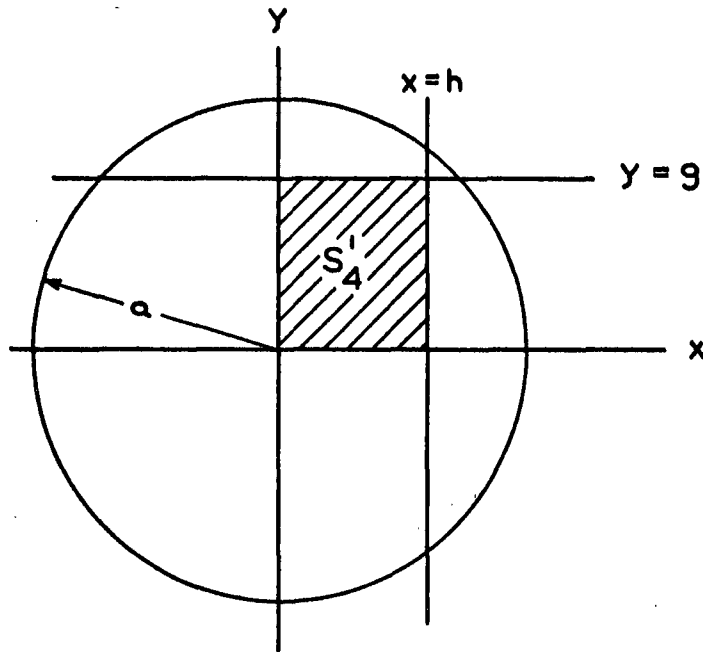
$$\bar{P}_1 = (16/b^2 L^2) \int_0^{L/2} \int_0^{\sqrt{L^2/4 - y^2}} S_3(L/2, x, y/\sqrt{L^2/4 - y^2}) dx dy \quad (49)$$

which can be easily integrated to yield Equation (28).

FOR  $L/b > 2\sqrt{2}$

As stated in the text, a fiber of this length will be intercepted by the grid if its lower half strikes any side of the opening. The lower end of the fiber can occupy any point on an imaginary hemisphere of diameter  $L$  whose center coincides with the fiber midpoint. The probability of the fiber being caught is then the area of the portion of the surface of the hemisphere whose projection falls outside the square opening under consideration divided by the total surface area of the hemisphere. The area of the portion of the surface which projects outside the square can be found as follows:

Consider a sphere,  $x^2 + y^2 + z^2 = a^2$ , which is intersected by the planes,  $x = h$  and  $y = g$ , such that  $h^2 + g^2 \leq a^2$ . The projection on the  $x$ - $y$  plane is shown in the following diagram:



An element of area on the surface of the sphere can again be represented by

$$dS = a(a^2 - x^2 - y^2)^{-1/2} dx dy$$

and thus the area  $S_4$  on one hemisphere which projects as the area  $S'_4$  in the  $x$ - $y$  plane can be represented by

$$S_4 = \int_0^g \int_0^h a(a^2 - x^2 - y^2)^{-1/2} dx dy \quad (50)$$

Upon performing the integration this yields

$$S_4(a, h, g) = ah \tan^{-1} g(a^2 - g^2 - h^2)^{-1/2} + 2ag \tan^{-1} Q - a^2 \tan^{-1} 2gQ/a(1 - Q^2) \quad (51)$$

where  $Q = (1/h)(\sqrt{a^2 - g^2} - \sqrt{a^2 - g^2 - h^2})$

Then for a fiber whose center is approaching at the point  $(\underline{x}, \underline{y})$  as in Fig. 20, the portion of the area of the lower hemisphere which projects into the opening can be given by

$$\underline{U} = \underline{S}_4(\underline{L}/2, \underline{x}, \underline{y}) + \underline{S}_4(\underline{L}/2, \underline{x}, \underline{b}-\underline{y}) + \underline{S}_4(\underline{L}/2, \underline{b}-\underline{x}, \underline{y}) + \underline{S}_4(\underline{L}/2, \underline{b}-\underline{x}, \underline{b}-\underline{y}) \quad (52)$$

And the probability of a fiber whose center approaches at  $(\underline{x}, \underline{y})$  being retained will then be

$$\underline{P} = 1 - \frac{2\underline{U}}{\pi \underline{L}^2} = 1 - \frac{\underline{U}}{\pi R^2} \quad R = \frac{\underline{L}}{2} \quad (53)$$

Substituting into Equation (26) gives

$$\bar{\underline{P}}_1 = 1 - (16/\pi \underline{L}^2 \underline{b}^2) \int_0^{\underline{b}/2} \int_0^{\underline{x}} \underline{U} \underline{d}\underline{x} \underline{d}\underline{y} \quad (54)$$

To facilitate the numerical integration of this expression, it can be written as

$$\bar{\underline{P}}_1 = 1 - (2/\pi \underline{L}^2 \underline{b}^2) \int_0^{\underline{b}} \int_0^{\underline{b}} \underline{U} \underline{d}\underline{x} \underline{d}\underline{y} \quad (55)$$

which is identical to

$$\bar{\underline{P}}_1 = 1 - (8/\pi \underline{L}^2 \underline{b}^2) \int_0^{\underline{b}} \int_0^{\underline{b}} \underline{S}_4(\underline{L}/2, \underline{x}, \underline{y}) \underline{d}\underline{x} \underline{d}\underline{y} \quad (56)$$

which was the expression that was numerically integrated to give the appropriate portion of Curve IV in Fig. 9.

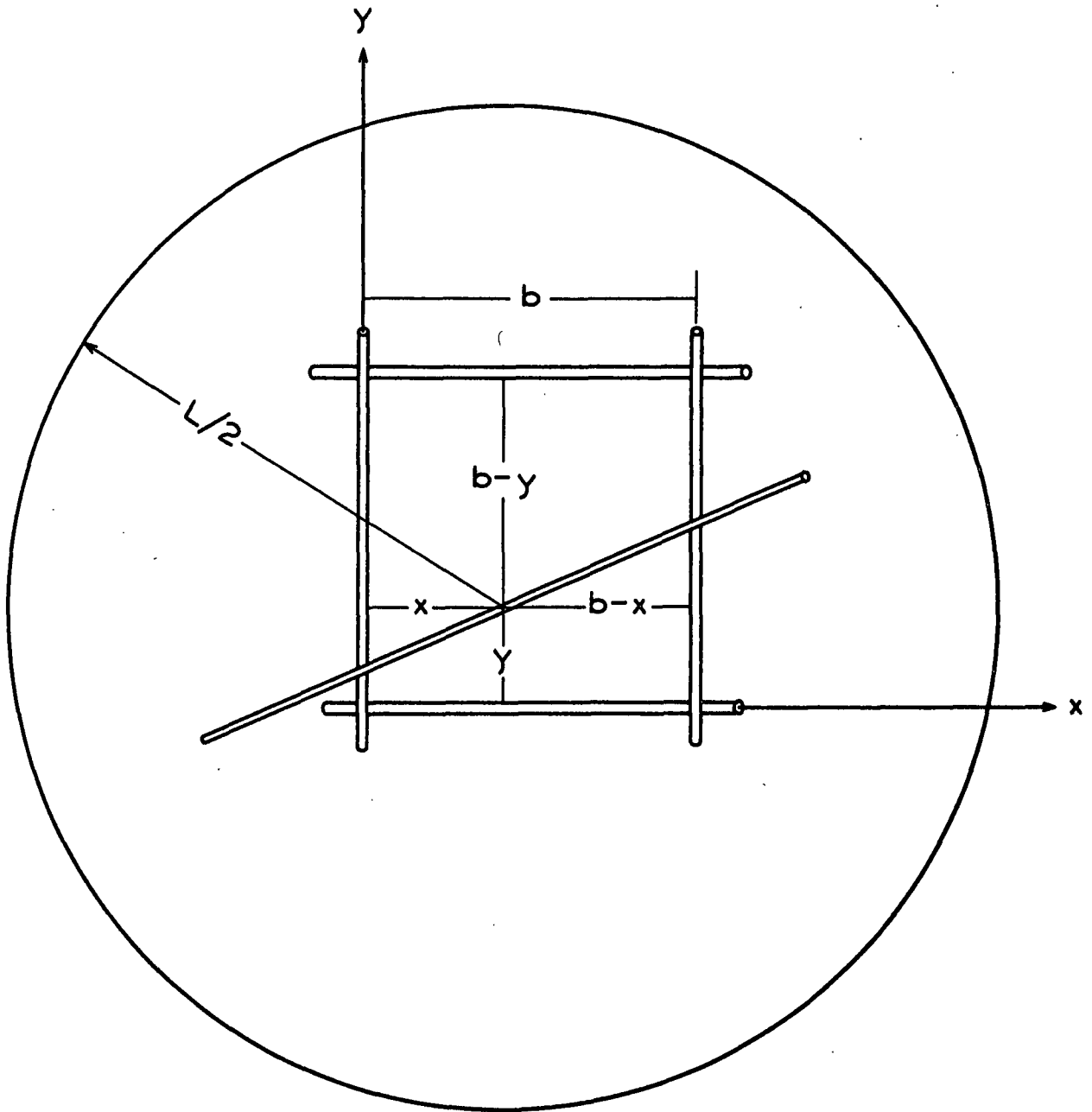


Figure 20. Projection of Fiber Approaching Square Grid,  
 $\underline{L/b} > 2\sqrt{2}$

FOR  $\underline{L}/\underline{b} = \sqrt{2}$

The octant of the square which is used for analysis is broken down into seven areas as in Fig. 21. These will be treated individually for the purpose of determining the probability function in each case.

Area A

Referring to Fig. 22A, if the fiber approaches with its midpoint in this area, the only possibility for bridging to occur is across the corner of the opening as in the case treated previously for  $\underline{L}/\underline{b} < 1$ . The probability function is the same also, and can be represented by

$$\underline{P}_A = (2/\pi\underline{L}^2) \left[ \underline{S}_3(\underline{L}/2, \underline{x}, \underline{y}/\sqrt{\underline{L}^2/4 - \underline{y}^2}) + \underline{S}_3(\underline{L}/2, \underline{y}, \underline{x}/\sqrt{\underline{L}^2/4 - \underline{x}^2}) \right] \quad (57)$$

Area B

In this case the fiber can bridge across the corner, or across the parallel sides I and III. Again consider the lower end of the fiber to occupy a point on the lower portion of the hemisphere of diameter  $\underline{L}$  and whose center coincides with the midpoint of the fiber. If this point lies on a portion of the hemisphere which projects as the shaded area in Fig. 22B then the fiber will be in position to bridge across the opening. The probability of bridging is the ratio of the area of this portion of the hemisphere to the total area of the hemisphere. The areas on the surface of the hemisphere which project as the shaded areas in the  $\underline{x}$ - $\underline{y}$  plane are indicated in the figure. The probability function can be represented for this area as

$$\underline{P}_B = \underline{P}_A + (1/2\underline{L} - \underline{b} + \underline{x})/\underline{L} + (4/\pi\underline{L}^2)\underline{S}_2(\underline{L}/2, \underline{x}, \sqrt{\underline{L}^2/4(\underline{b}-\underline{x})^2 - 1}) \quad (58)$$

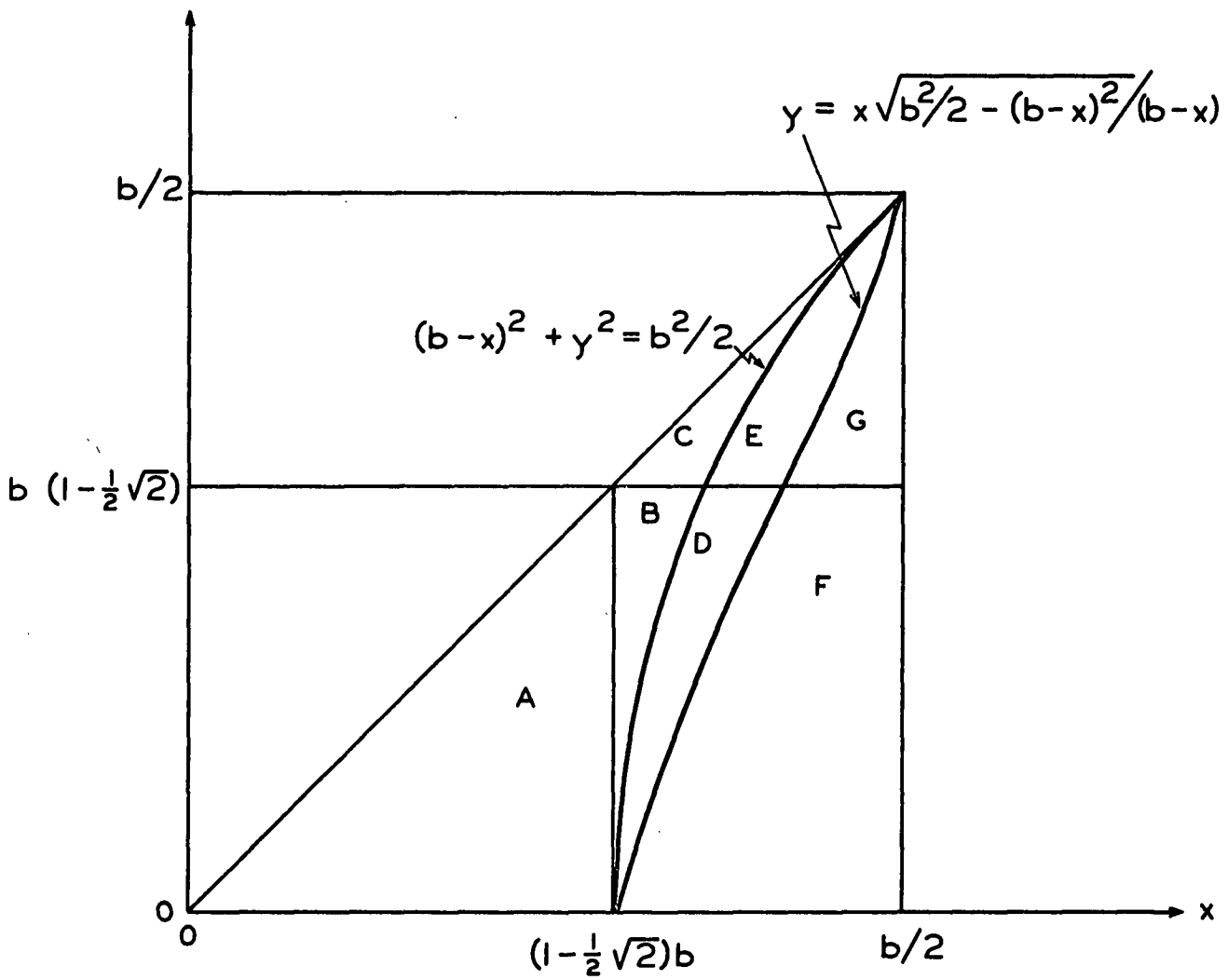


Figure 21. Division of the Octant for Purposes of Calculating  $\underline{P}$  for  $\underline{L}/\underline{b} = \sqrt{2}$

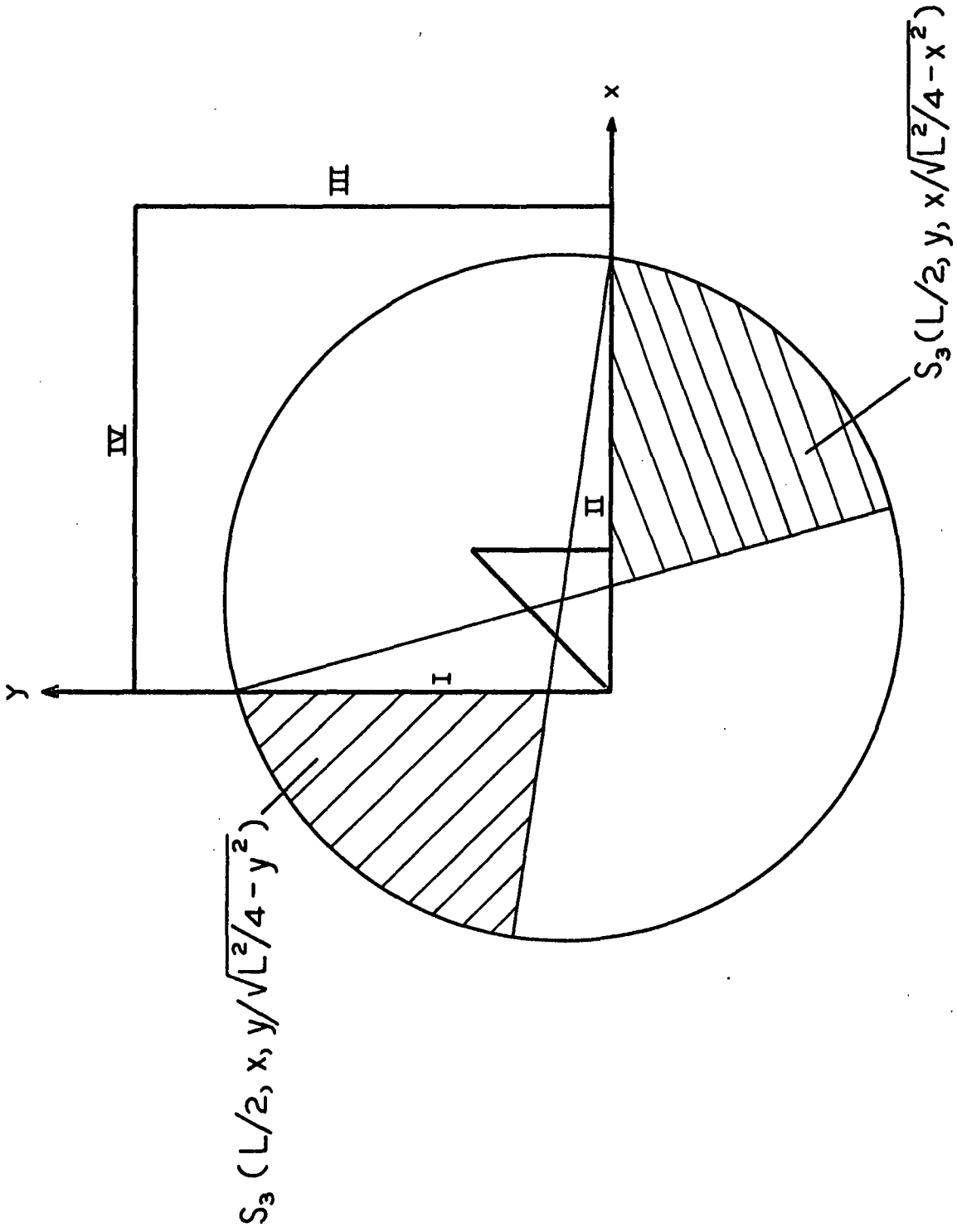


Figure 22A. Diagram for Determination of  $\bar{P}$  for Area  $\bar{A}$

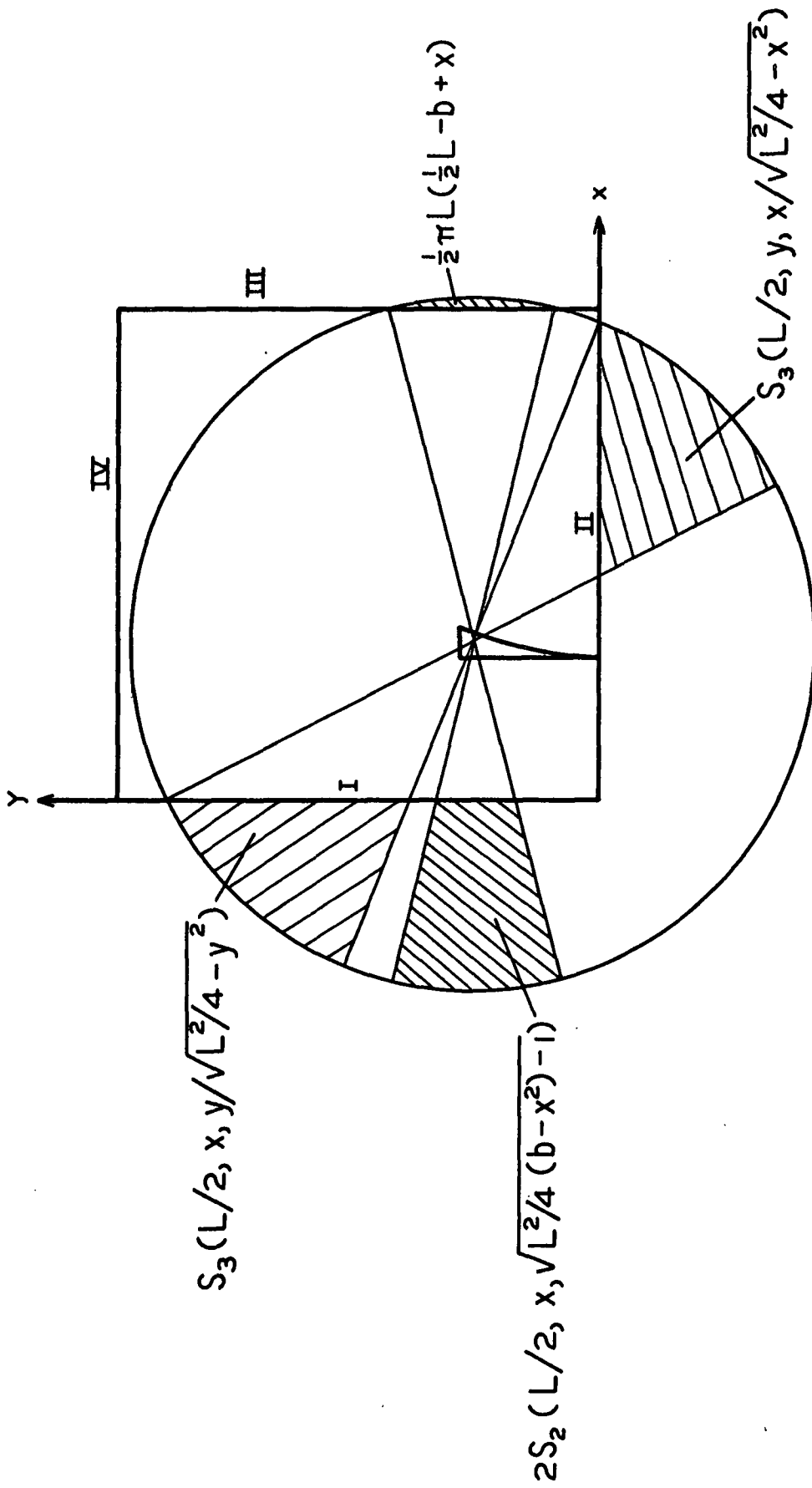


Figure 22B. Diagram for Determination of  $\underline{P}$  for Area  $\underline{B}$

Area C

In this case the fiber can bridge across the corner or across either pair of parallel sides of the opening. The probability function is the ratio of the area of the portion of the hemisphere which projects as the indicated area in Fig. 22C to the total area of the hemisphere, or

$$\underline{P}_C = \underline{P}_B + (1/2\underline{L} - \underline{b} - \underline{y})/\underline{L} + (4/\pi \underline{L}^2) \underline{S}_2(\underline{L}/2, \underline{y}, \sqrt{\underline{L}^2/4(\underline{b}-\underline{y})^2 - 1}) \quad (59)$$

Area D

In this case the fiber may again either bridge across the corner or across the two parallel sides I and III. However, there is some overlapping which distinguishes this from the case of area B. Using the same reasoning as in the previous cases and with the help of Fig. 22D, the probability function is found to be

$$\underline{P}_D = 1/2 + \underline{y}/2\underline{L} - \underline{b}/2\underline{L} + (2/\pi \underline{L}^2) \left[ \underline{S}_2(\underline{L}/2, \underline{x}, \sqrt{\underline{L}^2/4(\underline{b}-\underline{x})^2 - 1}) + \underline{S}_3(\underline{L}/2, \underline{y}, 1/\sqrt{\underline{L}^2/4\underline{x}^2 - 1}) - \underline{S}_4(\underline{L}/2, \underline{y}, \underline{b}-\underline{x}) \right] \quad (60)$$

Area E

If the fiber approaches with its midpoint in this area, it can be caught in the same manner as in the previous case and also by bridging across the parallel sides II and IV. Using Fig. 22E the probability function is found to be

$$\underline{P}_E = \underline{P}_D + \underline{P}_C - \underline{P}_B \quad (61)$$

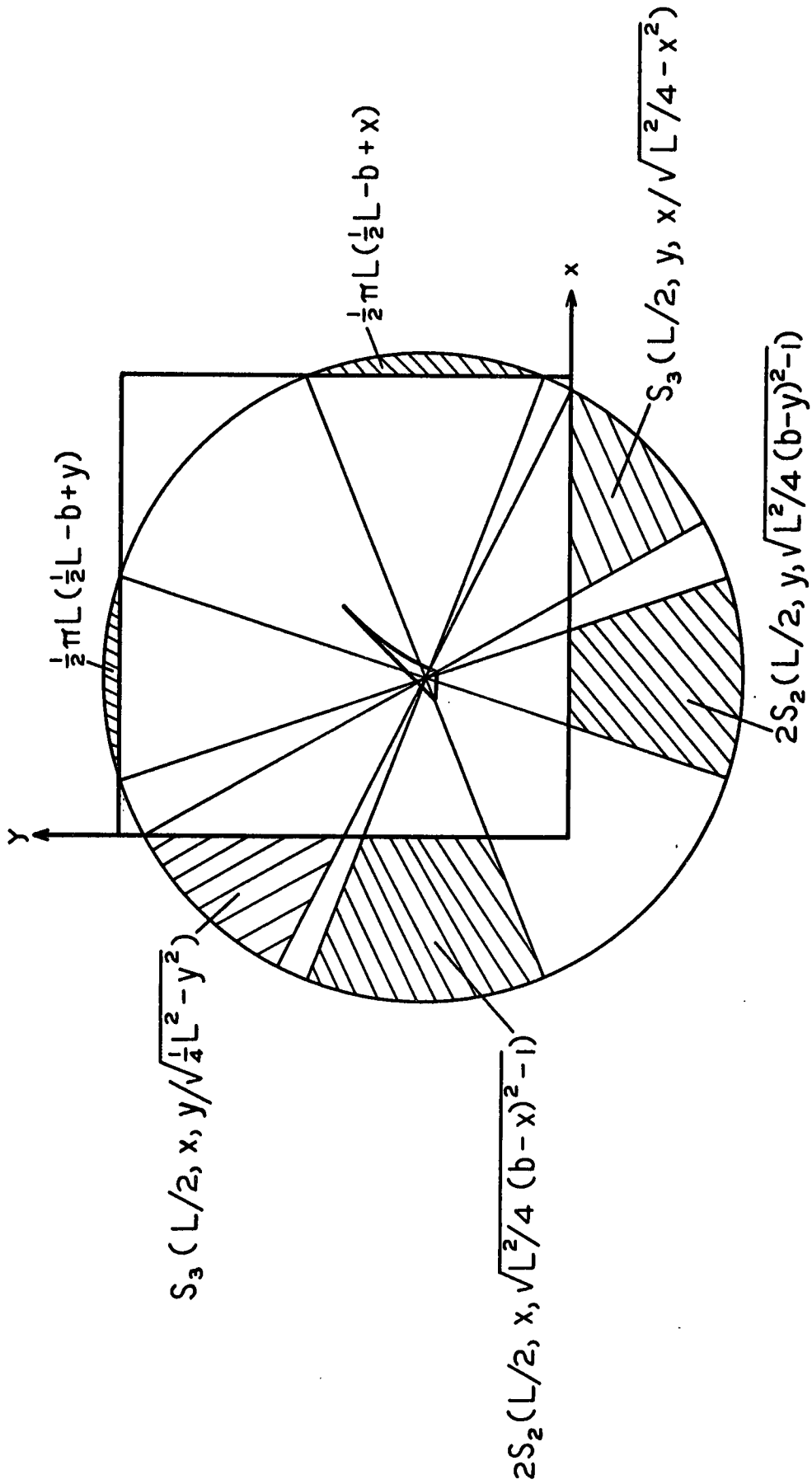


Figure 22C. Diagram for Determination of  $\underline{P}$  for Area  $\underline{C}$

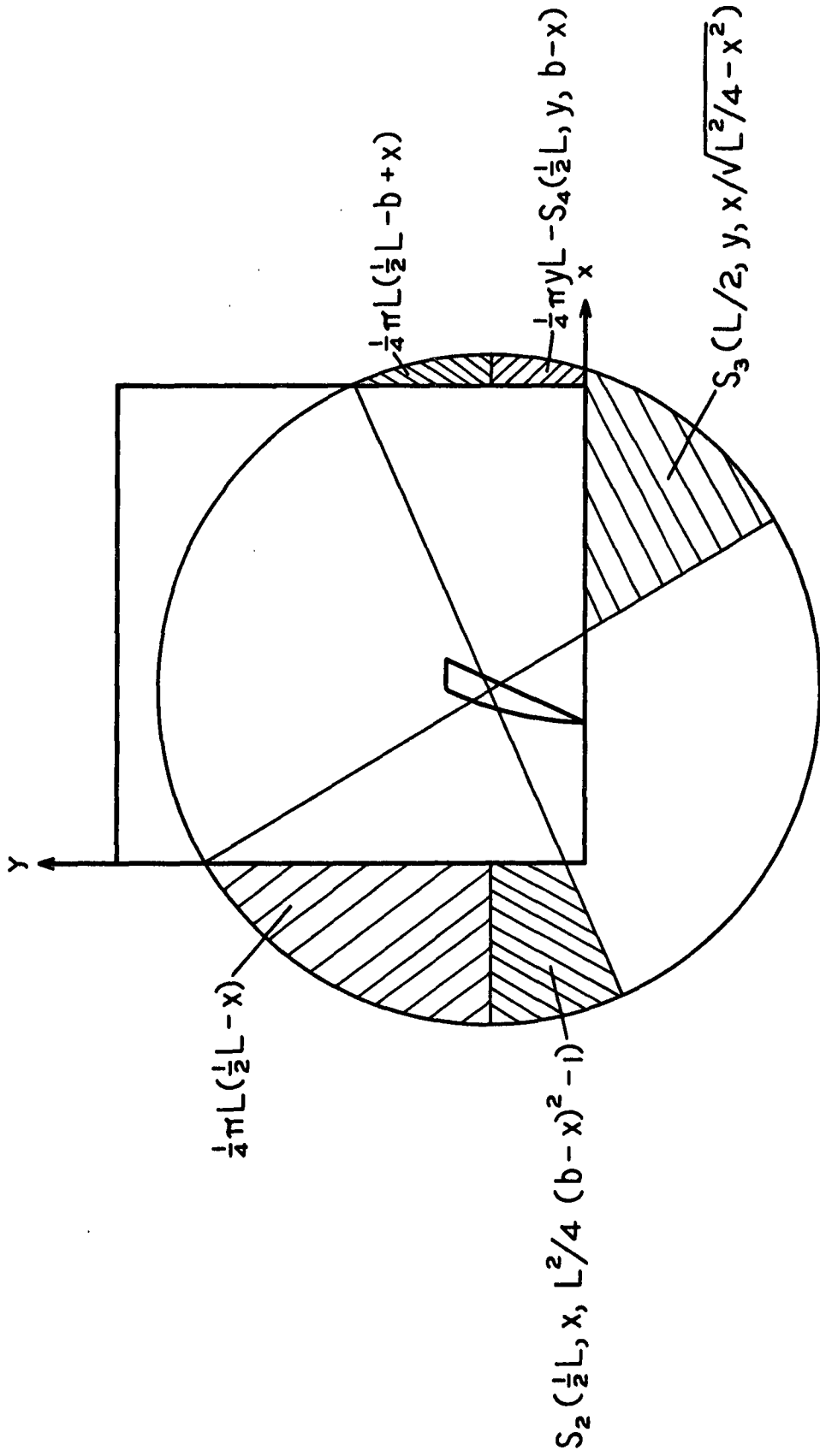


Figure 22D. Diagram for Determination of  $\underline{P}$  for Area  $\underline{D}$

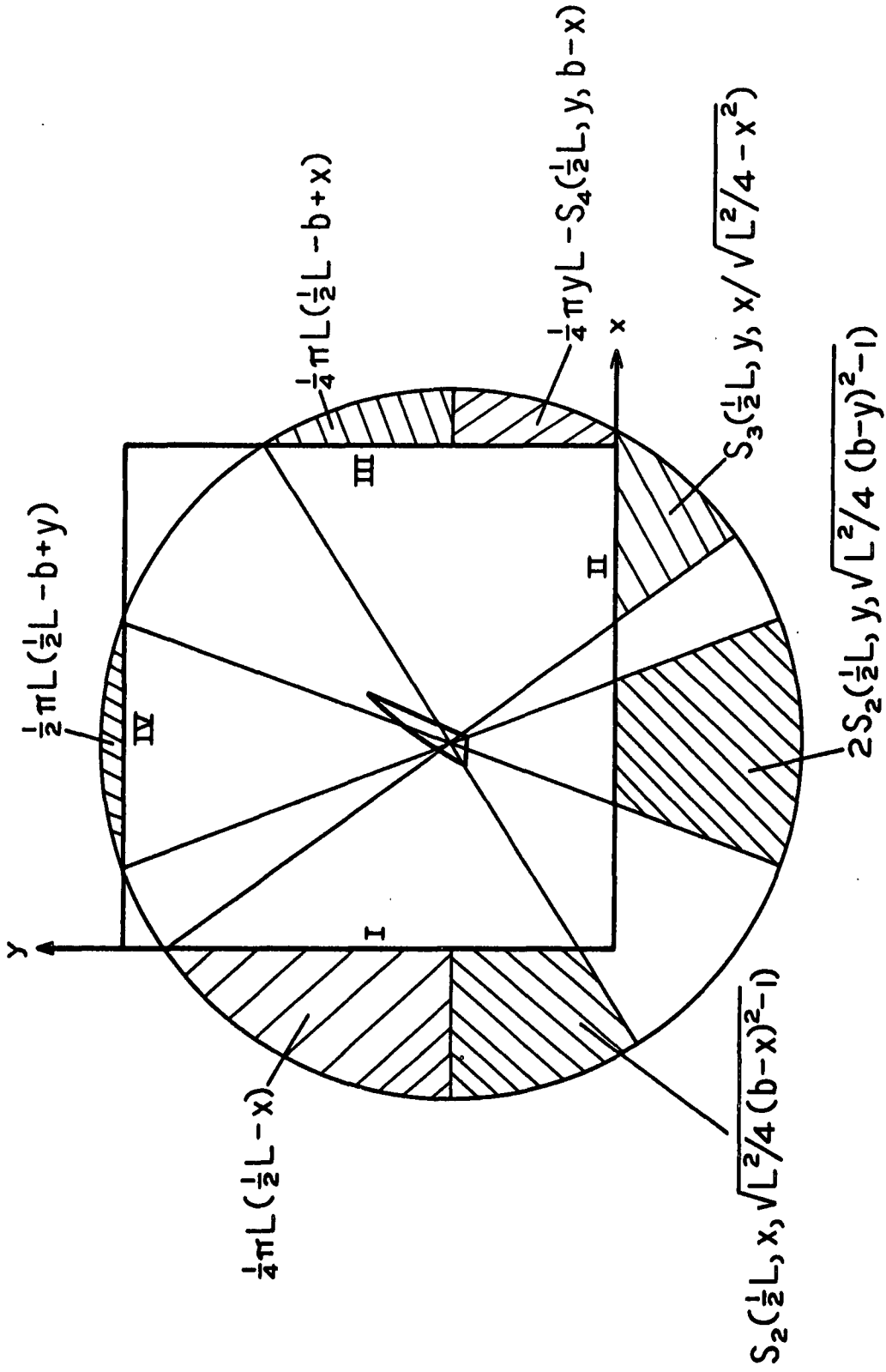


Figure 22E. Diagram for Determining P for Area E

Area F

In this case it is possible for the fiber to bridge across either of the corners formed by wires I, II, and III, or across the parallel sides I and III. Using the same reasoning as before with the aid of Fig. 22F, the probability function can be written as

$$\underline{P}_F = 1/2 + \underline{y}/\underline{L} - \underline{b}/2\underline{L} + (2/\pi\underline{L}^2) \left[ \underline{S}_3(\underline{L}/2, \underline{y}, \underline{x}/\sqrt{\underline{L}^2/4 - \underline{x}^2}) + \underline{S}_3(\underline{L}/2, \underline{y}, 1/\sqrt{\underline{L}^2/4(\underline{b}-\underline{x})^2 - 1}) - \underline{S}_4(\underline{L}/2, \underline{y}, \underline{b}-\underline{x}) - \underline{S}_4(\underline{L}/2, \underline{y}, \underline{x}) \right] \quad (62)$$

Area G

This case (Fig. 22G) is identical to the previous case except that it is possible for a fiber to also bridge across the parallel sides II and IV. The probability function is then

$$\underline{P}_G = \underline{P}_F + \underline{P}_C - \underline{P}_B \quad (63)$$

Since the probability function has now been defined over the entire octant of the square that is under analysis the value of  $\bar{P}_i$  can be evaluated by substituting into Equation (26) to give

$$\bar{P}_i = (8/\underline{b}^2) \left[ \iint_{(A)} \underline{P}_A \underline{dx} \underline{dy} + \iint_{(B)} \underline{P}_B \underline{dx} \underline{dy} + \iint_{(C)} \underline{P}_C \underline{dx} \underline{dy} + \iint_{(D)} \underline{P}_D \underline{dx} \underline{dy} + \iint_{(E)} \underline{P}_E \underline{dx} \underline{dy} + \iint_{(F)} \underline{P}_F \underline{dx} \underline{dy} + \iint_{(G)} \underline{P}_G \underline{dx} \underline{dy} \right] \quad (64)$$

The letters in parenthesis under each integral sign indicate that the expression for  $\underline{P}$  for each area is integrated over values of  $\underline{x}$  and  $\underline{y}$  only in that area. Most of this integration was carried out numerically, and the final result was that for  $\underline{L}/\underline{b} = \sqrt{2}$ ,  $\bar{P}_i = 0.41$ .

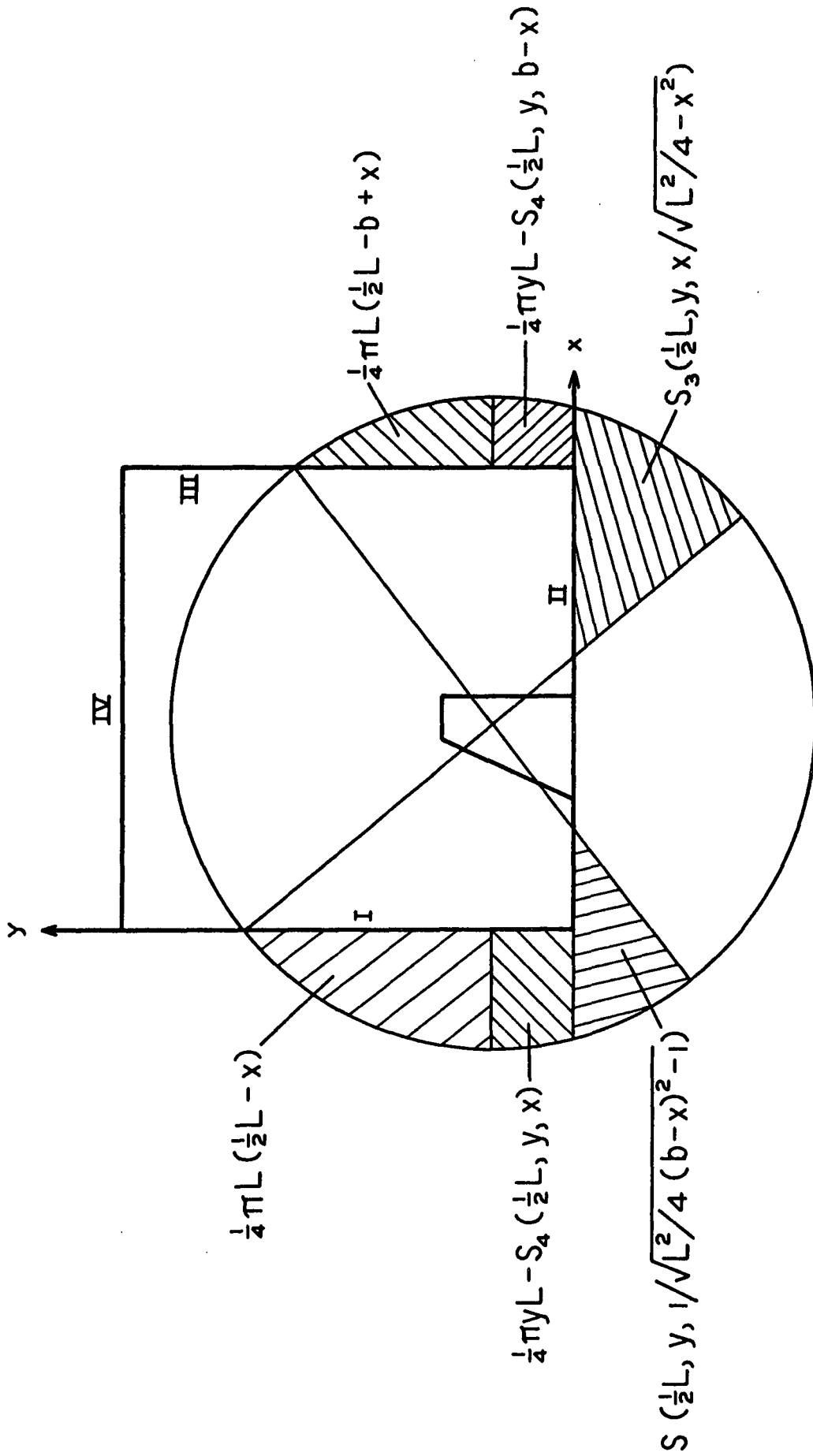


Figure 22F. Diagram for Determination of  $\underline{P}$  for Area  $\underline{F}$

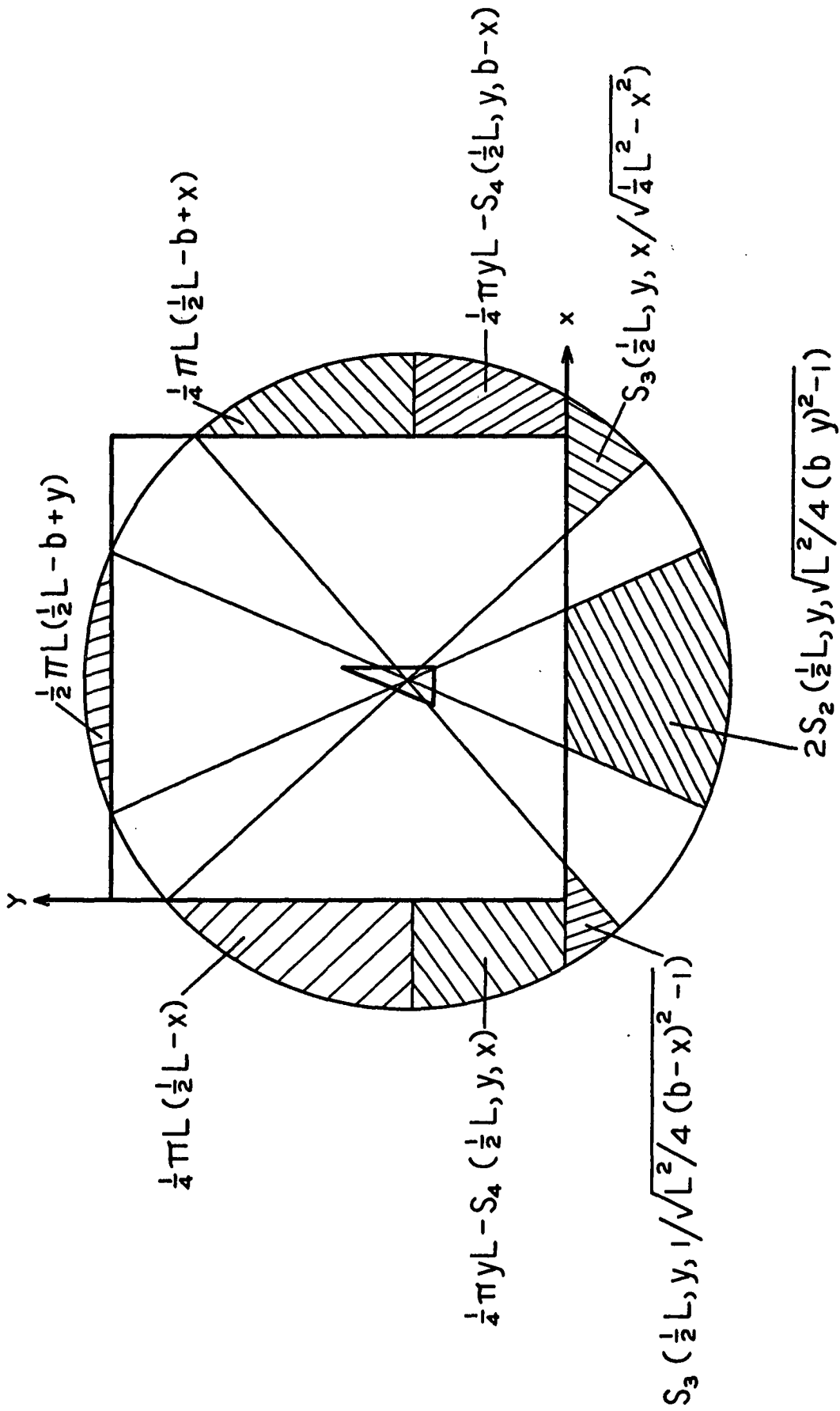


Figure 22G. Diagram for Determination of  $\bar{P}$  for Area G

APPENDIX II

TABLE I

CALCULATED THEORETICAL POINTS FOR THE CURVES OF FIGURE 9

Curve I		Curve II		Curve III		Curve IV	
$\underline{b/L}$	$\underline{\bar{P}}_1$	$\underline{b/L}$	$\underline{\bar{P}}_1$	$\underline{b/L}$	$\underline{\bar{P}}_1$	$\underline{b/L}$	$\underline{\bar{P}}_1$
0.10	0.87	0.10	0.87	0.10	0.90	0.18	0.97
0.20	0.75	0.20	0.75	0.20	0.81	0.26	0.95
0.30	0.61	0.25	0.68	0.25	0.75	0.36	0.91
0.40	0.48	0.33	0.58	0.33	0.66	0.71	0.41
0.50	0.32	0.42	0.47	0.42	0.56	1.00	0.12
0.60	0.18	0.45	0.41	0.50	0.44	1.20	0.09
0.70	0.09	0.50	0.34	0.45	0.51	1.40	0.06
0.80	0.03	0.62	0.17	0.62	0.22		
0.90	0.01	0.71	0.10	0.71	0.13		
1.00	0.00	0.83	0.03	0.83	0.05		
		0.91	0.01	0.91	0.02		
		1.00	0.00	1.00	0.00		

### APPENDIX III

#### EXPERIMENTAL

##### APPARATUS

A schematic diagram of the apparatus is shown in Fig. 10. This consists of two 60-gallon stainless steel tanks A and B, an eight inch diameter lucite flow tube C, a stainless steel centrifugal pump D, and auxiliary copper and brass piping. The flow tube is seven feet long, and the bottom of the tanks are about ten feet above the lower end of the tube. The tube can be filled from below using water from tank A through valves V<sub>4</sub> and V<sub>5</sub>. When the tube is filled, either water from tank A or fiber slurry from tank B can be drawn into the tube depending on the position of the three-way plug valve V<sub>3</sub>. The flow rate is measured by means of an orifice O and is controlled by valve V<sub>2</sub> as the water is returned to either tank. The flow tube can be drained by closing valve V<sub>1</sub>, opening the vent, and properly positioning the three-way valve V<sub>3</sub>. This arrangement allows the water to be re-used as is necessary.

A diagram of the entrance section at the top of the flow tube is shown in Fig. 23. All piping between the tanks and entrance section is two-inch brass or copper tubing. The water enters through the top of the tube into an annular region formed by two concentric cones which distributes the flow across the tube. The solid double cone in the center of the tube is twelve inches in over-all length and three inches in diameter at the base. The outer cone is 2-1/2 inches in diameter at

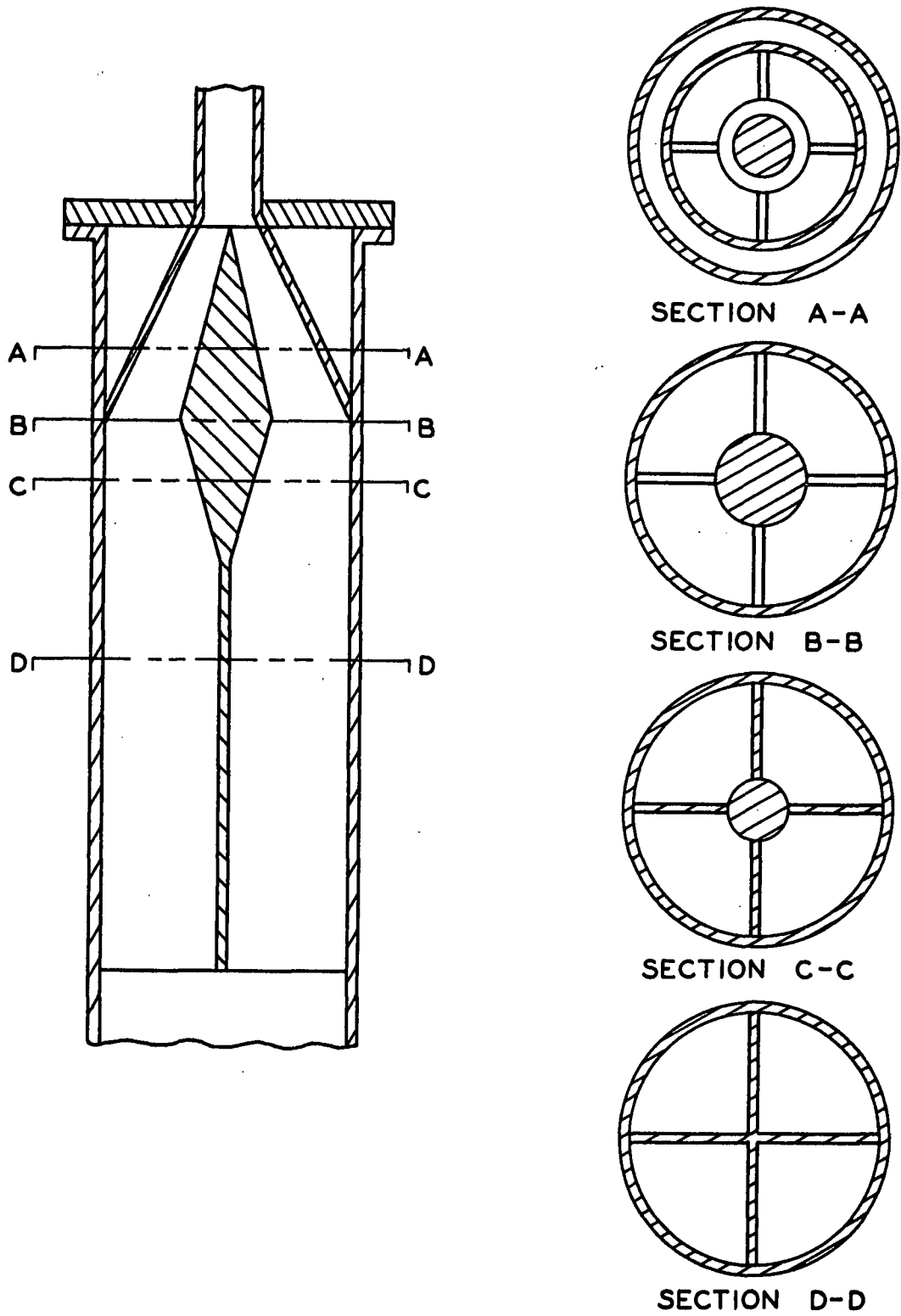


Figure 23. Entrance Section of Flow Tube

the top and eight inches at the bottom with a height of six inches. Vanes for the purpose of straightening the flow are placed at right angles and extend from the base of the central double cone eighteen inches down into the tube or to a point two feet from the top of the tube.

Details of the bottom section of the flow tube are shown in Fig. 24. This consists of a brass base E for the tube, a porous stainless steel plate F which collects all fibers which pass through the grid G under study, and a filter H which can be moved into the tube between the grid and the porous plate or completely out of the tube into a recessed water-tight housing. This filter is a brass ring with a 20-mesh wire cloth soldered across the opening. It is moved into and out of position by the rod J. The use of this movable filter will be discussed later when describing the procedure for making runs. Rubber retaining rings M are used for holding tared filter cloths in place on the porous plate and movable filter. A ring N supporting the grid to be studied fits into the flow tube between this bottom section and the main section of lucite flow tube. A distance of 2 inches is between the grid and the face of the porous plate when the flow tube is fully assembled, and a length of five feet of unobstructed tube is between the surface of the grid and the lower end of the vanes in the entrance section.

## MATERIALS

### FIBERS

Fiber samples were cut from Du Pont Type 300, 15-denier, continuous filament nylon. The fibers were cut by aligning a large number

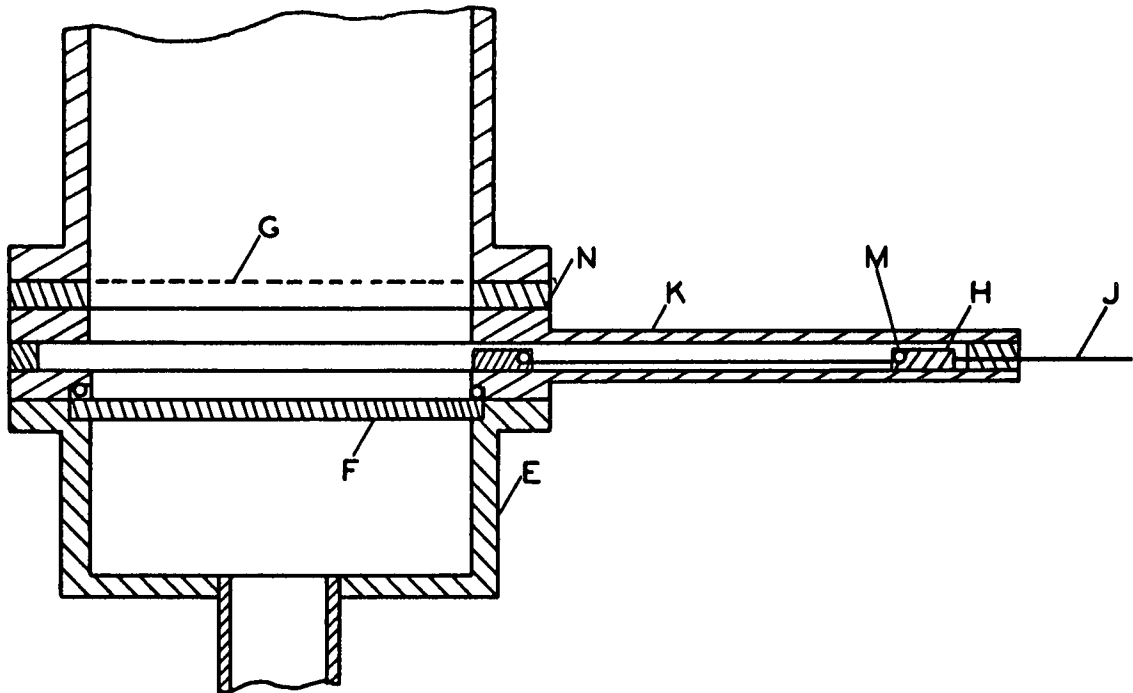


Figure 24. Diagram of Bottom Section of Flow Tube

of the filaments and cutting with a special cutter consisting of a number of equally spaced single-edge razor blades bolted rigidly together with spacers between them. The fiber-length distributions of these samples are shown in Table II. These distributions were determined by projecting fibers on The Institute of Paper Chemistry semi-automatic fiber-length machine but taking the measurements directly with a millimeter scale rather than using the recorder. About two hundred fibers were measured in each sample. The two samples with a mean length of 2.6 mm. were obtained using two different cutters which accounts for the difference in distributions. The sample designated 2.6b was used for all the work with square-mesh grids and for determining the effect of wire diameter on the retention by parallel grids; the sample designated 2.6a was used for all other work.

#### GRIDS

The grids were constructed by stringing small-diameter wire between accurately grooved bars on a jig made for this purpose. The tightly stretched wires were cemented with an epoxy resin to a 1/2-inch thick lucite ring while still held tightly on the jig. When the cement had set firmly the wires were cut free from the jig leaving the ring with the accurately spaced wires stretched across the opening to form the grid. The ring supporting the grid fits into the flow tube as shown in Fig. 24.

The dimensions of the grids which were used in this work are given in Table III.

Fiber Diameter.

-101-

44.47I 2,69 μ

From Myers Data

TABLE II

FIBER-LENGTH DISTRIBUTIONS

Interval, mm.	% by Number					
1.3-1.4	2.0					
1.4-1.5	4.9					
1.5-1.6	7.8					
1.6-1.7	18.1					
1.7-1.8	22.1	1.1				
1.8-1.9	23.5	5.3				
1.9-2.0	15.7	6.4				
2.0-2.1	5.9	22.8		0.4		
2.1-2.2		23.8		2.6		
2.2-2.3		23.8		4.8		
2.3-2.4		10.0	2.4	6.2		
2.4-2.5		4.7	18.7	14.1		
2.5-2.6		2.1	36.5	23.4		
2.6-2.7			24.5	21.2		
2.7-2.8			11.1	18.9		
2.8-2.9			5.3	4.9		
2.9-3.0			1.4	1.8	0.5	
3.0-3.1				0.9	3.2	
3.1-3.2				0.9	9.6	
3.2-3.3					19.6	
3.3-3.4					23.6	
3.4-3.5					19.1	
3.5-3.6					13.2	
3.6-3.7					10.0	
3.7-3.8					1.4	
3.8-3.9						
3.9-4.0						
4.0-4.1						
4.1-4.2						
4.2-4.3						
4.3-4.4						
4.4-4.5						
4.5-4.6						3.5
4.6-4.7						8.8
4.7-4.8						15.8
4.8-4.9						17.5
4.9-5.0						25.7
5.0-5.1						19.9
5.1-5.2						5.9
5.2-5.3						2.9
5.3-5.4						
Av.	1.8	2.1	2.6a	2.6b	3.4	4.9 mm.

TABLE III

DIMENSIONS OF GRIDS

Grid	Geometry	Interwire Spacing, in.	Wire Diameter, in.
A	Parallel	0.050	0.005
B	"	0.070	0.007
C	"	0.050	0.0018
D	"	0.050	0.020
E	Square	0.070	0.0018
F	"	0.100	0.0018
G	"	0.070	0.005

Grids C, E, and F were made of stainless steel wire while all the others were made of bronze. The bulk of the work done in this study was performed using parallel grids A and B and square grids E and F. The others were used only for the purpose of studying the effect of the wire diameter on the retention curves as shown in Fig. 27.

The square-mesh grids were not woven but were formed by placing in contact and at right angles two parallel grids. Thus, the wires running in the two perpendicular directions were in two different planes one wire diameter apart.

#### WATER

Because large volumes of water and very small amounts of fibers were used, small amounts of suspended impurities in the water which could be caught on the filter cloths used for collecting the fibers were found to cause considerable errors. Consequently, special precautions had to be taken to remove suspended matter and insure a reasonably constant water quality.

Water was supplied to the tanks through a Fulflow filter, a Culligan water-softening unit, and another Fulflow filter. When the tanks were filled, the water was filtered further by circulating through the flow tube and through a triple thickness of filter paper (Cenco no. 13255) placed over the porous plate. The circulation was continued until the pressure drop across the filter paper ceased to increase with time.

In order to remove excess dissolved air, the water was heated by injecting filtered steam directly into the tanks. After gently agitating for a short time to hasten the escape of the small air bubbles formed by heating, the water was then cooled to the desired temperature by means of cooling coils in the tanks. All runs were made with a water temperature of  $27^{\circ}\text{C.} \pm 2^{\circ}$ .

#### PROCEDURE

To make a series of runs, water was prepared as described in the previous section. A weighed amount of fibers which had been dispersed in water in a four-liter filter flask and deaerated under aspirator suction overnight was added to tank B. A 1/8-hp. Lightnin' mixer was used for gentle agitation to keep the fibers dispersed in the tank. To begin each run, tared circles of nylon filter cloth were placed over the porous plate and on the movable filter and were held in place with the retaining rings. The grid was put in place and the flow tube was assembled and filled slowly from below taking care not to entrap any air under the grid. When the tube was filled, flow through the tube was begun and adjusted to the desired rate, the water being obtained from and returned to tank A. Fiber slurry was then introduced into the top of the tube

from tank B by means of the three-way valve, and when the desired amount had been obtained, the valve was shifted back to tank A in order to maintain the head necessary to maintain a constant flow rate until all the fibers had reached the grid. Then, the vent was opened, valve V<sub>1</sub> was closed, and the tube was slowly emptied. As the air-water interface approached the grid, the movable filter was moved into position between the grid and the porous plate. This was necessary since the deposits on the grid were often so small that the surface tension would disrupt the deposit as the interface passed through the grid, causing some of the fibers to be carried through. The fibers that were carried through in this manner were collected by the filter cloth on the movable filter and combined with the remainder of the deposit which was washed off the grid into a large funnel, collected in a glass crucible, dried, and weighed. The fibers which had passed through the grid during the run were retained on the filter cloth on the porous plate; these were also dried and weighed.

A series of about six to eight of these runs could be made in a day. Before each series, a blank run was made with no fibers present. The value of the blank, which ranged from 0 to 0.2 g./m.<sup>2</sup>, was subtracted from the weights obtained for all runs of the series.

All runs were made at temperatures of 27°C.  $\pm$  2° and at an average linear velocity of 2.2 cm./sec. except for special runs to determine the effect of varying the flow rate. The consistency of the fiber suspensions used varied with the fiber length being used, but was less than one-twentieth of the critical concentration as defined by Mason (18) in all cases.

## EFFECTS OF OPERATING VARIABLES

It was felt that it was possible for certain of the arbitrary operating variables which were not taken into account in the derived retention relationships to appreciably affect the experimental results. To make certain that experimental conditions had been chosen which would eliminate or reduce to a minimum the effects of some of these variables, the following studies were performed.

### FLOW RATE

It was expected that the fluid velocity would have little or no effect on retention in the system used as long as it was high enough to keep the fibers randomly oriented as they approached the grid and low enough not to deform the fibers or create large eddies that would tend to wash the fibers off the grid. To determine if variations in flow rate would affect the retention curves, data was taken at three different flow rates. The results are shown in Fig. 25, from which it can be concluded that the effect of flow rate is negligible in the vicinity of that used for determining the retention curves reported in the body of this report.

### WIRE DIAMETER

One of the important geometrical variables which was not considered in the theoretical development is the diameter of the wires which compose the grid in relation to the spacing between them. For parallel grids this would be expected to affect retention primarily through its effect on the flow pattern in the vicinity of the grid. Experiments with three parallel grids having widely different pitch-to-

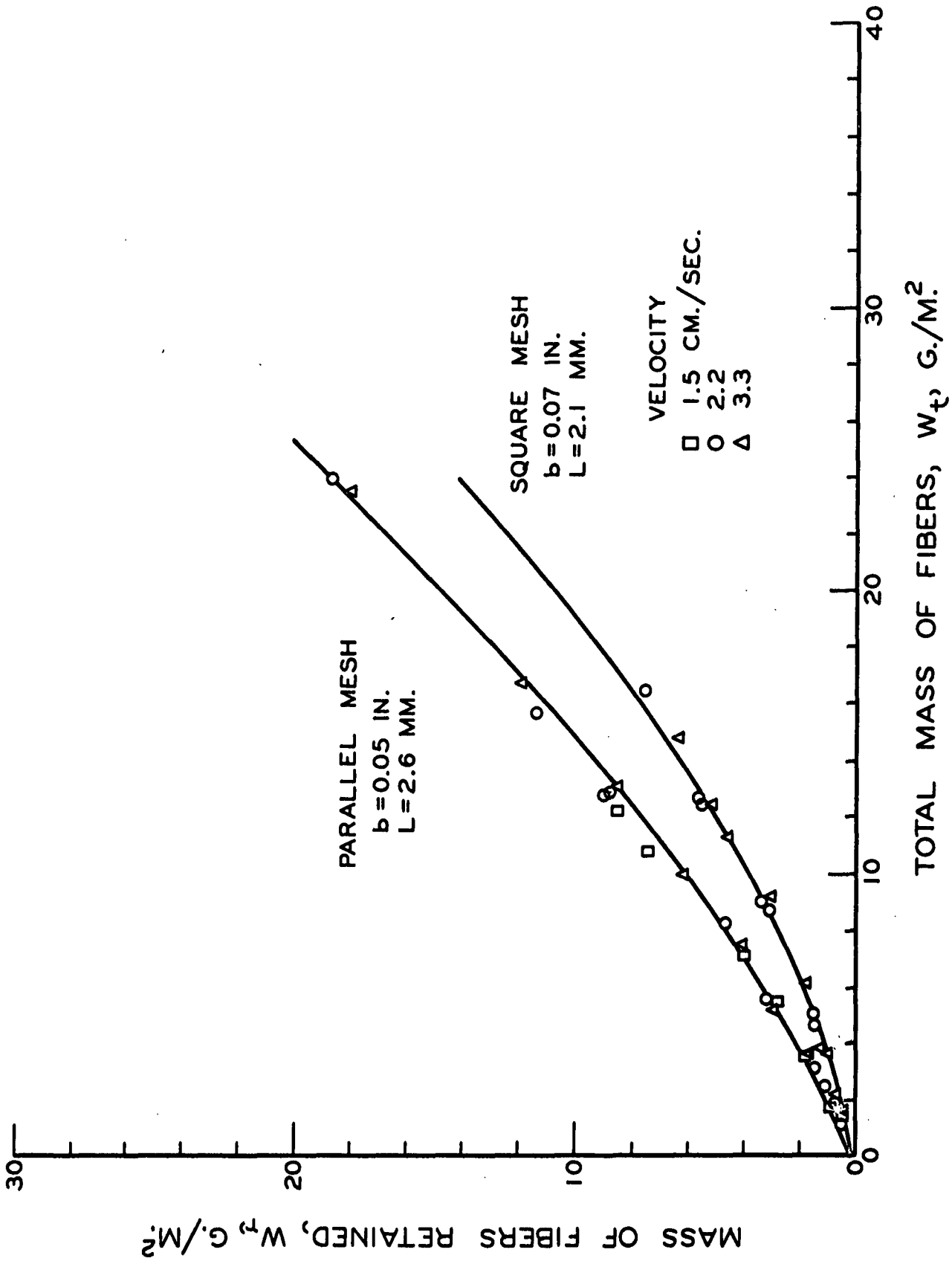


Figure 25. Effect of Flow Rate on Retention Curves

diameter ratios showed (Fig. 26) that this was not an important variable at the low flow rates used in this work.

For square-mesh grids of the construction used in this work, the wire diameter determines the offset of the two different sets of parallel wires running in the two perpendicular directions. This offset would be particularly important for short fibers which can bridge only across the corner of the square opening. The results shown in Fig. 26 indicate that the wire diameters used in this study are sufficiently small relative to the interwire spacings and fiber lengths used that this effect is negligible.

#### CONSISTENCY

To make certain that the slurries used were dilute enough so that each fiber would act independently, a set of experiments was carried out in which the consistency was varied as shown in Fig. 27. The values shown refer to consistency in the tank. The actual consistency in the flow tube will not be the same due to mixing and the consequent dilution that occurs upon entering the flow tube. However, the consistency in the flow tube must be a function of that in the slurry tank from which the slurry was drawn. The results show that in the range of consistencies that were used, fiber interactions were insufficient to affect the data.

#### PERMEATION TIME

As explained earlier, a certain amount of clear water had to be passed through the deposit after it was formed when making a run.

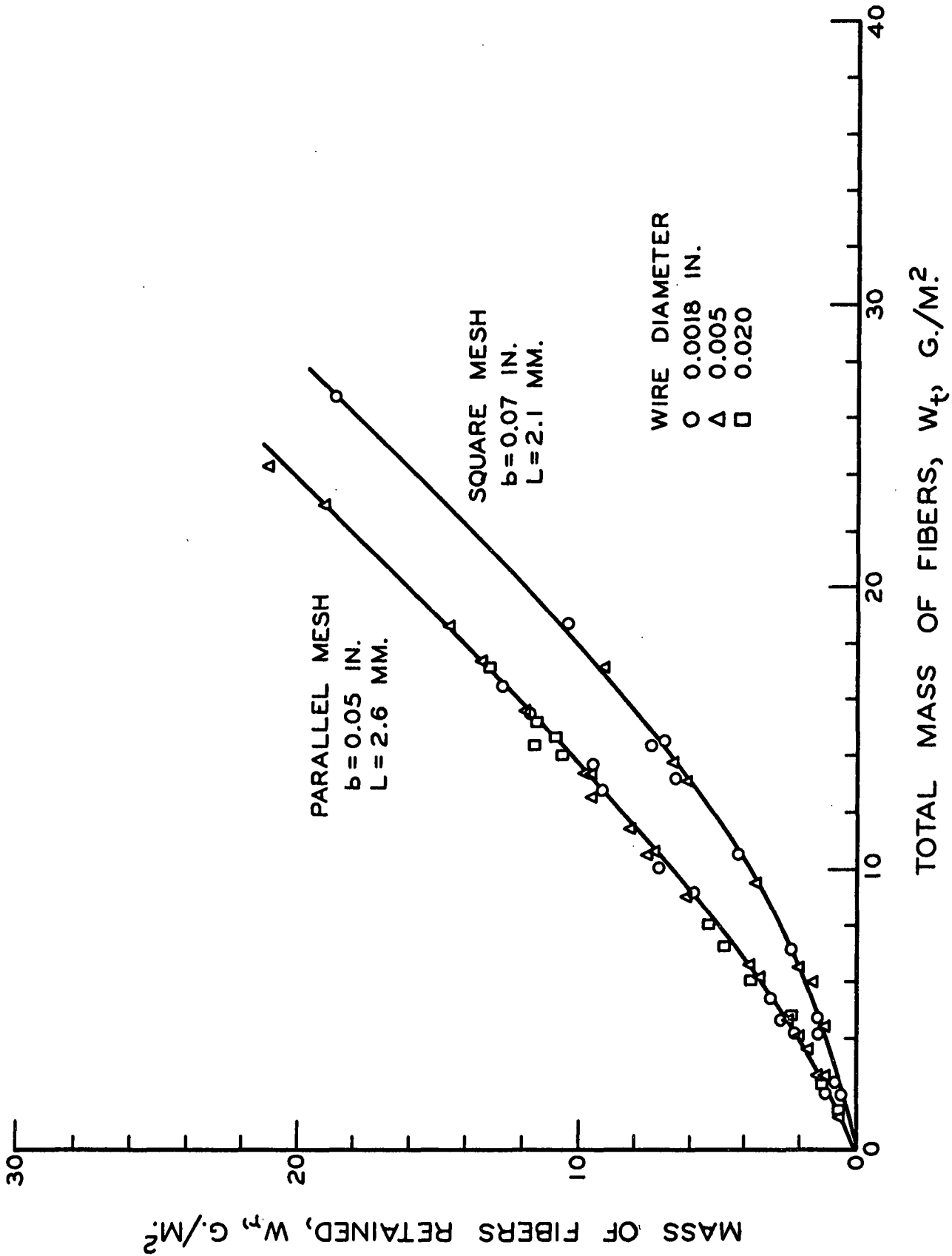


Figure 26. Effect of Wire Diameter on Retention Curves

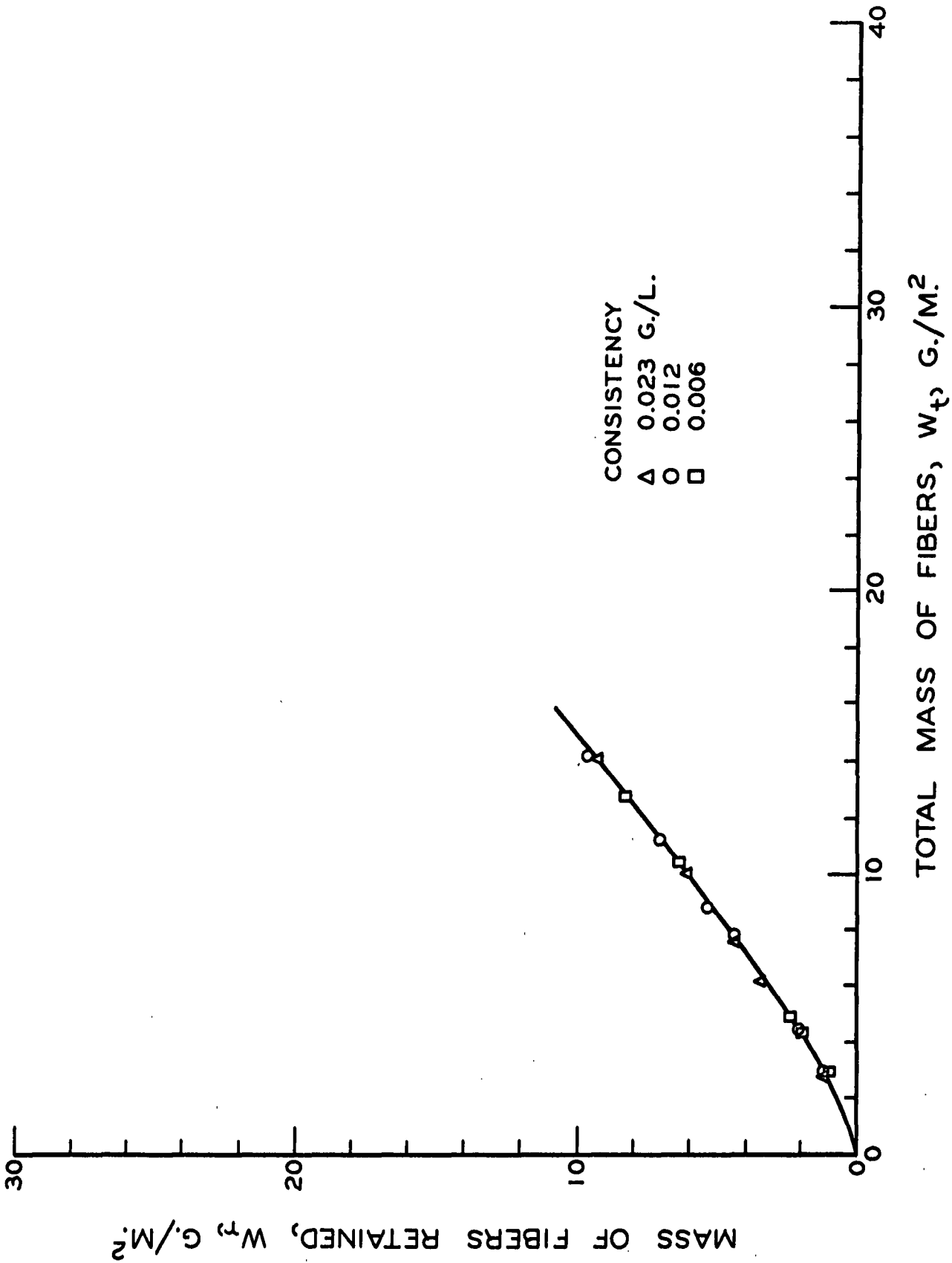


Figure 27. Effect of Consistency on the Retention of 2.6-mm. Fibers by Parallel-Mesh Grid ( $b = 0.05$  in.)

Standard practice in this work was to flow clear water for three minutes at a velocity of 2.2 cm./sec. after shifting the three-way valve from tank B back to tank A. This was done in order to maintain the velocity constant until all the fibers had reached the grid. To determine if there was any tendency for this water to wash fibers off the grid, the time of this permeation was varied. The data of Fig. 28 indicate that there was no tendency for the fibers to be washed off.

#### DISTRIBUTION OF FIBER ORIENTATIONS

In order to obtain an indication of whether or not the assumption of randomly oriented fibers approaching the grid was valid in the experimental system, photographs of the approaching fibers were made, and the distribution of angles was measured. The photographs were taken by focusing a 35-mm. camera equipped with a 135-mm. lens and 265-mm. extension tube on a point in the flow tube and taking series of exposures during actual runs. The camera was sighted through a flat lucite window in the flow tube at a point two inches above the grid and with the axis of the lens perpendicular to that of the flow tube. Exposures were made with the point of focus at the center of the tube and at one inch from the wall of the tube. Typical examples of the photographs obtained in this manner are shown in Fig. 29. The angles of all fibers which were in good enough focus were measured directly from the photographs, and the distributions are shown in Table IV. The angles measured by this means do not completely specify the orientation of the fibers. However, due to the symmetry of the flow tube, it would be expected that the distribution of  $\theta$  is random, and in this case the distribution of angles

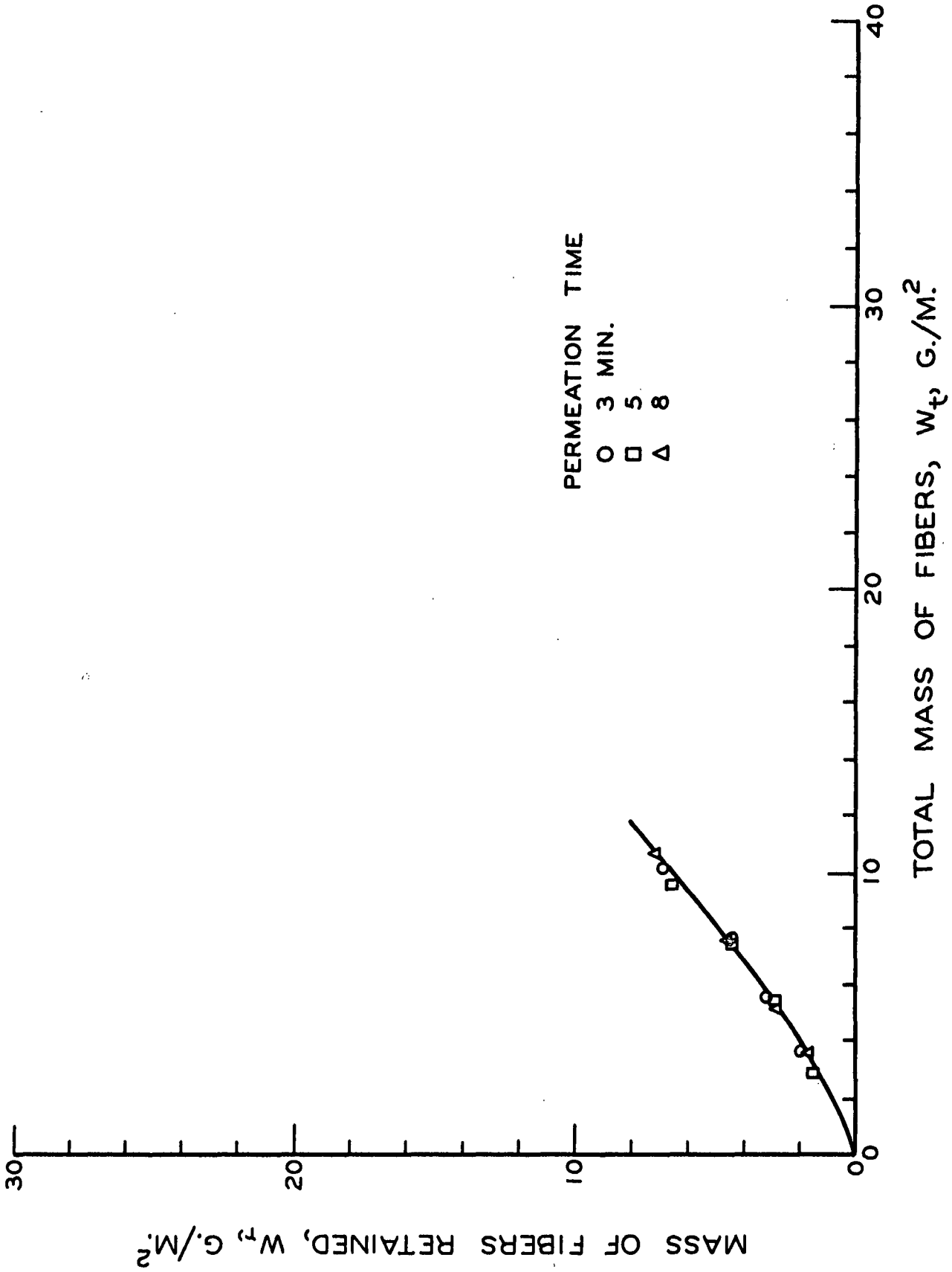


Figure 28. Effect of Permeation Time on the Retention of 2.6-mm. Fibers by Parallel-Mesh Grid ( $b = 0.05$  in.)

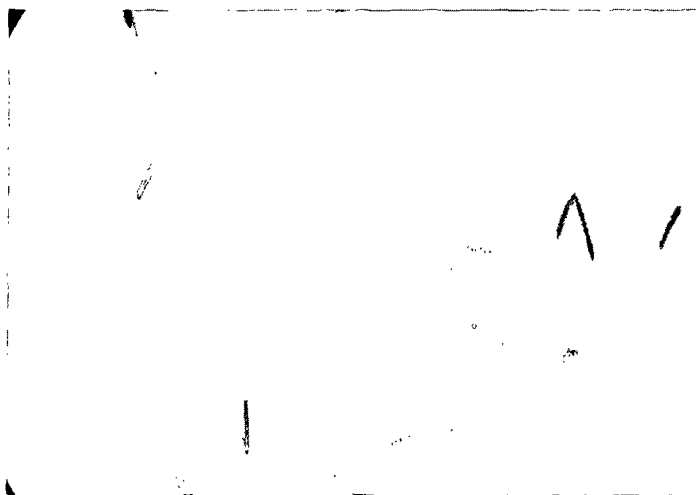
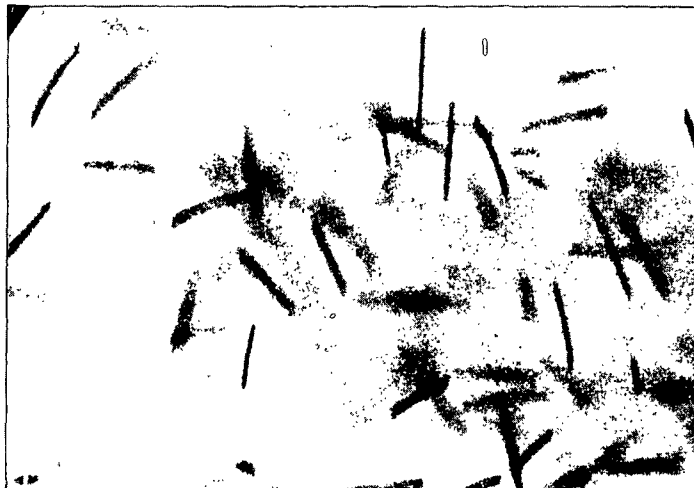


Figure 29. Photographs Used for  
Measuring Fiber Orientations

measured from the photographs gives an indirect indication of the distribution of  $\phi$ .

TABLE IV  
DISTRIBUTION OF FIBER ORIENTATIONS

Interval, degrees <sup>a</sup>	Center of Tube		1" from Wall
	3.4-mm. Fibers, %	2.1-mm. Fibers, %	2.1-mm. Fibers, %
0-30	21	18	12
30-60	16	18	16
60-90	14	14	24
90-120	17	13	21
120-150	17	18	16
150-180	15	19	11
Total fibers measured	275	709	751

<sup>a</sup> Measured from the horizontal.

The data show a definite tendency for the fibers to assume a horizontal orientation near the center of the tube and a vertical orientation near the wall. Neither tendency is extreme, and it is felt that the assumption of random orientation of the fibers approaching the grid is reasonably valid.

APPENDIX IV

EXPERIMENTAL RETENTION DATA

TABLE V

DATA FOR PARALLEL GRID,  $\underline{b} = 0.05$  IN.

$\underline{L} = 1.8$ mm.		$\underline{L} = 2.1$ mm.		$\underline{L} = 2.6$ mm.	
$\frac{W_r}{g \cdot \sqrt{m.}^2}$	$\frac{W_t}{g \cdot \sqrt{m.}^2}$	$\frac{W_r}{g \cdot \sqrt{m.}^2}$	$\frac{W_t}{g \cdot \sqrt{m.}^2}$	$\frac{W_r}{g \cdot \sqrt{m.}^2}$	$\frac{W_t}{g \cdot \sqrt{m.}^2}$
.99	6.26	.71	2.50	.52	1.23
1.17	7.04	1.05	3.30	.80	1.60
1.51	8.64	1.08	3.52	.83	1.79
1.88	10.71	1.64	4.72	.77	1.82
2.16	12.62	2.25	6.45	1.14	2.53
2.62	12.84	3.18	8.15	1.23	3.02
3.12	14.04	3.43	9.29	1.51	3.09
4.14	19.01	4.10	9.72	2.06	3.70
4.14	19.23	5.52	11.70	2.19	4.50
6.08	21.98	6.27	12.96	3.18	5.62
6.36	21.67	8.02	15.19	3.21	5.65
8.24	23.61	9.35	16.85	4.38	7.81
9.44	27.28	10.52	18.27	4.41	7.75
9.88	28.73	12.81	21.76	4.78	7.87
10.46	27.04	13.40	21.85	5.37	8.82
13.24	33.21	17.41	25.52	5.74	8.77
14.63	35.52	18.83	27.28	6.08	9.66
14.97	36.91	20.80	29.60	6.91	10.19
15.90	36.02	25.09	33.70	7.16	11.30
18.33	39.20			7.56	11.20
26.54	47.99			8.92	12.87
				9.01	12.81
				9.59	14.10
				11.39	15.64
				12.10	16.39
				16.85	21.70
				18.89	23.89
				23.39	28.12
				23.76	28.77
				4.69	8.18

TABLE V (CONT'D)

$\underline{L} = 3.4 \text{ mm.}$		$\underline{L} = 4.9 \text{ mm.}$	
$\frac{W_r'}{g \cdot 7m.}^2$	$\frac{W_t'}{g \cdot 7m.}^2$	$\frac{W_r'}{g \cdot 7m.}^2$	$\frac{W_t'}{g \cdot 7m.}^2$
1.48	2.22	.93	1.23
1.39	2.13	1.42	1.88
1.70	2.44	1.08	1.36
2.78	3.79	1.45	1.97
2.19	3.30	1.85	2.38
3.33	4.63	2.50	3.08
4.54	5.86	2.53	3.12
5.74	7.32	2.62	3.18
6.57	8.30	3.06	3.76
8.48	10.28	4.19	5.00
8.73	10.90	5.65	6.67
10.40	12.47	7.44	8.46
13.58	16.11	7.53	8.67
16.94	19.51	9.17	10.19
21.91	24.91	10.15	11.30
		11.88	13.18
		14.32	15.68
		17.04	18.43
		21.69	23.36

TABLE VI

DATA FOR PARALLEL GRID,  $\underline{b} = 0.07$  IN.

$\underline{L} = 2.5$ mm.		$\underline{L} = 3.4$ mm.		$\underline{L} = 4.9$ mm.	
$\frac{W_r}{g \cdot \sqrt{m}}^2$	$\frac{W_t}{g \cdot \sqrt{m}}^2$	$\frac{W_r}{g \cdot \sqrt{m}}^2$	$\frac{W_t}{g \cdot \sqrt{m}}^2$	$\frac{W_r}{g \cdot \sqrt{m}}^2$	$\frac{W_t}{g \cdot \sqrt{m}}^2$
.96	3.43	.74	1.48	.74	1.27
1.05	3.40	.86	1.76	1.02	1.73
1.11	4.41	1.36	2.78	1.34	2.10
1.45	4.32	1.67	3.30	1.94	2.84
2.10	6.54	2.78	5.00	2.41	3.55
2.25	6.61	3.12	5.43	3.06	4.07
2.65	8.12	3.92	6.05	4.60	5.71
3.74	9.26	4.29	6.91	4.88	6.08
4.32	10.25	5.03	7.90	5.40	6.85
6.61	13.09	6.79	9.97	6.36	7.84
9.35	16.61	8.73	11.67	10.80	12.53
13.61	20.90	9.57	12.38	12.38	14.07
15.12	22.22	12.75	16.20	13.46	15.34
20.40	28.18	20.93	24.94	15.90	17.65
				18.46	20.53

TABLE VII

DATA FOR SQUARE GRID,  $\underline{b} = 0.07$  IN.

$\underline{L} = 1.8$ mm.		$\underline{L} = 2.1$ mm.		$\underline{L} = 2.6$ mm.	
$\frac{W_r}{g \cdot \sqrt{m.}^2}$	$\frac{W_t}{g \cdot \sqrt{m.}^2}$	$\frac{W_r}{g \cdot \sqrt{m.}^2}$	$\frac{W_t}{g \cdot \sqrt{m.}^2}$	$\frac{W_r}{g \cdot \sqrt{m.}^2}$	$\frac{W_t}{g \cdot \sqrt{m.}^2}$
.62	4.63	.46	1.91	.99	2.07
.99	5.46	.77	2.43	1.24	2.25
1.08	7.44	.90	3.36	1.79	3.18
1.42	9.35	1.33	4.14	2.07	3.89
1.48	11.76	1.42	4.69	2.65	4.38
1.82	11.23	1.45	4.66	3.43	5.90
1.88	12.22	2.35	7.10	3.49	5.71
3.02	15.77	1.54	4.97	4.57	7.13
3.06	19.41	3.15	8.74	5.71	8.86
3.73	16.11	4.32	10.56	8.83	12.19
6.11	25.77	5.49	12.38	8.89	12.32
8.67	28.92	5.65	12.65	9.41	12.93
12.65	36.42	6.94	14.54	14.75	18.76
		7.53	14.32	24.23	28.77
		7.72	16.48		
		10.34	18.61		
		18.80	26.73		
		20.46	28.30		

$\underline{L} = 3.4$ mm.		$\underline{L} = 4.9$ mm.	
$\frac{W_r}{g \cdot \sqrt{m.}^2}$	$\frac{W_t}{g \cdot \sqrt{m.}^2}$	$\frac{W_r}{g \cdot \sqrt{m.}^2}$	$\frac{W_t}{g \cdot \sqrt{m.}^2}$
.68	.86	.43	.46
.86	1.17	1.08	1.20
1.20	1.64	1.36	1.54
1.33	1.67	2.78	3.06
1.94	2.53	2.81	3.09
2.99	3.77	3.98	4.29
3.46	4.35	3.98	4.35
5.81	6.92	5.46	6.02
6.76	7.90	8.24	8.86
8.12	9.54	10.74	11.42
10.03	11.67	14.01	14.91
12.50	14.23	17.10	17.90
20.28	22.32	7.44	8.15

TABLE VIII

DATA FOR SQUARE GRID,  $\underline{b} = 0.10$  IN.

$\underline{L} = 2.1$ mm.		$\underline{L} = 2.6$ mm.		$\underline{L} = 3.4$ mm.	
$\frac{W_r'}{g \cdot \sqrt{m.}^2}$	$\frac{W_t'}{g \cdot \sqrt{m.}^2}$	$\frac{W_r'}{g \cdot \sqrt{m.}^2}$	$\frac{W_t'}{g \cdot \sqrt{m.}^2}$	$\frac{W_r'}{g \cdot \sqrt{m.}^2}$	$\frac{W_t'}{g \cdot \sqrt{m.}^2}$
.56	5.49	.59	4.23	.71	1.70
.68	7.28	.90	5.28	.96	2.59
.80	8.77	1.02	7.13	1.42	3.33
.93	9.72	1.14	7.19	1.70	3.74
1.14	11.82	1.11	6.33	2.22	4.63
1.82	17.10	1.79	8.58	3.15	5.80
1.85	16.98	2.38	11.36	3.33	6.48
1.57	14.04	2.87	11.88	4.32	7.65
2.84	22.93	4.07	14.72	7.68	11.54
2.96	23.40	6.57	18.03	10.83	15.03
3.27	25.80	6.11	17.62	14.20	18.64
2.78	22.22	7.28	19.41	15.15	19.69
6.08	32.72	12.96	26.64		

$\underline{L} = 4.9$  mm.

$\frac{W_r'}{g \cdot \sqrt{m.}^2}$	$\frac{W_t'}{g \cdot \sqrt{m.}^2}$
.80	1.05
1.14	1.54
2.35	2.75
1.39	1.82
1.79	2.22
2.41	2.87
3.43	3.95
3.70	4.35
5.00	5.59
6.76	7.59
8.18	9.07
10.46	11.51
14.54	15.46

APPENDIX V

DETERMINATION OF INITIAL SLOPES

In the following Fig. 30-33, the initial slopes of the retention curves are determined as the intercept on the  $\frac{W_r}{W_t}$  axis of a plot of  $\frac{W_r}{W_t}$  vs.  $\frac{W_r}{W_t}$ . There is a degree of uncertainty in this extrapolation technique due to the large relative errors which are present in measurements at low retentions. This error is due in part to true experimental error and in part to the fact that the retention of fibers by the grid is a statistical process. The retention curve for any fiber length-grid combination is a statistical average curve, and the data observed for any particular run does not have to fall on this curve even if the experimental errors were not present. Due to this error and to the steepness of the curves at low values of  $\frac{W_r}{W_t}$ , the accuracy of the initial slopes shown in Fig. 14 is probably no better than about  $\pm 0.05$  units for the square-mesh data and about  $\pm 0.075$  units for the parallel-mesh data. The better accuracy for the square-mesh data is due to the fact that the curves to be extrapolated are less steep in the vicinity of  $\frac{W_r}{W_t} = 0$  than for the parallel mesh. This is easily understood if it is recognized that the rate of change of the slope of the retention curve is an indication of the rate at which the geometry of the openings in the grid is changing due to the deposited fibers. A given weight of fibers will change the geometry of a parallel-mesh grid much more radically than that of a square-mesh grid.

The extrapolation procedure is made somewhat easier if a few facts about the nature of the curves are understood. For each grid

studied, the curves to be extrapolated form a family, the two limiting cases being horizontal lines at values of  $\frac{W_r}{W_t}$  of zero and unity. For extremely low or high values of the initial slope, the curves must approach these horizontal lines. As a zero value of  $\frac{W_r}{W_t}$  is approached the curves must continue smoothly downward to the intercept; it is not possible for them to level off or turn upward. It is possible that the curves could turn downward more sharply and reach a considerably lower intercept than that indicated. The argument against this possibility is supported by the photographs in Appendix IV. At retention of much less than  $1/2 \text{ g./m.}^2$ , there are so few fibers on the grid, that extremely rapid changes in the slope of the retention curves in this range would be unexpected.

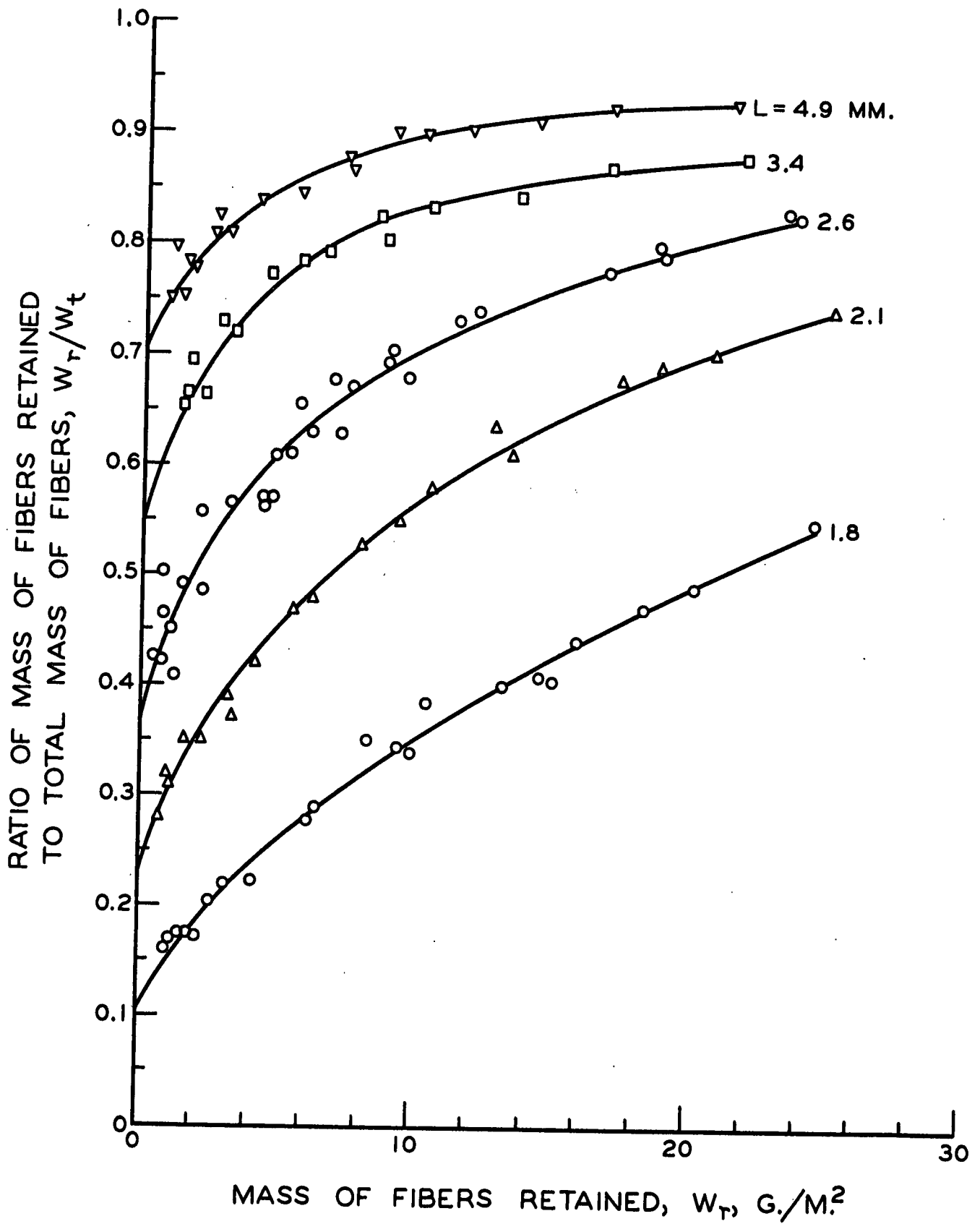


Figure 30. Determination of Initial Slopes.  
Parallel Grid,  $b = 0.050$  in.

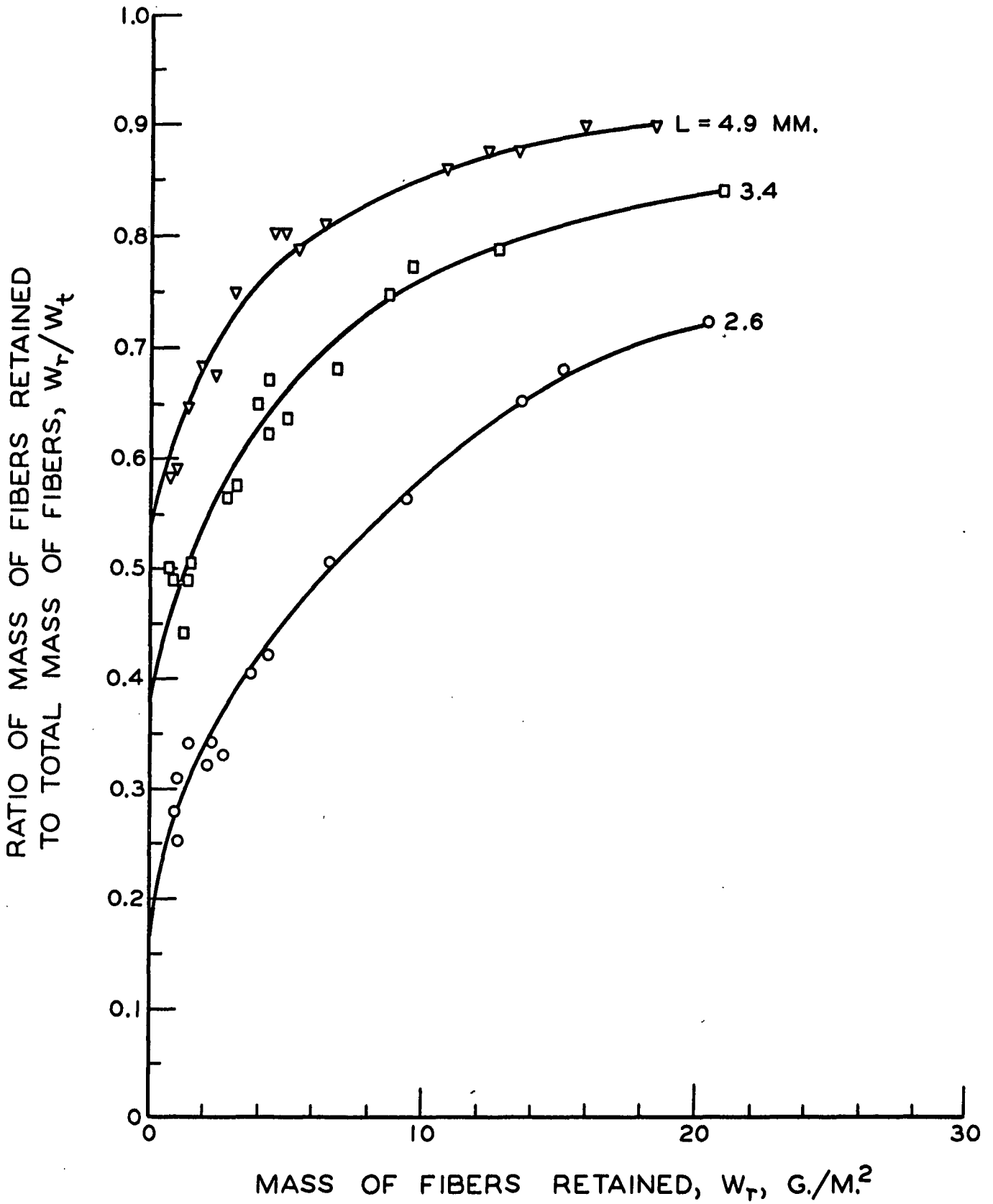


Figure 31. Determination of Initial Slopes  
Parallel Grid,  $b = 0.070$  in.

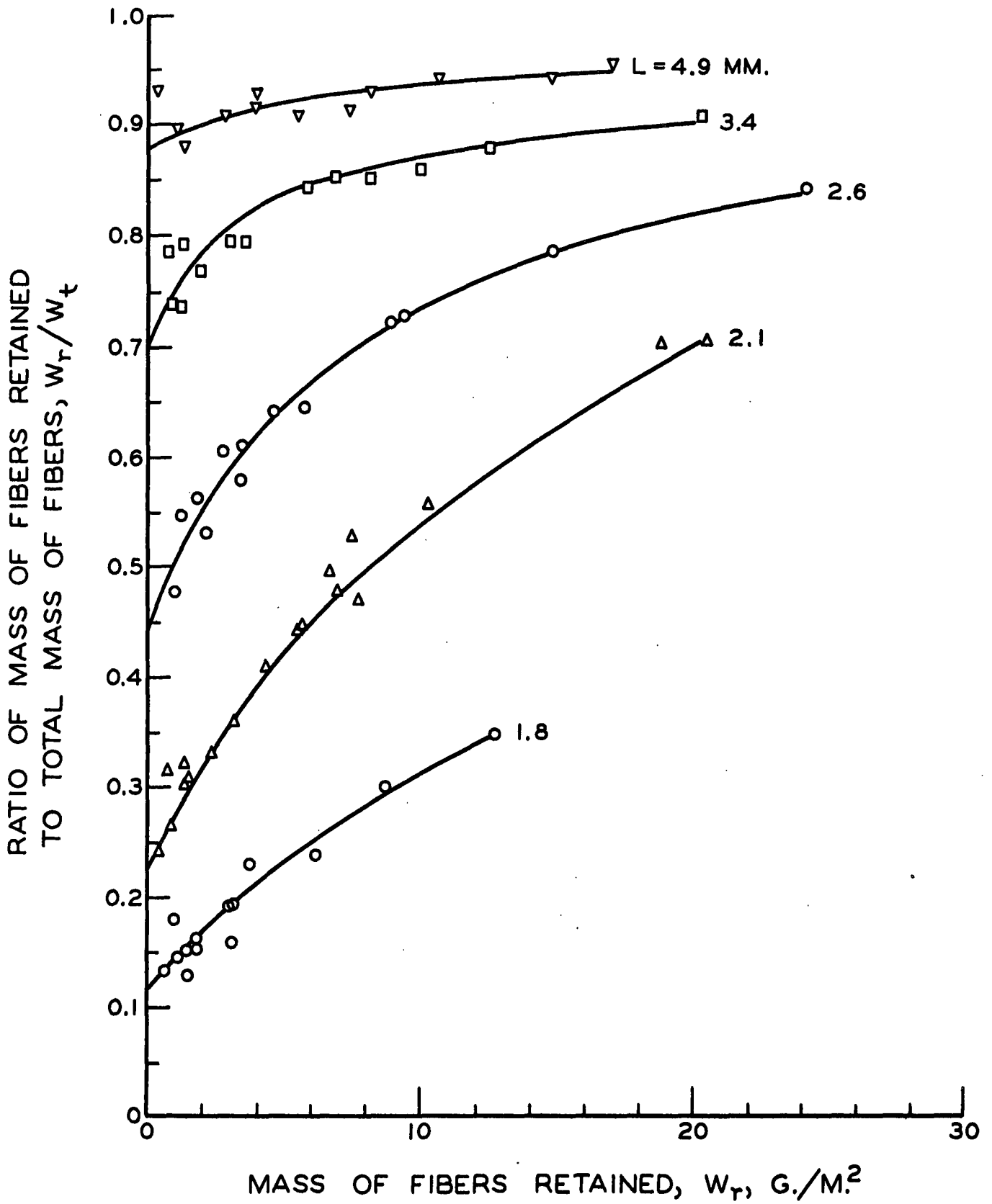


Figure 32. Determination of Initial Slopes  
Square Grid,  $b = .070$  in.

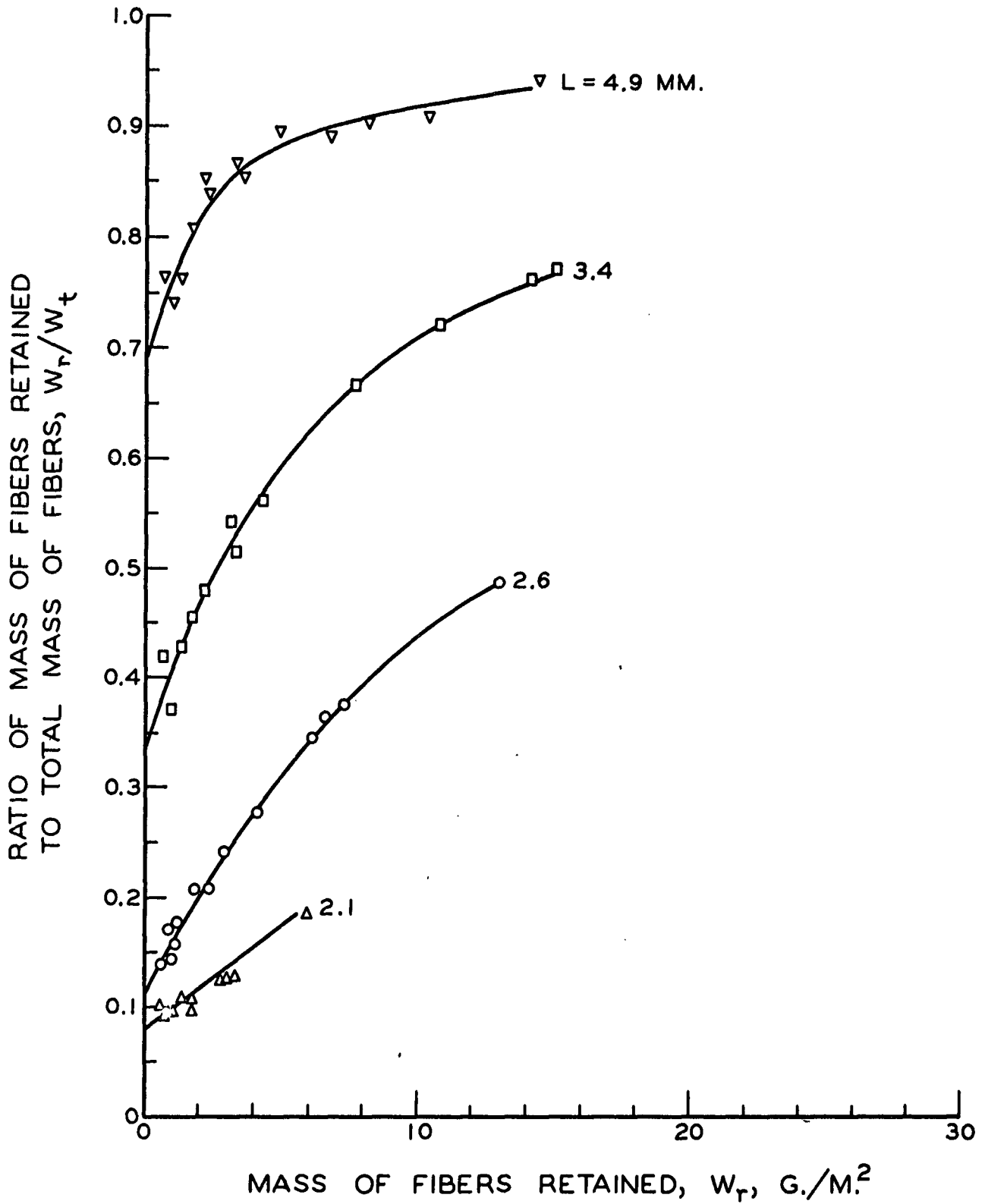
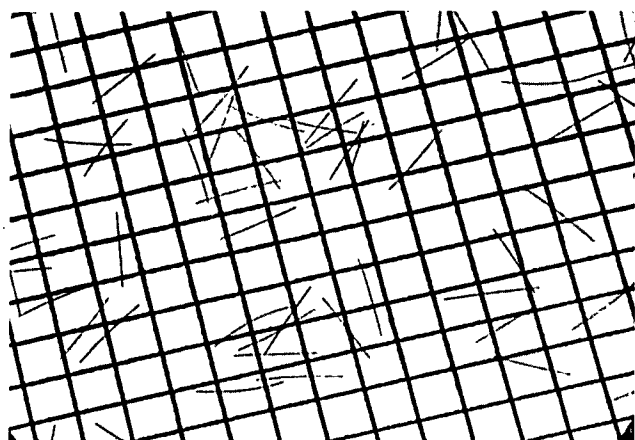


Figure 33. Determination of Initial Slopes  
Square Grid,  $b = 0.10$  in.

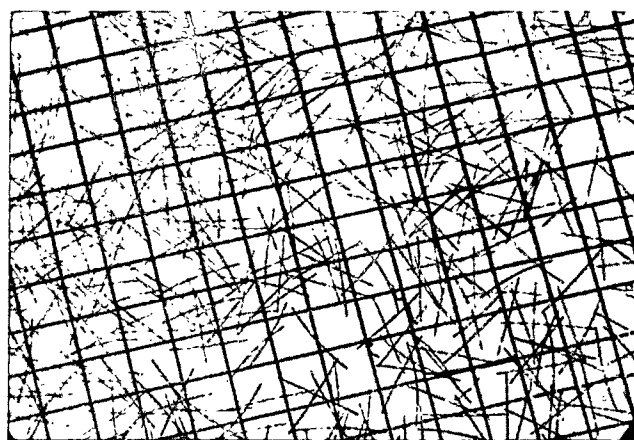
APPENDIX VI

PHOTOGRAPHS OF FIBER DEPOSITS

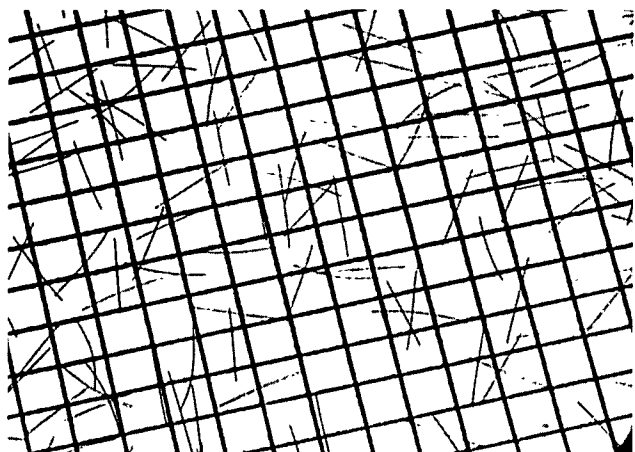
The photographs on the following pages were made to illustrate the appearance of the fiber deposits during its formation. They will serve to orient the reader as to the structure of the fiber deposit at different points along the retention curves. With the exception of the fibers being dyed and the grids being sprayed with black paint, all the conditions were the same when these photographs were taken as during normal runs. The photographs were taken through the flat lucite window in the side of the flow tube with the axis of the camera lens making about a thirty degree angle with the angle of the tube. A 35-mm. camera with 135-mm. lens and 155-mm. extension tube was used for this work. Each photograph represents a different run, and the exposure was made just before the air-water interface passed through the grid when draining the flow tube.



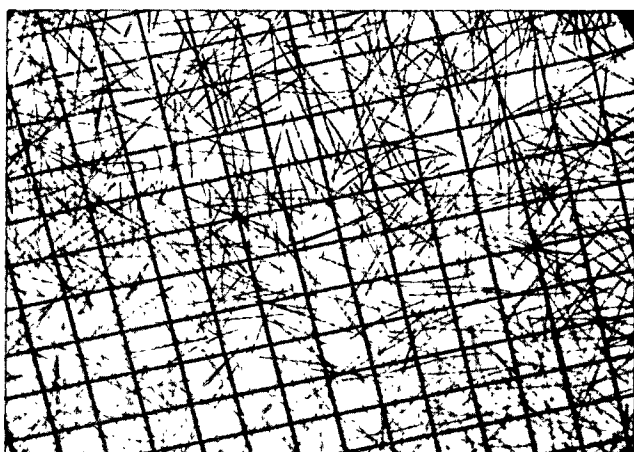
$$\frac{W}{r} = 0.6 \text{ g./m.}^2$$



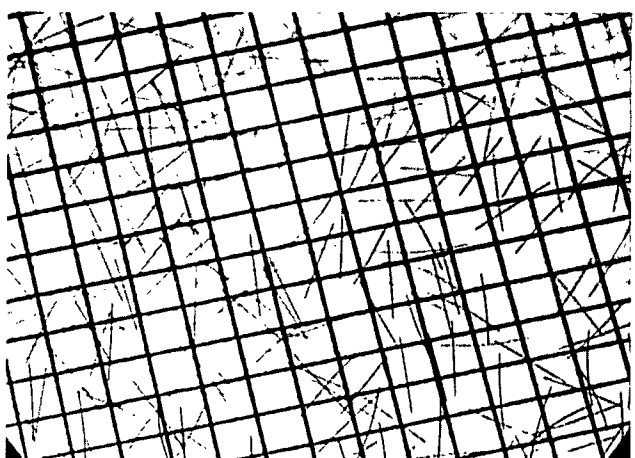
$$\frac{W}{r} = 3.3 \text{ g./m.}^2$$



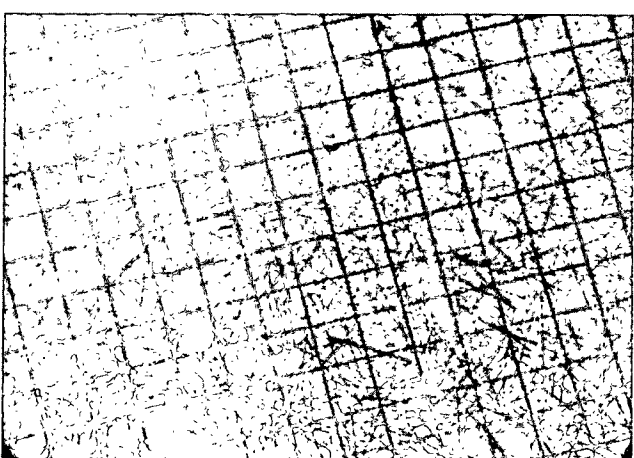
$$\frac{W}{r} = 0.8 \text{ g./m.}^2$$



$$\frac{W}{r} = 5.5 \text{ g./m.}^2$$

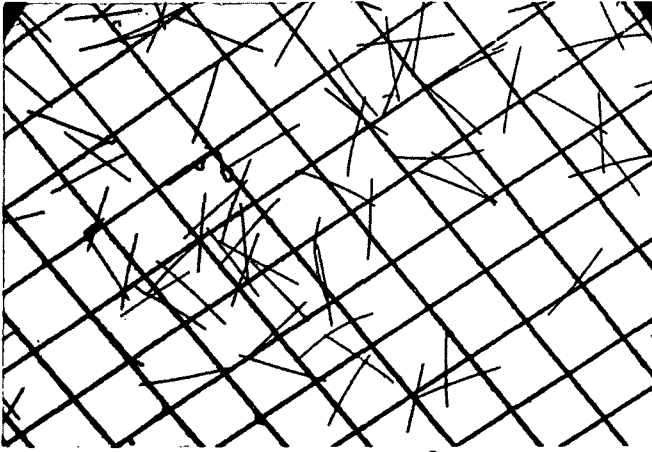


$$\frac{W}{r} = 1.7 \text{ g./m.}^2$$

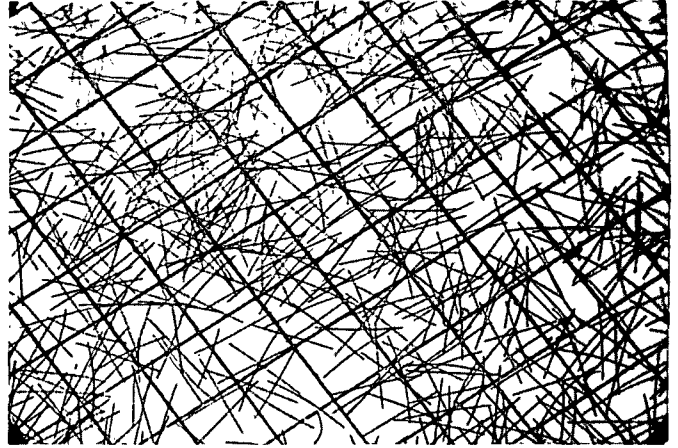


$$\frac{W}{r} = 10.8 \text{ g./m.}^2$$

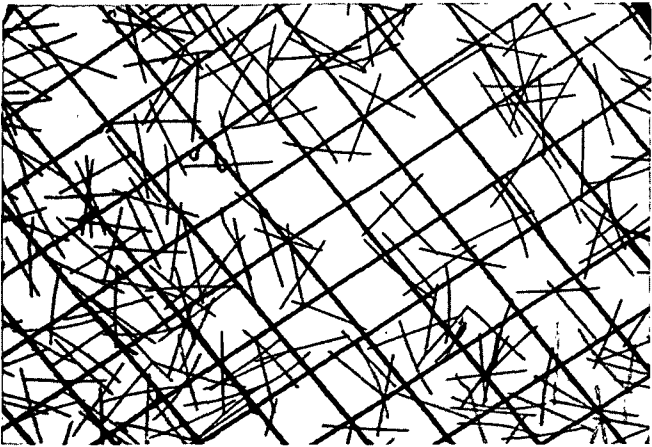
Figure 34. Deposits of Fibers on Square-Mesh Grid,  
 $\underline{b} = 0.07 \text{ in.}$ ,  $\underline{L} = 3.4 \text{ mm.}$



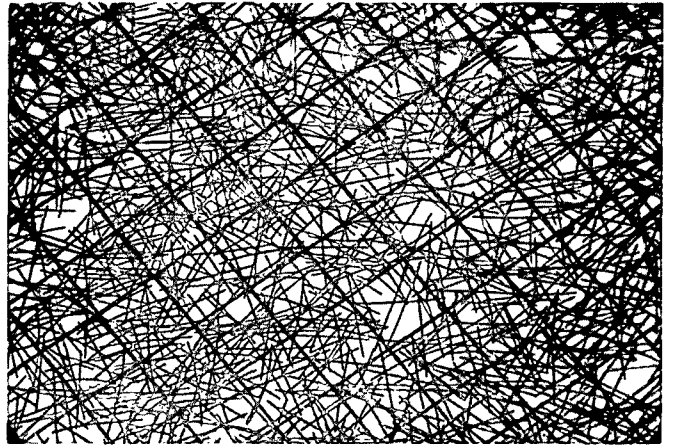
$$\frac{W}{r} = 0.8 \text{ g./m.}^2$$



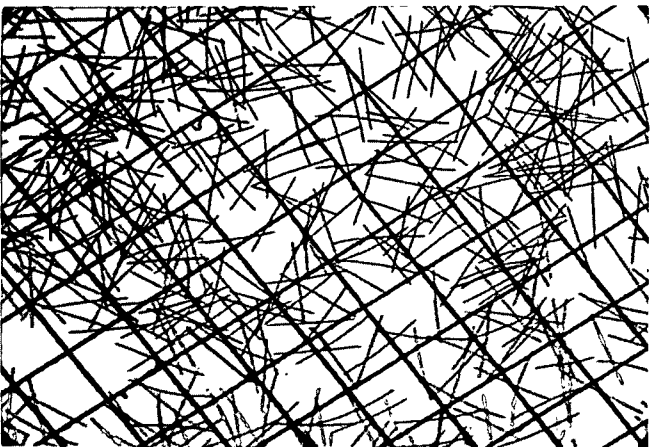
$$\frac{W}{r} = 4.6 \text{ g./m.}^2$$



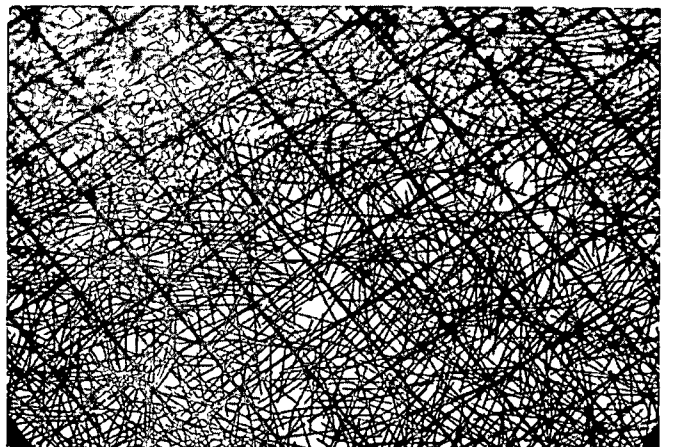
$$\frac{W}{r} = 2.1 \text{ g./m.}^2$$



$$\frac{W}{r} = 8.9 \text{ g./m.}^2$$



$$\frac{W}{r} = 3.0 \text{ g./m.}^2$$

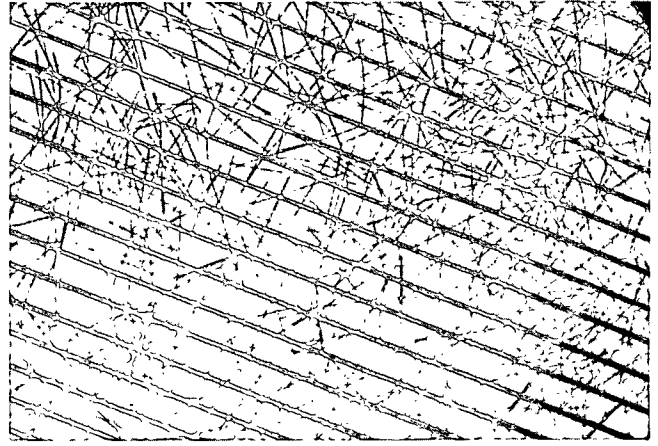


$$\frac{W}{r} = 12.6 \text{ g./m.}^2$$

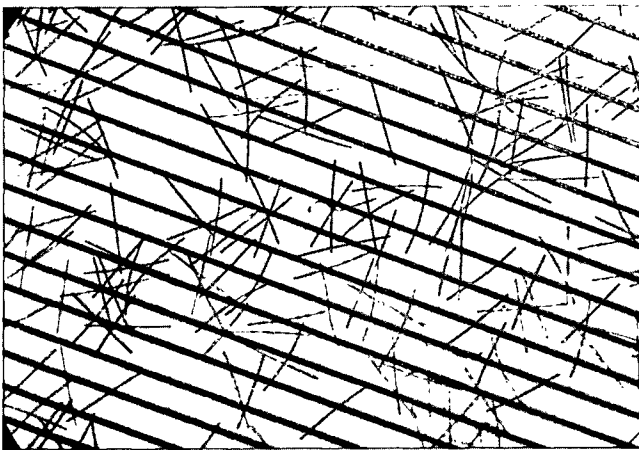
Figure 35. Deposits of Fibers on Square-Mesh Grid,  
 $\underline{b} = 0.10 \text{ in.}$ ,  $\underline{L} = 3.4 \text{ mm.}$



$$\frac{W_r}{\underline{r}} = 0.6 \text{ g./m.}^2$$



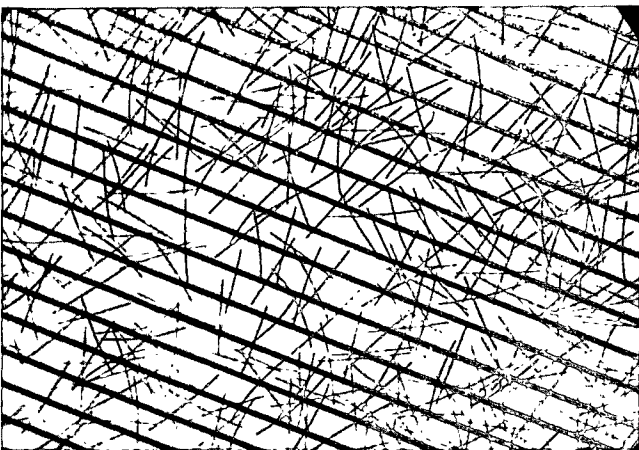
$$\frac{W_r}{\underline{r}} = 4.6 \text{ g./m.}^2$$



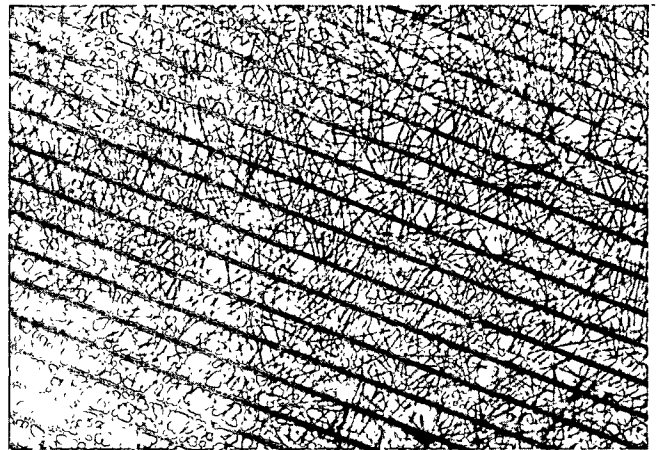
$$\frac{W_r}{\underline{r}} = 1.5 \text{ g./m.}^2$$



$$\frac{W_r}{\underline{r}} = 7.4 \text{ g./m.}^2$$

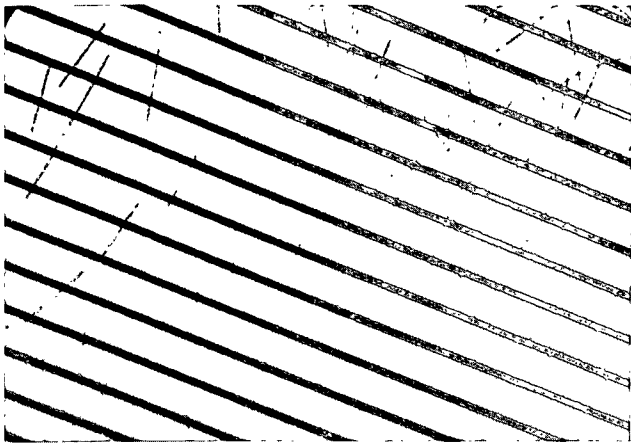


$$\frac{W_r}{\underline{r}} = 3.4 \text{ g./m.}^2$$

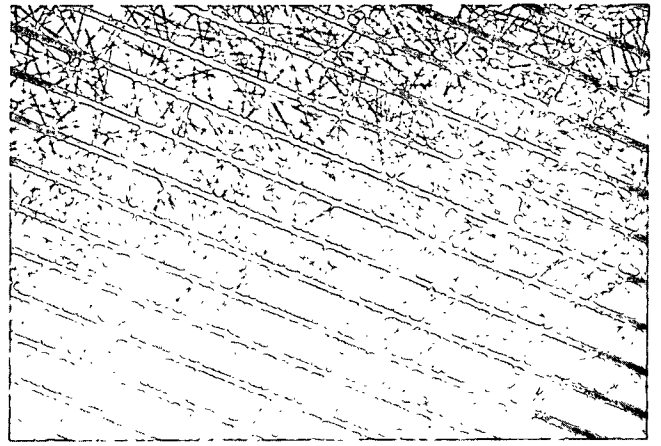


$$\frac{W_r}{\underline{r}} = 10.5 \text{ g./m.}^2$$

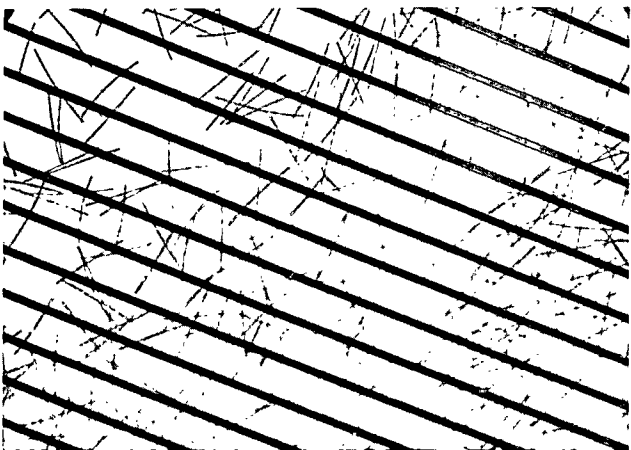
Figure 36. Deposits of Fibers on Parallel Grid,  
 $\underline{b} = 0.05 \text{ in.}$ ,  $\underline{L} = 3.4 \text{ mm.}$



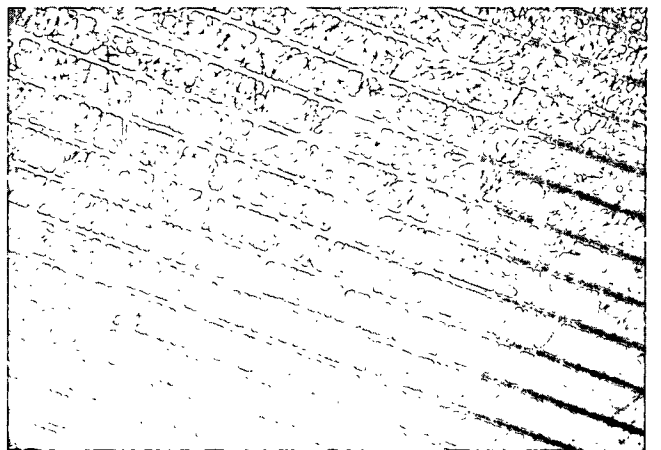
$$\frac{W}{r} = 0.6 \text{ g./m.}^2$$



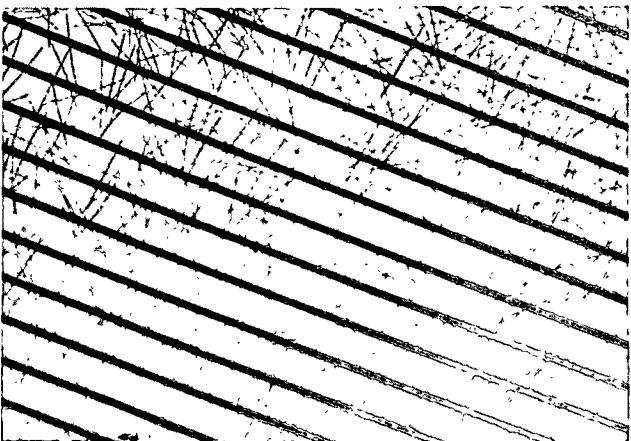
$$\frac{W}{r} = 6.0 \text{ g./m.}^2$$



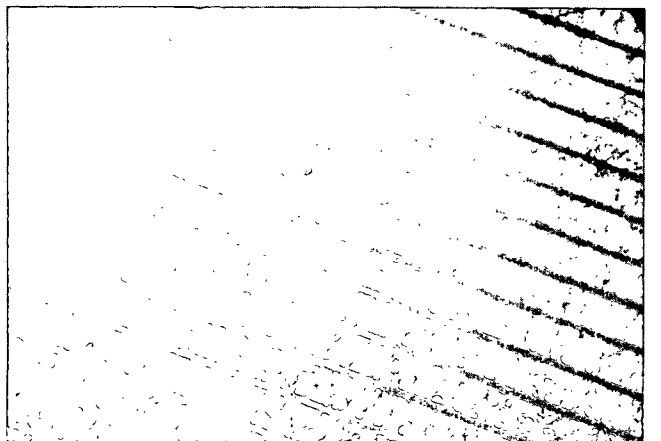
$$\frac{W}{r} = 1.8 \text{ g./m.}^2$$



$$\frac{W}{r} = 9.9 \text{ g./m.}^2$$



$$\frac{W}{r} = 2.8 \text{ g./m.}^2$$



$$\frac{W}{r} = 12.3 \text{ g./m.}^2$$

Figure 37. Deposits of Fibers on Parallel Grid,  
 $\underline{b} = 0.07$  in.,  $\underline{L} = 3.4$  mm.